Behavior of a Steel Girder Bolted Splice Connection

PUBLICATION NO. FHWA-HRT-17-042

NOVEMBER 2017

U.S. Department of Transportation
Federal Highway Administration

Research, Development, and Technology
Turner-Fairbank Highway Research Center
6300 Georgetown Pike
McLean, VA 22101-2296

FOREWORD

This report documents the finite element modeling of a bolted steel girder field splice connection designed using the traditional method and using a new method that makes conservative assumptions resulting in a simpler, streamlined procedure. The results of the analysis demonstrated the efficacy of the new design procedure, which resulted in fewer bolts compared to the traditional design approach, making the connection more economical. The results of this work would benefit those interested in behavior of bolted connections used for the construction of steel bridges, including State transportation departments, researchers, and design consultants.

Cheryl Allen Richter, Ph.D., P.E.
Director, Office of Infrastructure
Research and Development

TECHNICAL REPORT DOCUMENTATION PAGE

1. Report No. FHWA-HRT-17-042	2. Government Accession No.	3. Recipient's Catalog No.
4. Title and Subtitle Behavior of a Steel Girder Bolted Splice Connection		5. Report Date November 2017
		6. Performing Organization Code:
7. Author(s) Justin M. Ocel, Ph.D. P.E.		8. Performing Organization Report No.
9. Performing Organization Name and Address Federal Highway Administration Bridge and Foundation Engineering Team Turner-Fairbank Highway Research Center 6300 Georgetown Pike McLean, VA 22101-2296		10. Work Unit No.
		11. Contract or Grant No.
12. Sponsoring Agency Name and Address Office of Infrastructure Research and Development Federal Highway Administration 6300 Georgetown Pike McLean, VA 22101-2296		13. Type of Report and Period Covered Final Report; December 2015–May 2016
		14. Sponsoring Agency Code HRDI-40

15. Supplementary Notes
This was a staff study; no funds were expended performing this effort. Justin Ocel (HRDI-40) performed the finite element analysis and wrote the report.

16. Abstract
This report documents the finite element analysis of a bolted field splice connection from a hypothetical three-span continuous bridge with back spans 234 ft long, and a 300-ft center span. The connection was designed using a traditional approach and then by using a new simplified method that required fewer bolts for the web splice component. The results of the analysis demonstrated the efficacy of the new design method in that it did not result in overstressing of the girder or bolts at the strength limit state. In part because of this work, the American Association of State and Highway Transportation Officials voted in June 2016 to adopt a new design method for the design of bolted connections for steel bridges.

17. Key Words Steel bridges, Bolted connection, Modeling, Finite element analysis	18. Distribution Statement No restrictions. This document is available through the National Technical Information Service, Springfield, VA 22161. http://www.ntis.gov

19. Security Classif. (of this report) Unclassified	20. Security Classif. (of this page) Unclassified	21. No. of Pages 86	22. Price N/A

Form DOT F 1700.7 (8-72) Reproduction of completed page authorized.

SI* (MODERN METRIC) CONVERSION FACTORS

APPROXIMATE CONVERSIONS TO SI UNITS

Symbol	When You Know	Multiply By	To Find	Symbol
		LENGTH		
in	inches	25.4	millimeters	mm
ft	feet	0.305	meters	m
yd	yards	0.914	meters	m
mi	miles	1.61	kilometers	km
		AREA		
in^2	square inches	645.2	square millimeters	mm^2
ft^2	square feet	0.093	square meters	m^2
yd^2	square yard	0.836	square meters	m^2
ac	acres	0.405	hectares	ha
mi^2	square miles	2.59	square kilometers	km^2
		VOLUME		
fl oz	fluid ounces	29.57	milliliters	mL
gal	gallons	3.785	liters	L
ft^3	cubic feet	0.028	cubic meters	m^3
yd^3	cubic yards	0.765	cubic meters	m^3
	NOTE: volumes greater than 1000 L shall be shown in m^3			
		MASS		
oz	ounces	28.35	grams	g
lb	pounds	0.454	kilograms	kg
T	short tons (2000 lb)	0.907	megagrams (or "metric ton")	Mg (or "t")
		TEMPERATURE (exact degrees)		
^oF	Fahrenheit	5 (F-32)/9 or (F-32)/1.8	Celsius	^oC
		ILLUMINATION		
fc	foot-candles	10.76	lux	lx
fl	foot-Lamberts	3.426	$candela/m^2$	cd/m^2
		FORCE and PRESSURE or STRESS		
lbf	poundforce	4.45	newtons	N
lbf/in^2	poundforce per square inch	6.89	kilopascals	kPa

APPROXIMATE CONVERSIONS FROM SI UNITS

Symbol	When You Know	Multiply By	To Find	Symbol
		LENGTH		
mm	millimeters	0.039	inches	in
m	meters	3.28	feet	ft
m	meters	1.09	yards	yd
km	kilometers	0.621	miles	mi
		AREA		
mm^2	square millimeters	0.0016	square inches	in^2
m^2	square meters	10.764	square feet	ft^2
m^2	square meters	1.195	square yards	yd^2
ha	hectares	2.47	acres	ac
km^2	square kilometers	0.386	square miles	mi^2
		VOLUME		
mL	milliliters	0.034	fluid ounces	fl oz
L	liters	0.264	gallons	gal
m^3	cubic meters	35.314	cubic feet	ft^3
m^3	cubic meters	1.307	cubic yards	yd^3
		MASS		
g	grams	0.035	ounces	oz
kg	kilograms	2.202	pounds	lb
Mg (or "t")	megagrams (or "metric ton")	1.103	short tons (2000 lb)	T
		TEMPERATURE (exact degrees)		
^oC	Celsius	1.8C+32	Fahrenheit	^oF
		ILLUMINATION		
lx	lux	0.0929	foot-candles	fc
cd/m^2	$candela/m^2$	0.2919	foot-Lamberts	fl
		FORCE and PRESSURE or STRESS		
N	newtons	0.225	poundforce	lbf
kPa	kilopascals	0.145	poundforce per square inch	lbf/in^2

*SI is the symbol for the International System of Units. Appropriate rounding should be made to comply with Section 4 of ASTM E380.
(Revised March 2003)

TABLE OF CONTENTS

LIST OF FIGURES

LIST OF TABLES

LIST OF ABBREVIATIONS

AASHTO	American Association of State Highway and Transportation Officials
FHWA	Federal Highway Administration
LRFD	load and resistance factor design
MPC	multi-point constraint
NSBA	National Steel Bridge Alliance
PEEQ	plastic strain equivalent
SCOBS	Subcommittee on Bridges and Structures
SRSS	square root sum of the squares

INTRODUCTION

The American Association of State Highway Officials and later the American Association of State Highway and Transportation Officials (AASHTO) specifications have required for many years that all steel splices and connections be designed for the average of calculated stress and strength of the member but not less than 75 percent of the strength of the member. This approach is straightforward when applied to axial truss members where the stress is equal in the various components of the member. However, such an approach does have its disadvantages. For example, application of this approach to a composite steel girder is generally more complex because the stresses in the flanges are not equal, and the distribution of the stress in the web is a function of the loads applied to the composite and noncomposite sections. In most designs of steel splices and connections, member strength controls the design because the designer usually intentionally places the splice in a low-moment region near the point of dead load inflection. The present traditional method for designing bolted splices in these regions uses a combination of designing for 75 percent of the strength of each flange at a minimum and then designing the web for a design moment determined based on the corresponding design stress in the flange with the largest design stress. The resulting connection design is tedious and can result in a large number of bolts in the web connection.

Experimental research by Ibrahim at the University of Texas showed that a simpler method of design produced a connection with adequate design capacity.[(1)] Rather than trying to proportion the primary bending moment to flanges and web, this method suggests decoupling the design so the flanges resist the primary bending moment and the web resists shear force. An ad hoc group consisting of representatives from AASHTO, steel bridge design consultants, a steel bridge fabricator, and representatives from the Federal Highway Administration (FHWA) was formed in 2015 to implement the findings of Ibrahim and develop a simpler design method that could be proposed to AASHTO.[(1)] The simpler method included designing the bolted flange and web splice connections for 100 percent of the individual capacities of the flange and web; the flange splices were designed for the yield capacity of the flange, and the web splices were designed for the shear capacity of the web. Therefore, the method satisfied the AASHTO design criteria because the web and flange splices have strengths equal to the design strengths of the respective components. No further check of the shear capacity of the connection was required; however, additional forces in the web connection may need to be considered if the flanges are not adequate to develop the factored design moment.

To better understand the ramifications of implementing the simpler design method, the ad hoc group worked with 11 different continuous span arrangements and 2 different girder spacings and compared the bolted splice designs using the 2 design philosophies. The ad hoc group felt detailed finite element modeling on the most extreme outlier connection that had the largest disparity in the required number of bolts would lend credit to the simpler design philosophy. The work reported herein only covers the finite element modeling effort in support of the ad hoc group recommendations.

A ballot to revise the language covering splice design in the *AASHTO Load and Resistance Factor Design (LRFD) Bridge Design Specifications* was presented to the AASHTO Subcommittee on Bridges and Structures (SCOBS) in June 2016.[(2)] A concurrent ballot was

passed at the 2016 SCOBS meeting that revised the shear strength of high-strength bolts to align with the latest specification of the Research Council of Structural Connections.[3] The revised shear strength of high-strength bolts was not originally considered when performing the finite element analysis for the ad hoc group. All references made throughout this report to the current design method are those published in the seventh edition of the *AASHTO LRFD Bridge Design Specifications*; references to the new method refer to those that appear in the eighth edition of the *AASHTO LRFD Bridge Design Specifications*.[2,4]

EXAMPLE SPLICE CONNECTION

The outlier bolted splice was from a three-span continuous girder with 234-ft long back spans, a 300-ft long center span, and a girder spacing of 12 ft. The girder was designed using ASTM A709 grade 50 steel and $^{7}/_{8}$-inch-diameter ASTM A325 bolts.[5,6] An 8-inch concrete deck was used in the design. At the spliced section, the girder flange and web plates had dimensions as shown in table 1.

Table 1. Example girder plate dimensions.

Side of Splice	Top Flange Width (inches)	Top Flange Thickness (inches)	Web Depth (inches)	Web Thickness (inches)	Bottom Flange Width (inches)	Bottom Flange Thickness (inches)
Left	19	1	109	0.75	19	1
Right	22	2	109	0.75	22	2

A design program was used to iteratively proportion the girder and select the optimum location for the splice, which was 64 ft away from the first interior support in the first span. The unfactored moments required for AASHTO design at the splice location from the continuous girder analysis are as shown in table 2. However, the factored shear demand was only 853 kip based on an assumed shear panel dimension ratio (d_o/D) of 3.0 used in the program. The author herein was most interested in pushing the demand as far as possible for the connection, and the factored shear force was reevaluated for a d_o/D of 2.0, thus resulting in a factored shear of 1,312 kip.

Table 2. Design forces in splice.

Design Force Component	Unit	Magnitude
M_{DC1}	kip-ft	-333.4 (steel only)
M_{DC}	kip-ft	-1,230.6 (concrete deck)
M_{DC2}	kip-ft	-242.3
M_{DW}	kip-ft	-315.3
M_{pos_LL+IM}	kip-ft	5,626.9
M_{neg_LL+IM}	kip-ft	-7,116.9
V_u	kip	1,312

Comparison of Splice Designs

This report does not delve into the detailed calculations of each design method; only the end result is discussed herein. A side-by-side comparison of the current and new design methods is shown in 0 and 0. The design methods resulted in no difference between the number of bolts in the flange splices; however, there was a significant difference between the required bolts for the web splices, with the new method requiring only two rows of bolts at a much larger spacing. Overall, the new method required 104 fewer bolts than the current method.

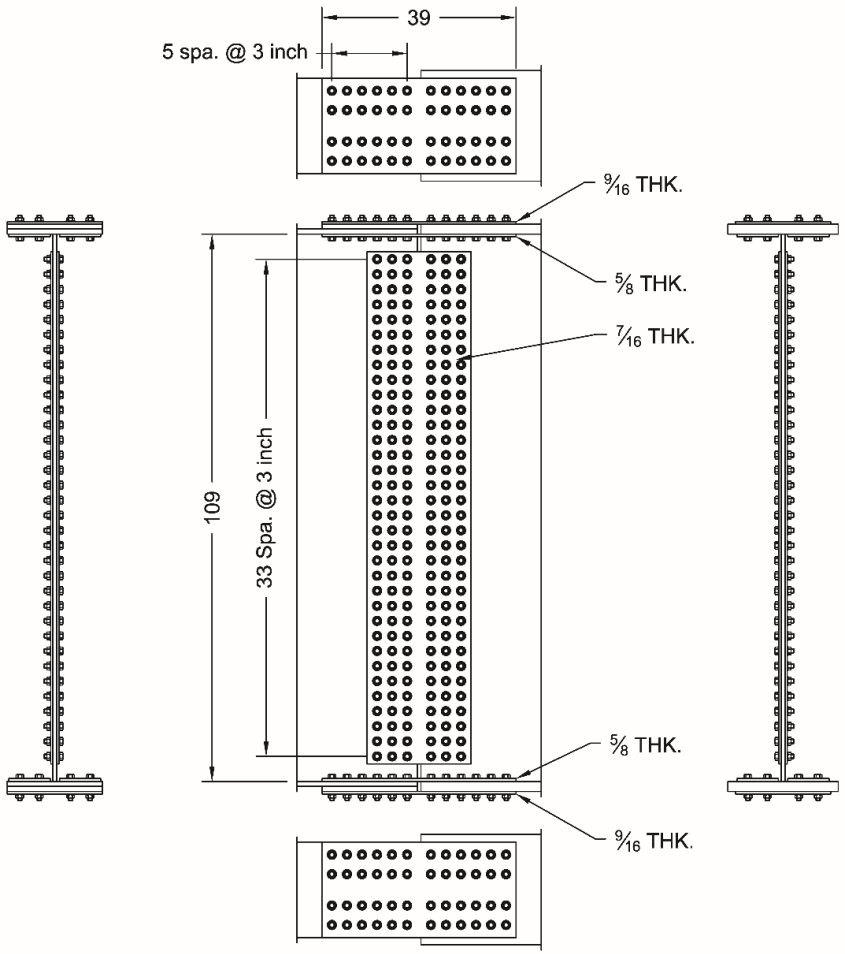

Source: FHWA

Figure 1. Illustration. Detailing of the field splice using current method.

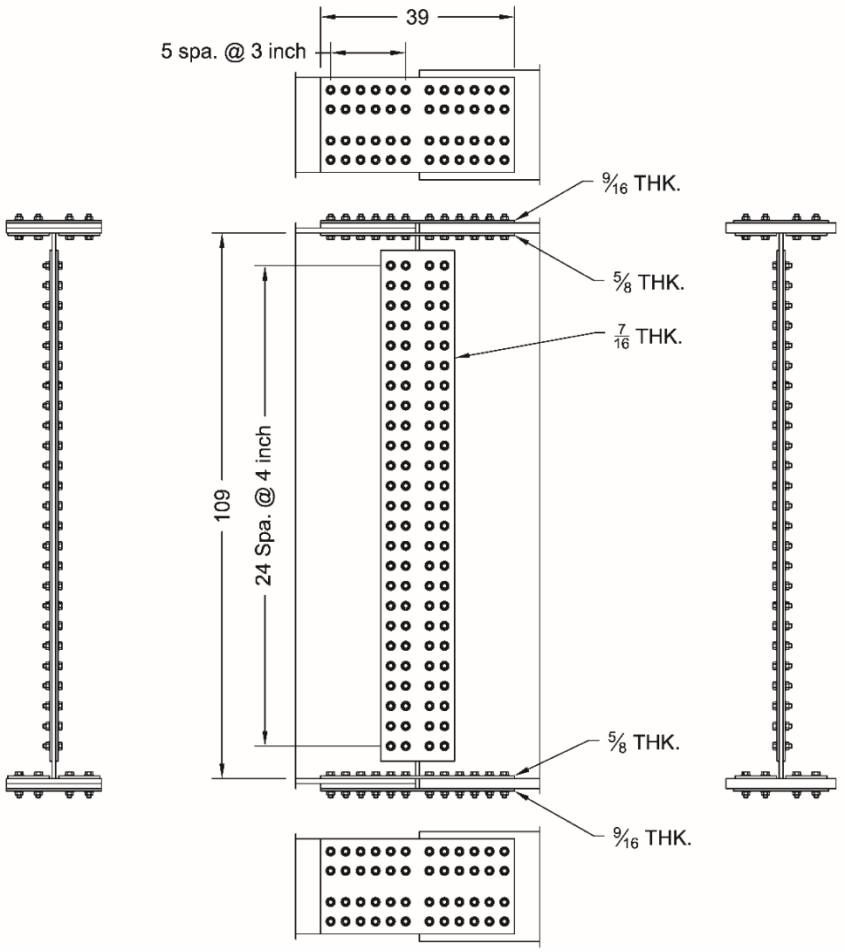

Source: FHWA

Figure 2. Illustration. Detailing of the field splice using new method.

MODEL DESCRIPTION

The two connection details shown in 0 and 0 were modeled with Abaqus®
version 6.11-1 to explore the limit states for each of the connections.[7] This chapter discusses the details of how the connections were modeled and the various inputs that were used within the model.

LOADING SCENARIOS

A total of 5 load/boundary condition scenarios were investigated for each of the connection designs (i.e., a total of 10 models). The five scenarios were (1) pure positive moment, (2) pure negative moment, (3) high shear, (4) combined shear and positive moment, and (5) combined shear and negative moment. The first scenario was a displacement controlled analysis of pure positive moment, as illustrated in 0, with a fixed rotation of 0.01 radians at the left support. The deck was present for this first scenario.

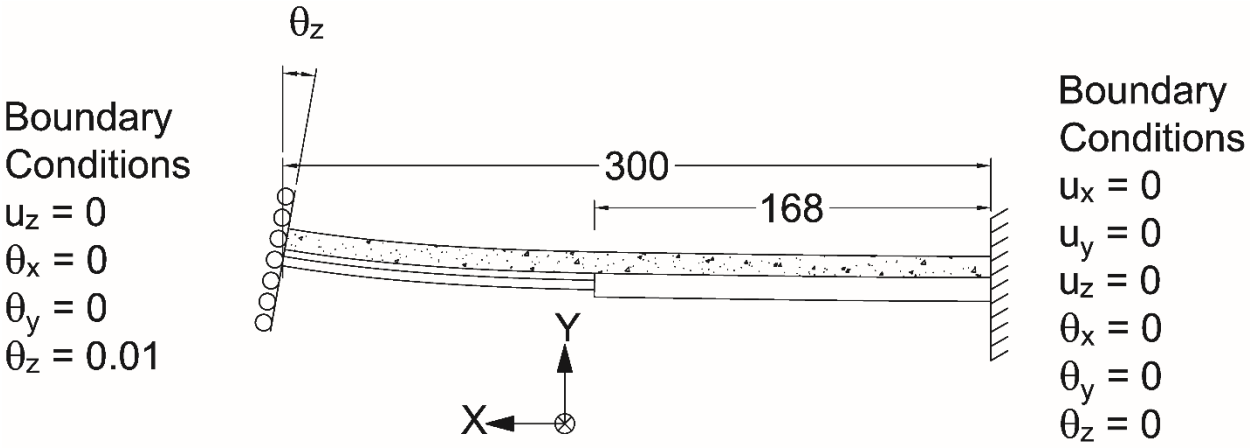

Source: FHWA

Figure 3**. Illustration. Boundary conditions and loading for constant positive moment loading.**

Where:

u_x = translation in X-direction.
u_y = translation in Y-direction
u_z = translation in Z-direction
θ_x = rotation about X-axis.
θ_y = rotation about Y-axis.
θ_z = rotation about Z-axis.

The second scenario was a displacement controlled analysis of pure negative moment, as illustrated in 0, with a fixed rotation of -0.015 radians at the left support. The deck was not present in the pure negative moment scenario.

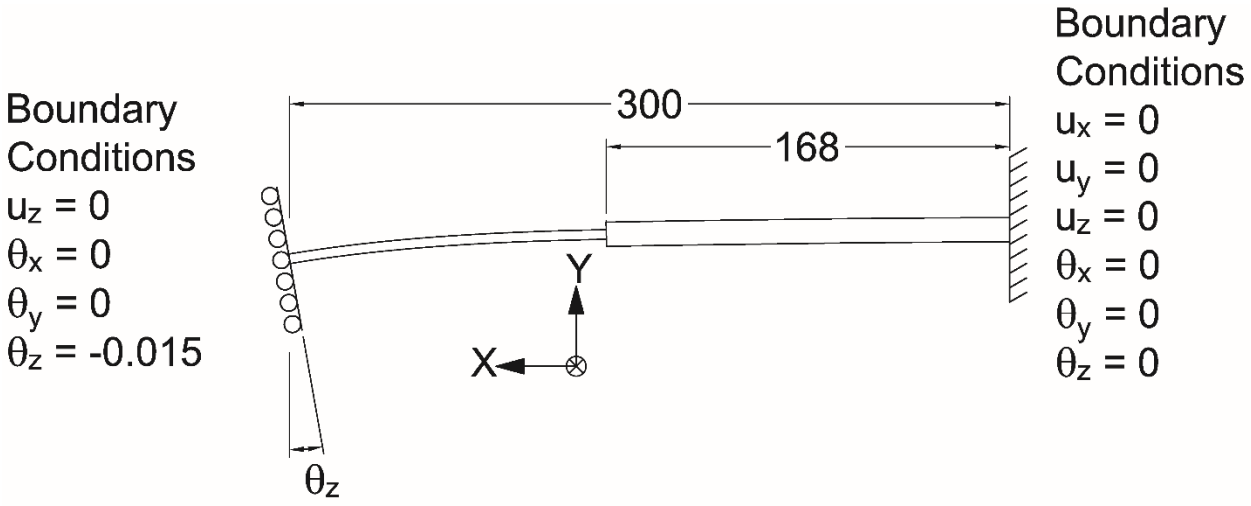

Source: FHWA

Figure 4. Illustration. Boundary conditions and loading for constant negative moment loading.

The third scenario was the imposition of high shear with minimal moment in the splice, as shown in 0. A fixed-fixed beam with a 2.5-inch support settlement analogy was used, and this scenario forced the splice to be located 132 inches from the right support, which is the theoretical inflection point. Because the internal and external moments at the supports in the high shear scenario eventually exceeded the yield moment of the girder sections, the ends were modeled with elastic elements, as shown in the figure. It is also important to note that the deck was not present in the high shear scenario. The first three scenarios were displacement-controlled analyses because the ultimate limit state was being explored, which could be readily compared to the design demand.

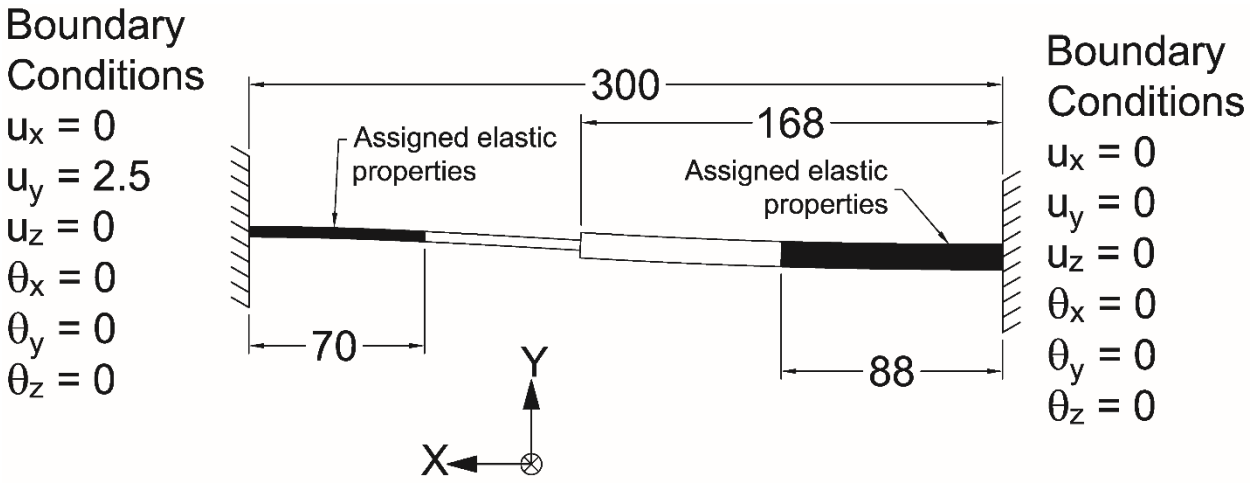

Source: FHWA

Figure 5. Illustration. Boundary conditions and loading for high shear loading.

The fourth scenario was a load-controlled analysis that investigated the model under a proportional application of the factored positive moment and shear ($M_{u,pos}$ = 8,016 kip-ft and

V_u = 1,312 kip, respectively). In this scenario, a cantilevered beam, where the right support was fixed, was used, as shown in 0. Loads were applied to the free end, which created a constant shear along the entire model, and the moments applied at the left support were chosen so that the design moment was imposed at the location of the splice. However, loads at the free end were also amplified by a factor of two so that the analysis could continue beyond the design loading. The deck was present for this scenario. Because the internal moment at the right support eventually exceeded the yield moment of the girder sections, that end was modeled with elastic elements as shown in the figure.

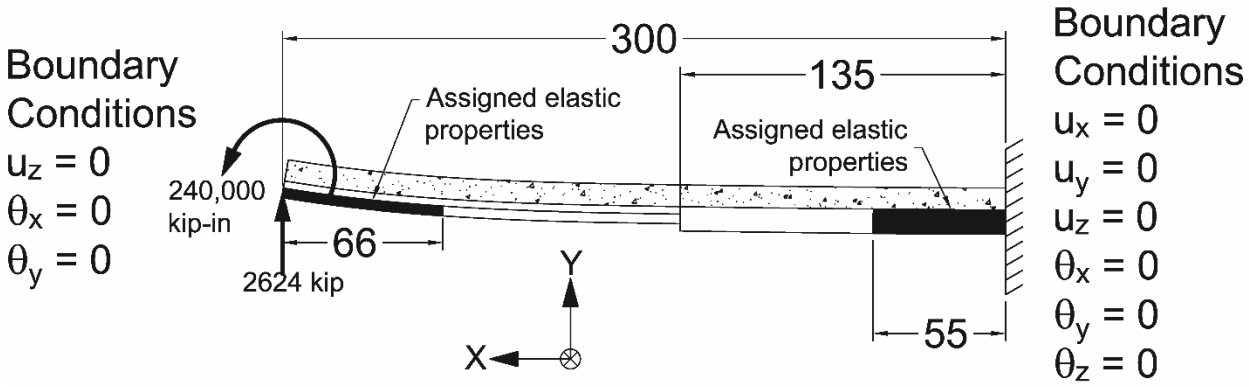

Source: FHWA

Figure 6. Illustration. Boundary conditions and loading for positive moment proportional loading.

The fifth scenario was a load-controlled analysis that investigated the model under a proportional application of the factored negative moment loading in the presence of the design shear ($M_{u,neg}$ = 15,185 kip-ft and V_u = 1,312 kip, respectively). The same philosophy of loading was used as in the positive moment proportional loading scenario; however, the length of the overall model was reduced, and the loads had to change. The scenario is fully shown in 0 and also used elastic elements near the fixed support.

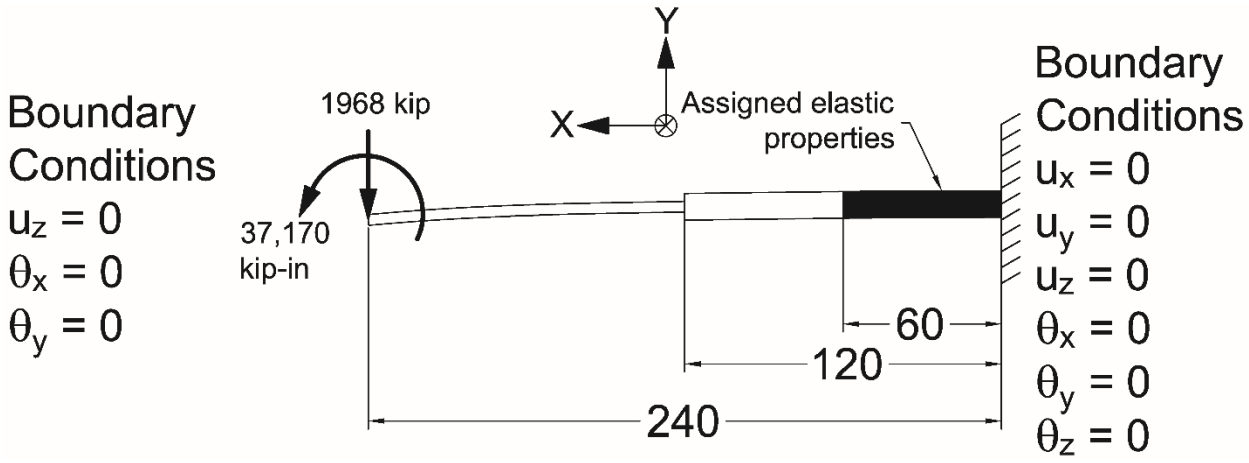

Source: FHWA

Figure 7. Illustration. Boundary conditions and loading for negative moment proportional loading.

GEOMETRIC AND MATERIAL DESCRIPTION

The 10 models were built within the preprocessor in accordance with the splice detailing shown in 0 and 0. The models were built mostly with three-dimensional shell elements for all of the plate elements, but the bolts were modeled with fastener elements described in the Fastener Properties section in this chapter.

Each end of the model was kinematically constrained to a reference point located at the centroid of the girder on each end. This is shown in 0 by the lines emanating from the reference point to the entire cross section of the girder and the concrete deck. A multi-point constraint (MPC) was used to enforce the kinematic constraint; the Beam MPC was used to enforce all six degrees of freedom to be the same on the cross section as the reference point. This essentially forced plane sections to remain plane and normal. This offered the advantage that all loads and boundary conditions could be specified on just the reference point and evenly distributed to the entire cross section. For the scenarios in which the deck was not present, the MPC only constrained the portions of the model representing the girder.

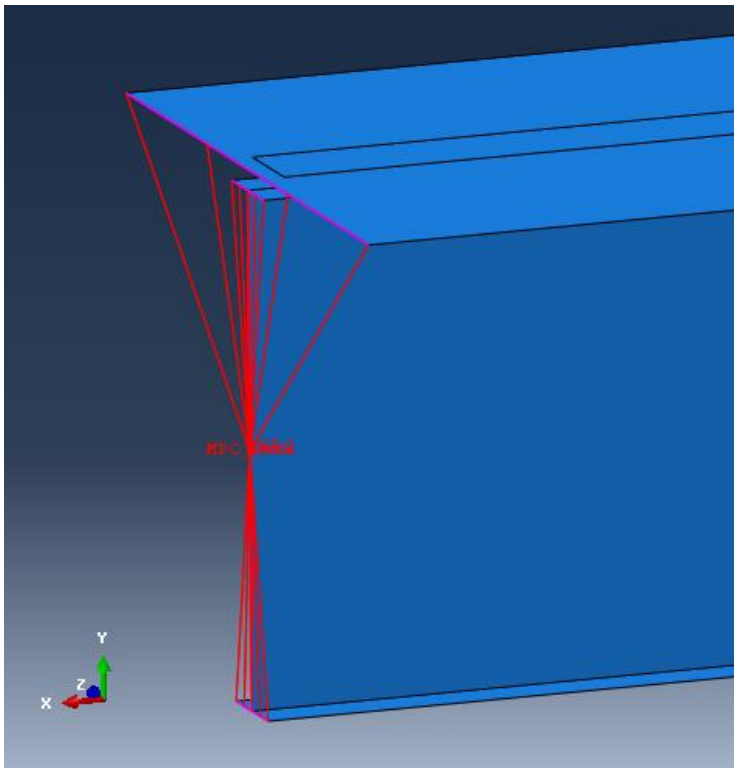

Source: FHWA
Note: Only the left side is shown in the figure.

Figure 8. Illustration. Example of end kinematic constraint.

When the deck was present for some scenarios, it was modeled with elastic shell elements and assigned a thickness of 8 inches, E = 3,600 ksi, and ν = 0.2. The deck was 12 ft wide (because the girder spacing was specified as 12 ft). The deck was attached to the girders with tie constraints. This is best shown in 0, where the circles represent potential shear connector locations (four across the flange and 6-inch pitch). Any nodes within the circles are the master

nodes in the constraint, and the three translational degrees of freedom are constrained between the master nodes and the slave nodes within the purple rectangle on the deck.

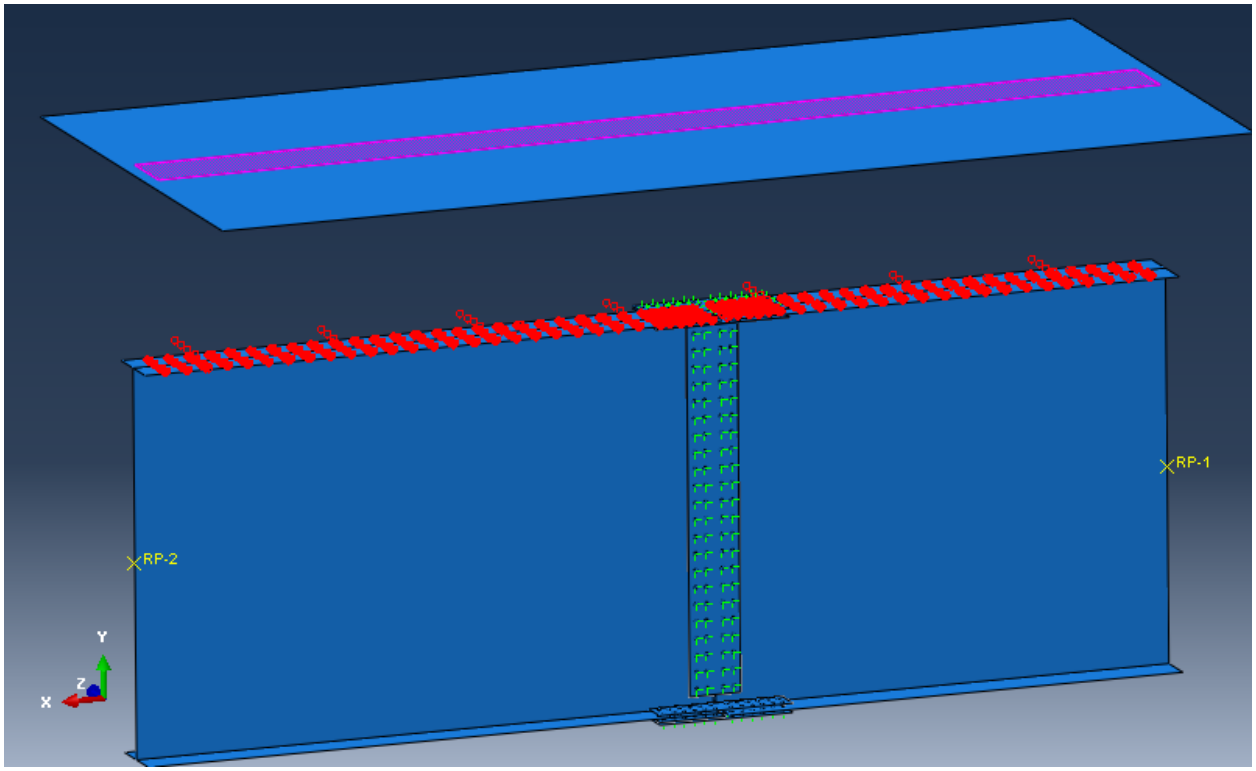

Source: FHWA
Note: The deck is overly offset from the girder for illustrative purposes only.

Figure 9. Illustration. Example of constraint between deck and girders.

All steel was given elastic properties of E = 29,000 ksi and ν = 0.3. For areas of the girder that were not specified as "only elastic," they were assigned additional nonlinear material properties with an initial assumed yield stress of 50 ksi. After yielding, the steel had a strain hardening relationship as shown in 0. This model was based on real coupon data tested by FHWA but scaled so that the yield stress was ideally 50 ksi and the tensile strength was ideally 65 ksi, which are the design values for ASTM A709 Grade 50 steel.[(5)]

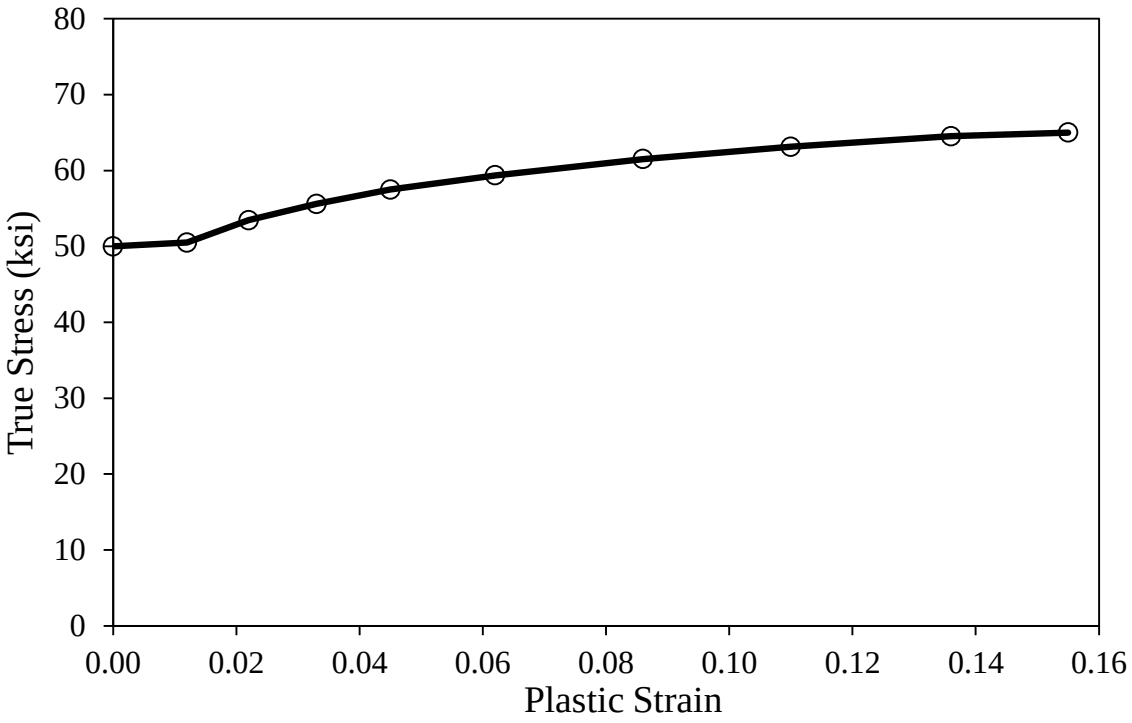

Source: FHWA

Figure 10**. Graph. Nonlinear material properties for steel plate elements.**

Finally, preliminary model runs experienced nonlinear geometric effects through certain buckling modes (i.e., web buckling). Because this study was trying to identify strength, not stability limit states, the final analysis results reported herein were conducted with the nonlinear geometry turned off.

Fastener Properties

The $^{7}/_{8}$-inch ASTM A325 bolts were modeled with discrete connector elements.[(6)] These are point-based elements that impose kinematic relationships between surfaces, and the connector can be assigned nonlinear properties. 0 shows an example of one connector element passing from top to bottom through an inner flange splice plate, the lower girder flange, fill plate, and outer splice plate. The "Cartesian + Align" is the combined Abaqus® connector element used to represent bolts. Furthermore, the connector element has the benefit of being applied over an influence area in each ply of the splice. In this case, an influence radius of 0.75 inch was specified, which ties the nodes within this radius on each surface to the other surfaces with the designated fastener properties. This somewhat replicates how a real nut and washer would spread load.

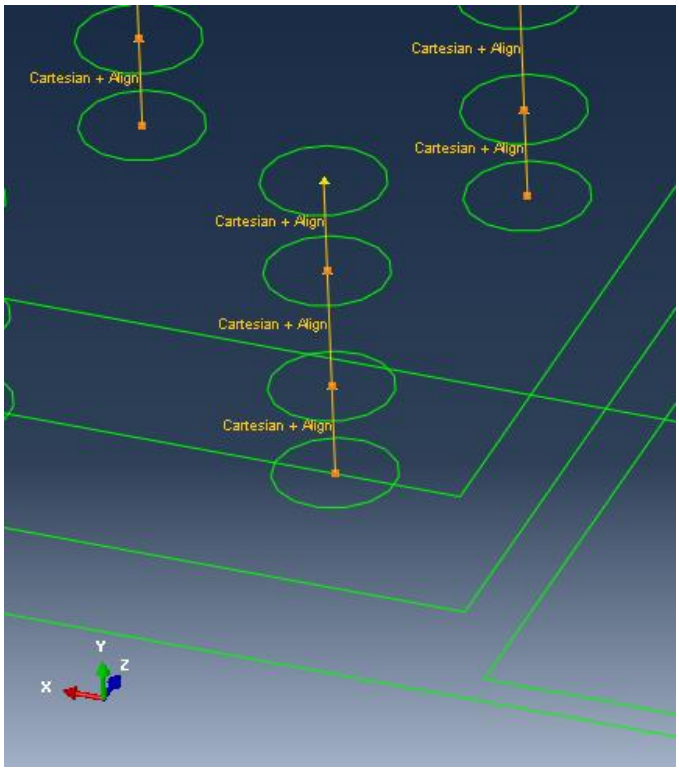

Source: FHWA

Figure 11**. Illustration. Example connector element at lower flange of left girder with the connector passing through the inner splice, flange, fill, and outer splice plates.**

To determine the material properties of the actual connector elements, a quarter space model of a butt joint with a single pin was modeled using solid elements where the pin represented a loose bolt. A representation of this model is shown in 0. The steel plate was assigned the nonlinear material properties shown in 0, and the pin was assigned the nonlinear material properties shown in 0. Post-processing was done by outputting the *z*-displacement of the two red dots shown in 0 and plotting that displacement against the applied shear force. Because the girder splice models used shell elements representing mid-plane thickness, the red dots correspond to the displacement at the mid-thickness of the plates being joined. In the model shown, a $^{9}/_{16}$-inch-thick plate was joined to a 2-inch-thick plate. The actual plot of the assumed fastener shear force and displacement values for the refined fastener model is shown in 0. It was found that an elastic stiffness of 4,000 kip/inches was appropriate based on the solid modeling. This is not shown in the plot because the plastic deformation is separated from the elastic deformation.

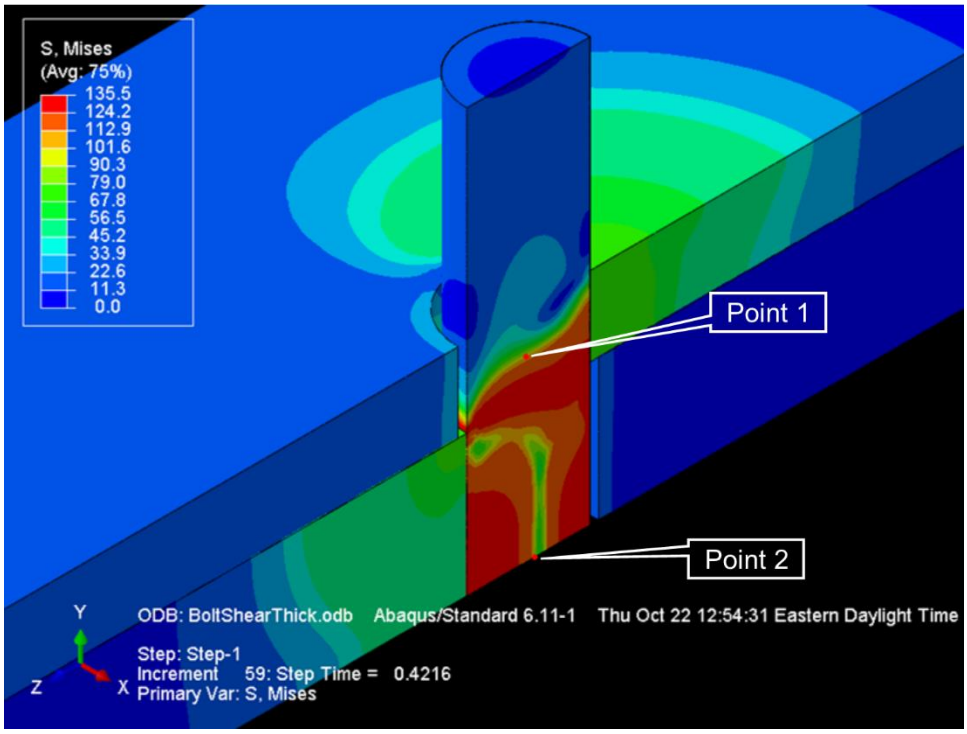

Source: FHWA

Figure 12**. Illustration. Quarter space model of butt joint for fastener characterization.**

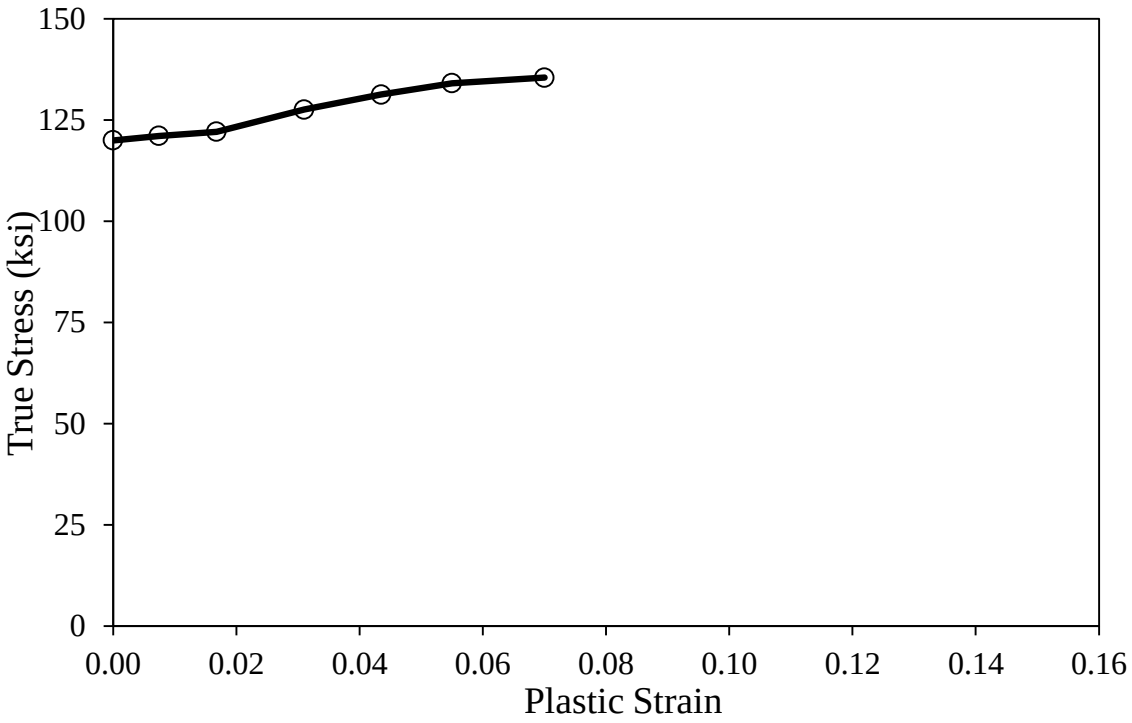

Source: FHWA

Figure 13**. Graph. Nonlinear material properties assigned to pin.**

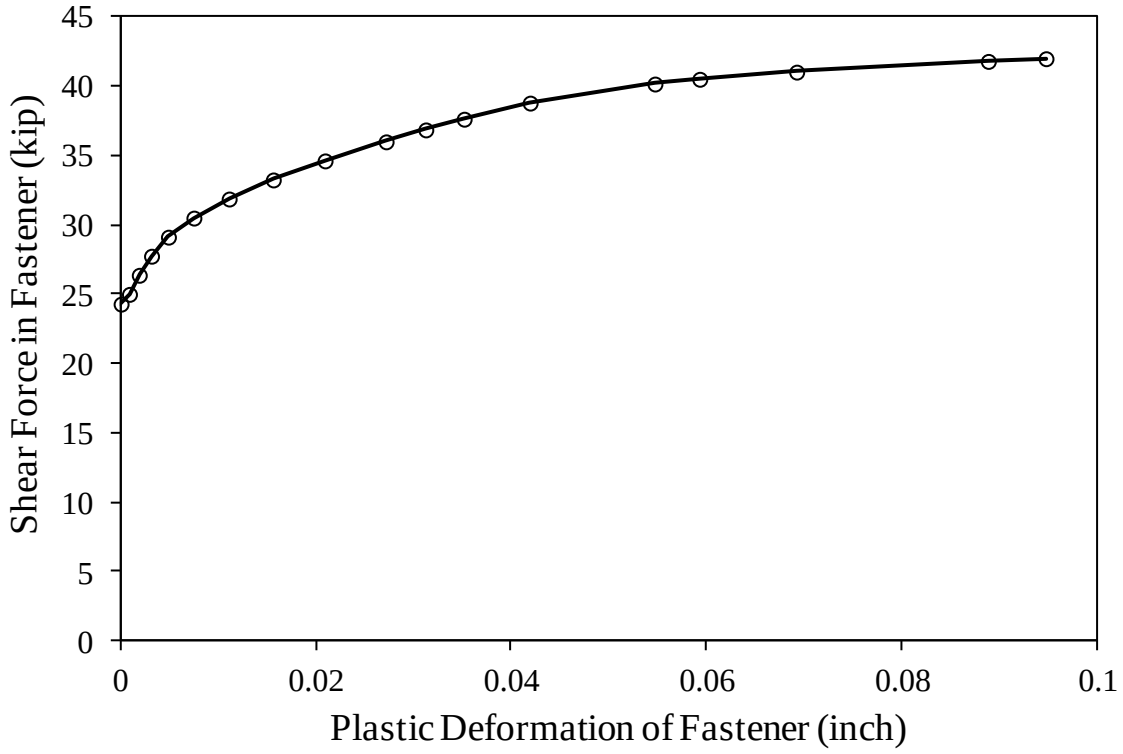

Source: FHWA

Figure 14**. Graph. Shear force versus plastic deformation of fastener elements.**

The shear forces from the solid element model were ultimately scaled to represent the actual design strength of a $^{7}/_{8}$-inch ASTM A325 bolt. In single shear, this bolt could have an ultimate shear resistance of $0.58(120)(\pi/4)(0.875^2) = 41.9$ kip. Therefore, the maximum shear force in the bolt was assumed to be 42 kip. This assumes that the connection length effect did not have to be included in this strength calculation because the model should capture any shear lag effects. Assuming an ultimate shear strength of 42 kip meant that the yield of the bolt was 24.3 kip according to the solid model output. The ultimate plastic deformation of the bolt was approximately 0.09 inch, which was considered reasonable compared to the bolt shear results of Moore, Rassati, and Swanson.[8] Finally, the failure criterion for the fastener elements was based on a circular yield surface with isotropic hardening. That is, an individual fastener element had two local directions of in-plane shear, and the hardening model shown in 0 was enforced to the square root sum of the squares (SRSS) of the two in-plane shear forces. The axial stiffness of the fastener was considered purely elastic with a stiffness of 10,000 kip/inches and uncoupled from the shear stiffness.

Other Considerations

Modeling the spliced girder with three-dimensional shells and connecting them together with discrete line elements representing high-strength bolts did not fully capture the reality of a physical connection. Slip, bolt tension, and contact were not considered in the model, but rationale for their omission is provided in the following subsections.

Slip

Effectively, the way the fastener elements were defined meant that in a physical sense, each bolt was a perfect pin within a clearance hole, and the plates they connected together had no friction between them. In reality, bolts are installed in oversized holes, and, considering large bolt patterns, some bolts will initially be in bearing, and others may not. There is no good way to model the random variation in bolt hole clearance over a connection with hundreds of bolts. The models were used to investigate strength limit states, so the assumption being made relied on the inherent ductility of steel, and the shear forces on a bolt in a real connection eventually redistribute into the idealization seen in the model at the strength limit state.

Bolt Tension

The fastener definition did not consider that in bridge construction, bolts are fully tensioned. Therefore, no friction could develop between plies of the connection, and all force had to go through the bolts. In reality, there will be some load transfer through friction, so neglecting it should be a lower bound assumption. Additionally, at the strength limit state, it is doubtful whether frictional forces are prevalent.

Contact

The elements defining each ply of the connection had no contact interaction defined. The only thing maintaining separation of connection plies was the axial stiffness of the fastener elements. The ends of the left and right girder sections also did not have a contact interaction defined. Because the results were trying to define the distribution of bolt forces across the connection, contact was not believed to be highly influential.

RESULTS

This chapter presents the data from the five loading scenarios that were explored. For every loading scenario, the same data plots are shown in the same order as a means to provide easy context for how things change from one loading scenario to another. Additionally, every data plot shows a side-by-side output of the current and new design methods, with the size of the web splice plate being the identifying difference. For each scenario, contour plots are presented for the step that achieves the factored design forces, and, for a later step, that was either the last step or the step where the analysis could no longer converge to a solution. To assist in decoding the contour outputs, the following list defines the six types of stress/strain/force contours that are presented:

- **Mises stress**: Mises stress is a bulk measure of normal and shear stresses used to define failure, which, in this case, is yielding. Mises stress is always plotted from 0 to 50 ksi with a rainbow color palette. If the legend has a value higher than 50 ksi, then those areas with that color (if present) represent areas in the model where the Mises stress exceeds 50 ksi and is actively yielding.

- **Longitudinal stress**: Longitudinal stress is the Abaqus® S11 output, and, with the way the element local coordinate systems were defined, this represents the normal stress in the shell elements in the x-direction as defined in 0 through 0. Longitudinal stress is always plotted between -50 and 50 ksi with a rainbow color palette. If the legend has values greater than 50 ksi (if present) or less than -50 ksi (if present), then those represent areas where the longitudinal stress exceeds the yield.

- **Shear stress**: Shear stress is the Abaqus® S12 output, which represents the in-plane shear stress in the shell elements. With the way the element local coordinate systems were defined, this plots the xy-shear stress for the girder web and xz-shear stress for the girder flanges. Shear stress is always plotted between -29 and 29 ksi with a rainbow color palette because shear yield is approximately $0.58F_y$ = 29 ksi. If the legend has values greater than 29 ksi (if present) or less than -29 ksi (if present), then those represent areas where the shear stresses exceed the shear yield criteria.

- **Plastic strain equivalent (PEEQ)**: This is an Abaqus® term that represents a bulk strain measure output. Any area that is yielding will have a PEEQ value, and this value gives a sense for how far out that particular area is along the material failure model (shown in 0). The PEEQ plots, if shown, are always plotted from 0 to 0.05 with a rainbow color palette. Sometimes, for better resolution, a second PEEQ plot is provided with a smaller-scale legend.

- **Resultant bolt forces**: The connector elements used to represent bolts have the capability to output six internal force components within the fastener. For this analysis, the only two of interest are the two in-plane shear components (what Abaqus® calls CTF1 and CTF2) at the shear interface between the plates. The resultant force is the SRSS of CTF1 and CTF2 and is referred to as "CTF_SRSS." The post-processor plots this resultant force as a colored point for each element between shear planes. The forces are always plotted

from 0 to 42 kip because 42 kip is the unfactored shear strength of the $^{7}/_{8}$-inch ASTM A325 bolt.

- **Web splice bolt shear vectors**: These plots are generated outside of the post-processor but are effectively plotting CTF1 and CTF2 at the same time for just one shear plane of the web bolts. For each bolt location, a colored vector is shown where the length of that vector is scaled to CTF_SRSS, but the direction of the vector gives a sense for the ratio between the CTF1 and CTF2 forces. The vectors are scaled in length and assigned a different color based on their CTF_SRSS magnitude using a rainbow color palette.

PURE POSITIVE MOMENT

0 shows the moment versus rotation plot for the left support. The current design method results are plotted with circle data points, and the new design method results plotted with square data points. The overall response of the two models does not differ much between the two methods other than a slight reduction in moment strength after yielding. Contour plots present the results for the step with approximately M_u = 8,016 kip-ft applied (see 0 through 0) and for the last step in each analysis (see 0 through 0).

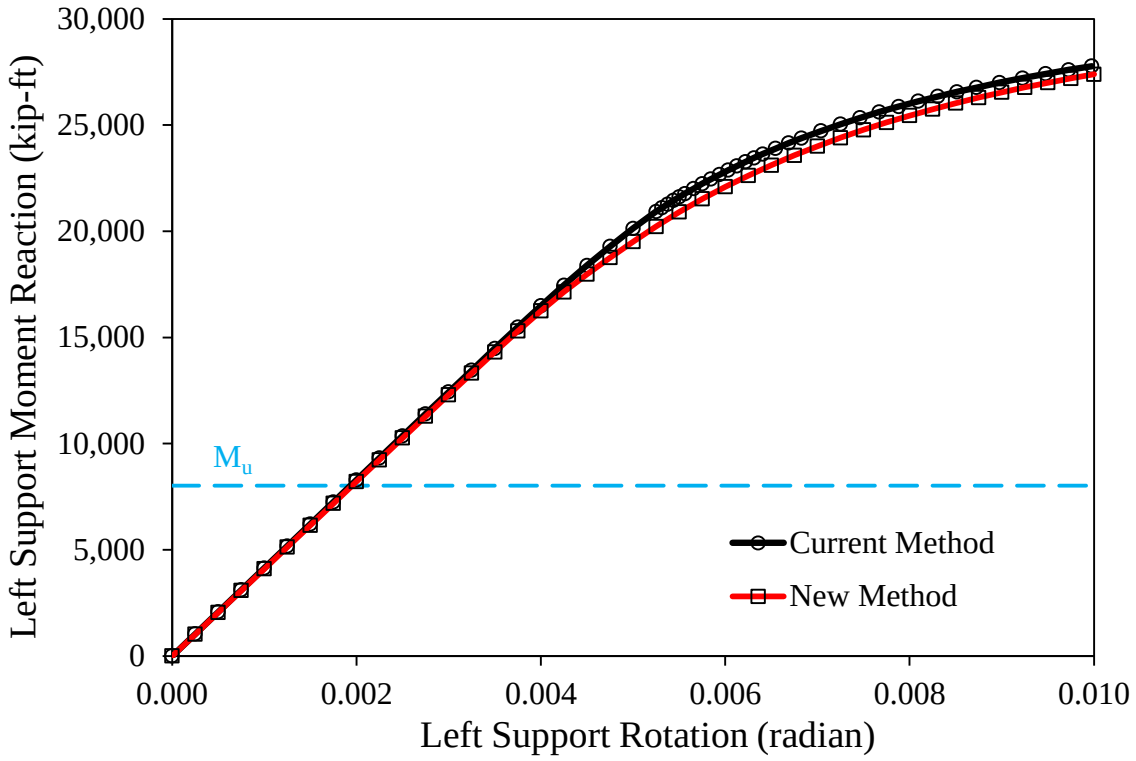

Source: FHWA

Figure 15. Graph. Moment versus rotation of the left support under pure positive moment for the splice designed using the current and new methods.

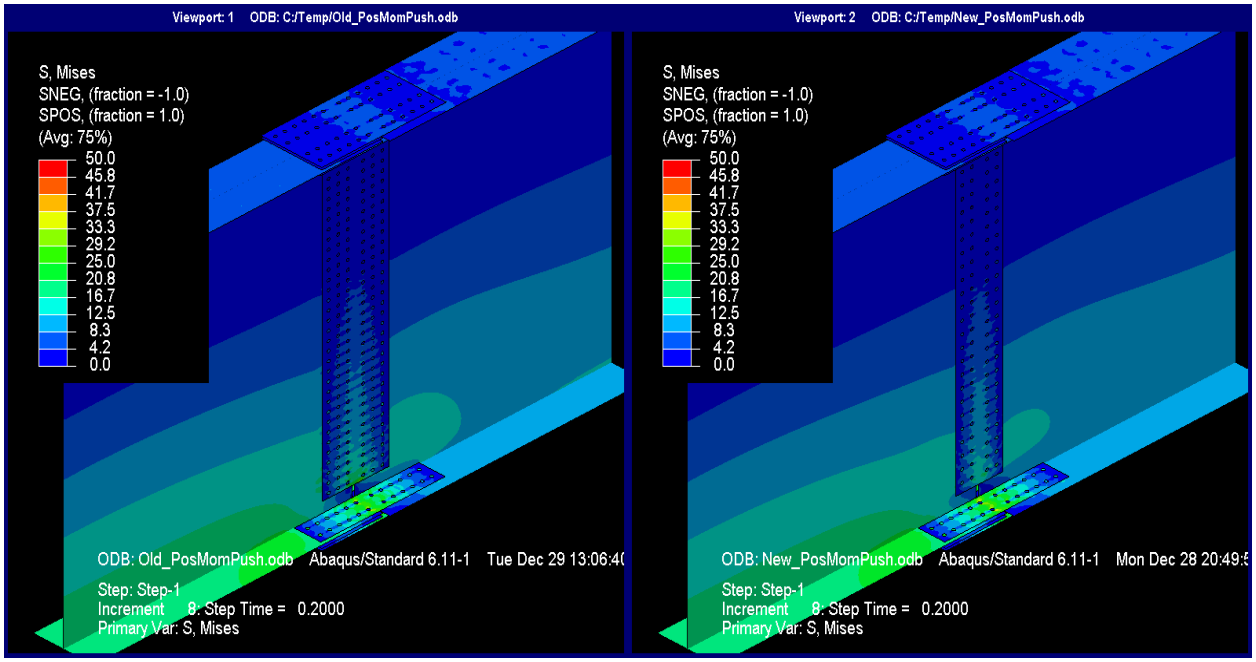

Source: FHWA

Figure 16**. Illustration. Mises stresses at pure positive M_u (deck not shown for clarity).**

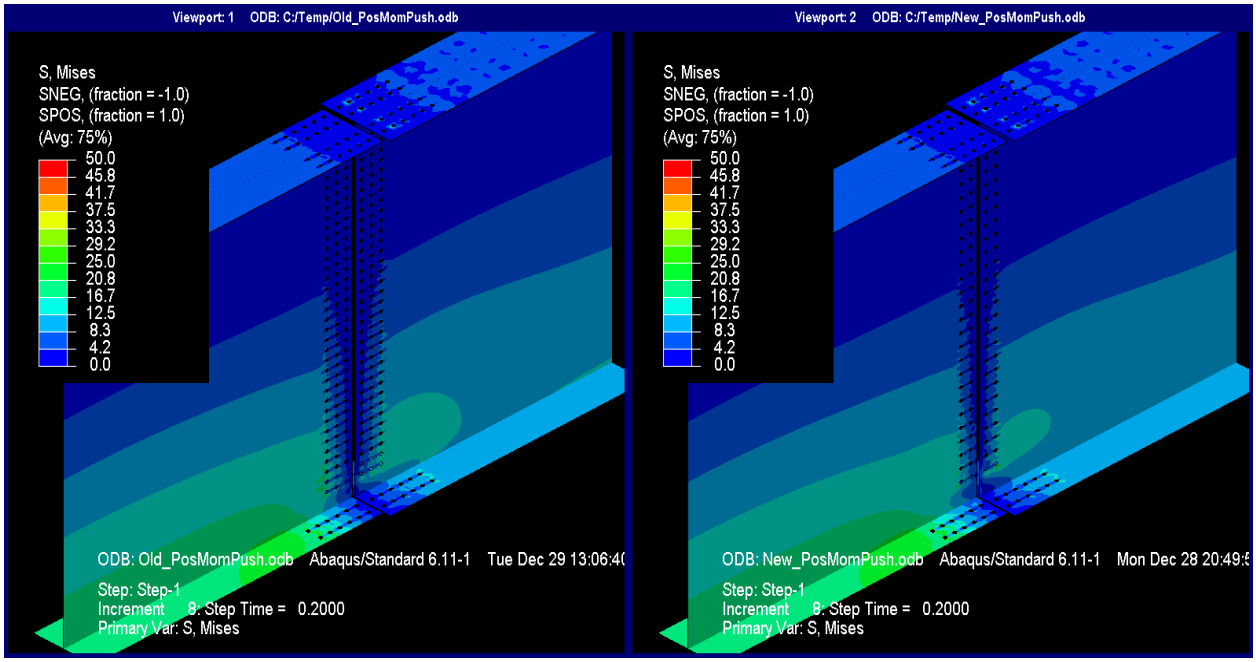

Source: FHWA

Figure 17**. Illustration. Mises stresses at pure positive M_u (splice plates and deck not shown for clarity).**

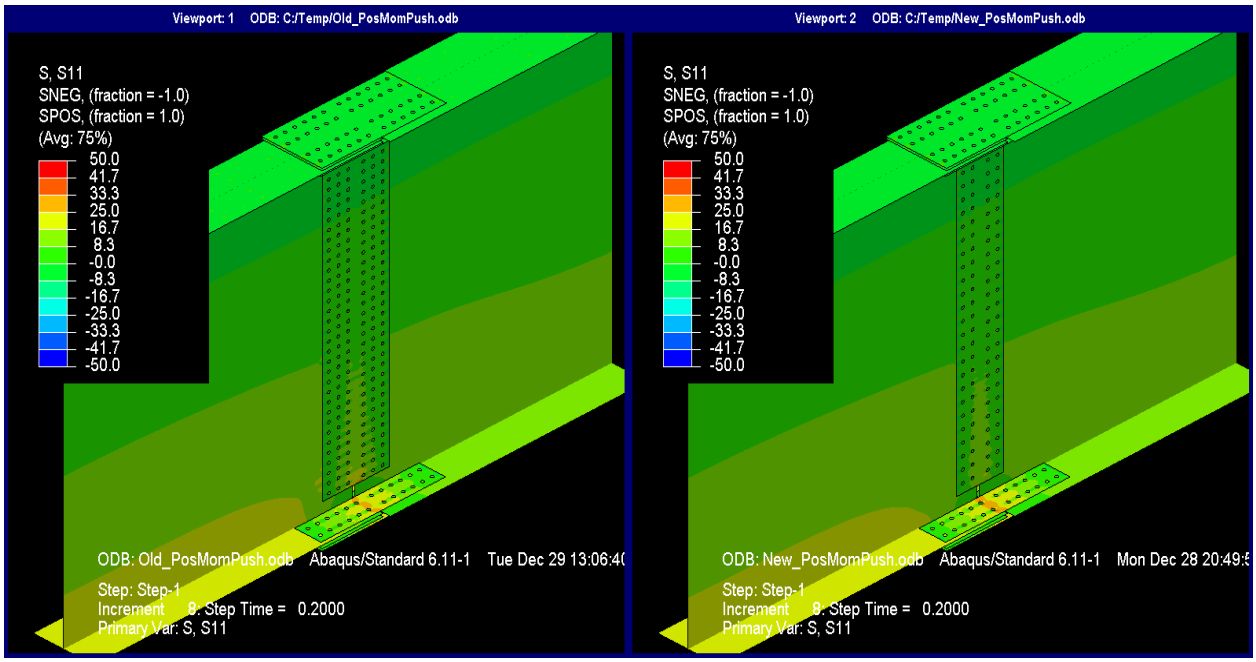

Source: FHWA

Figure 18**. Illustration. Longitudinal stresses at pure positive M_u (deck not shown for clarity).**

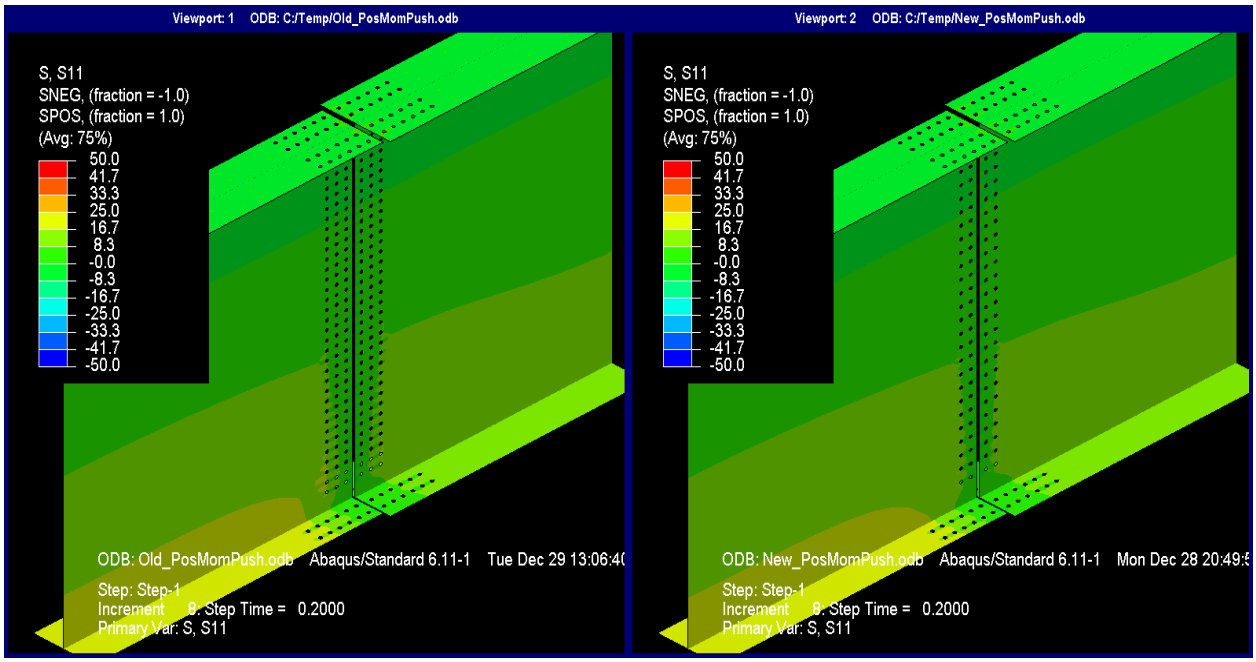

Source: FHWA

Figure 19**. Illustration. Longitudinal stresses at pure positive M_u (splice plates and deck not shown for clarity).**

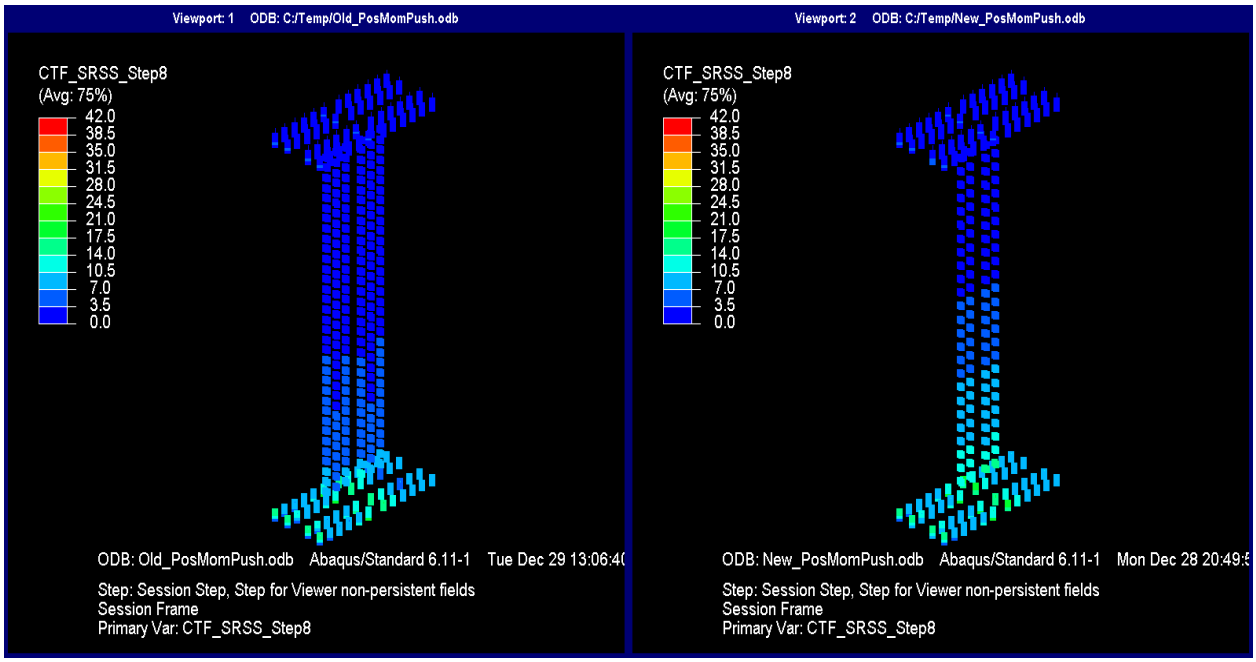

Source: FHWA

Figure 20**. Illustration. Resultant forces on bolt shear planes at pure positive M_u.**

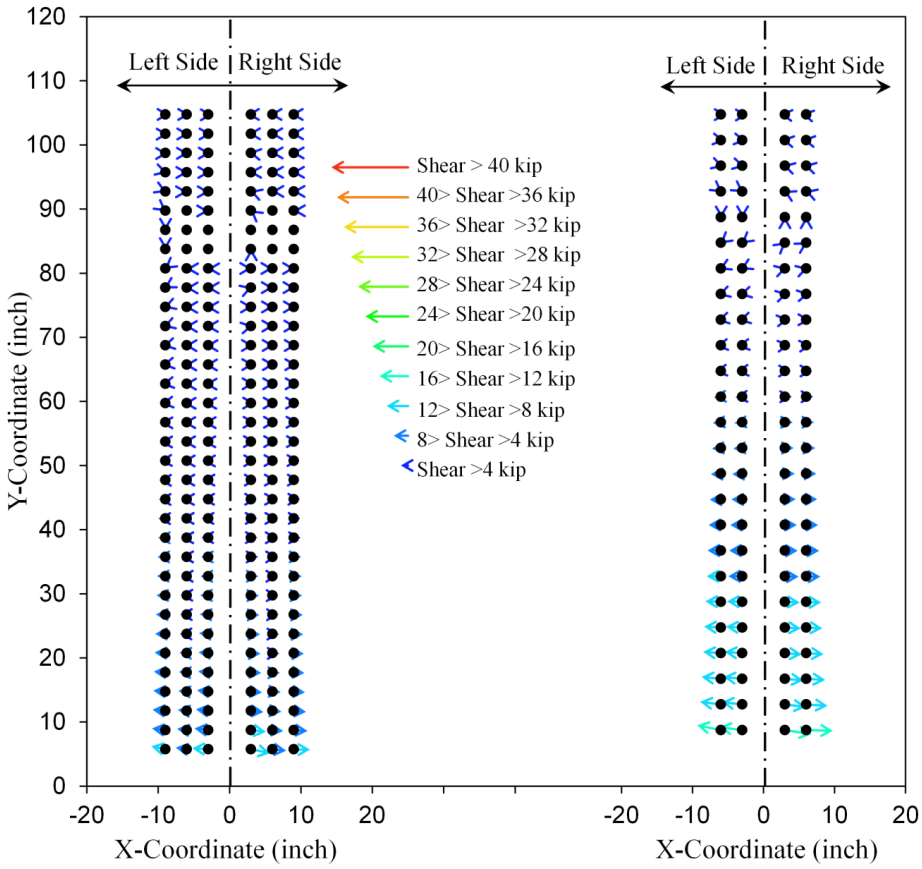

Source: FHWA

Figure 21**. Graph. Web splice bolt shear vectors at pure positive M_u.**

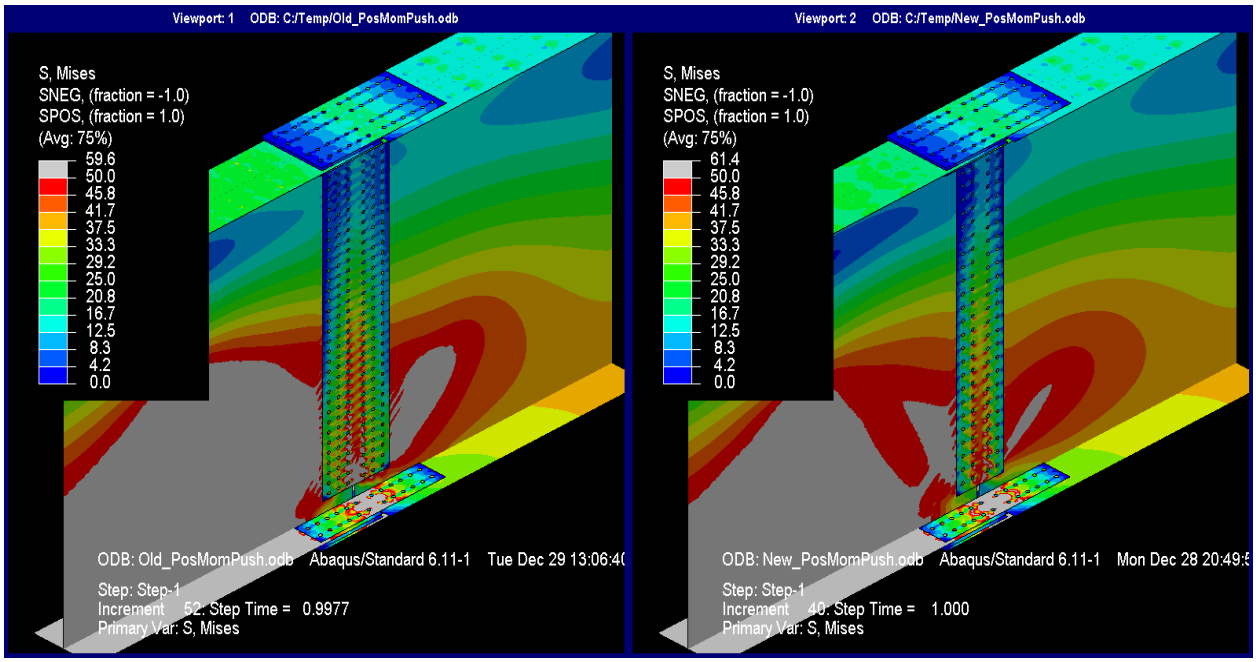

Source: FHWA

Figure 22. Illustration. Mises stresses at last step of pure positive moment (deck not shown for clarity).

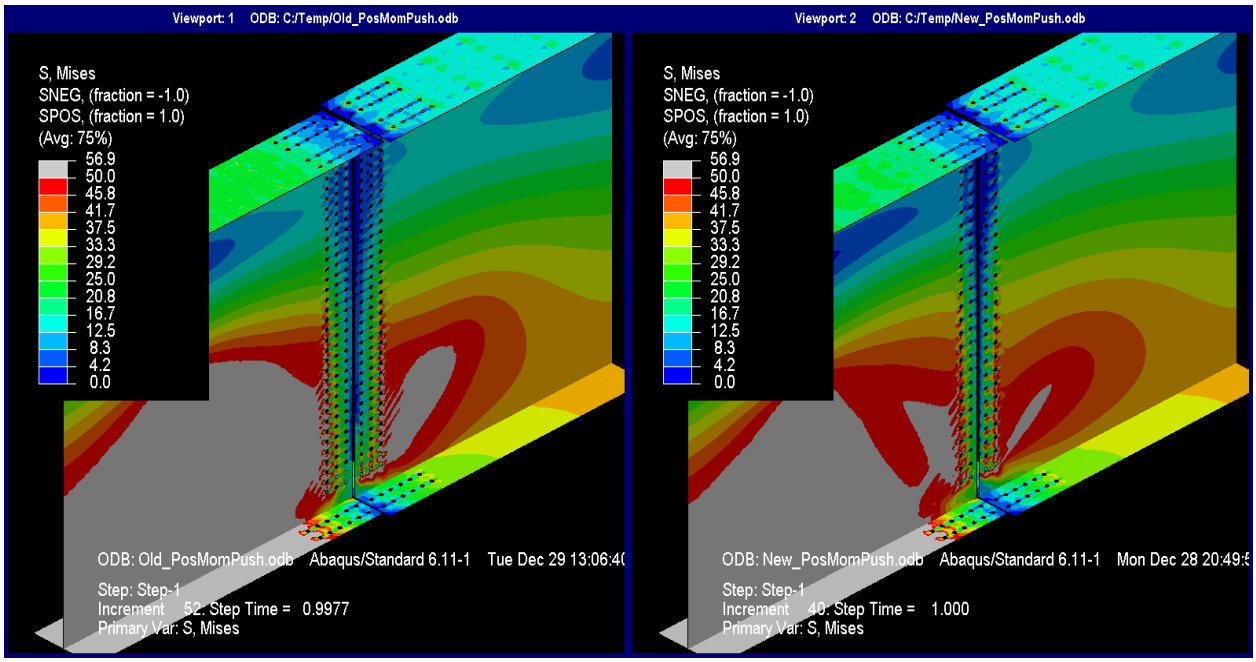

Source: FHWA

Figure 23. Illustration. Mises stresses at last step of pure positive moment (splice plates and deck not shown for clarity).

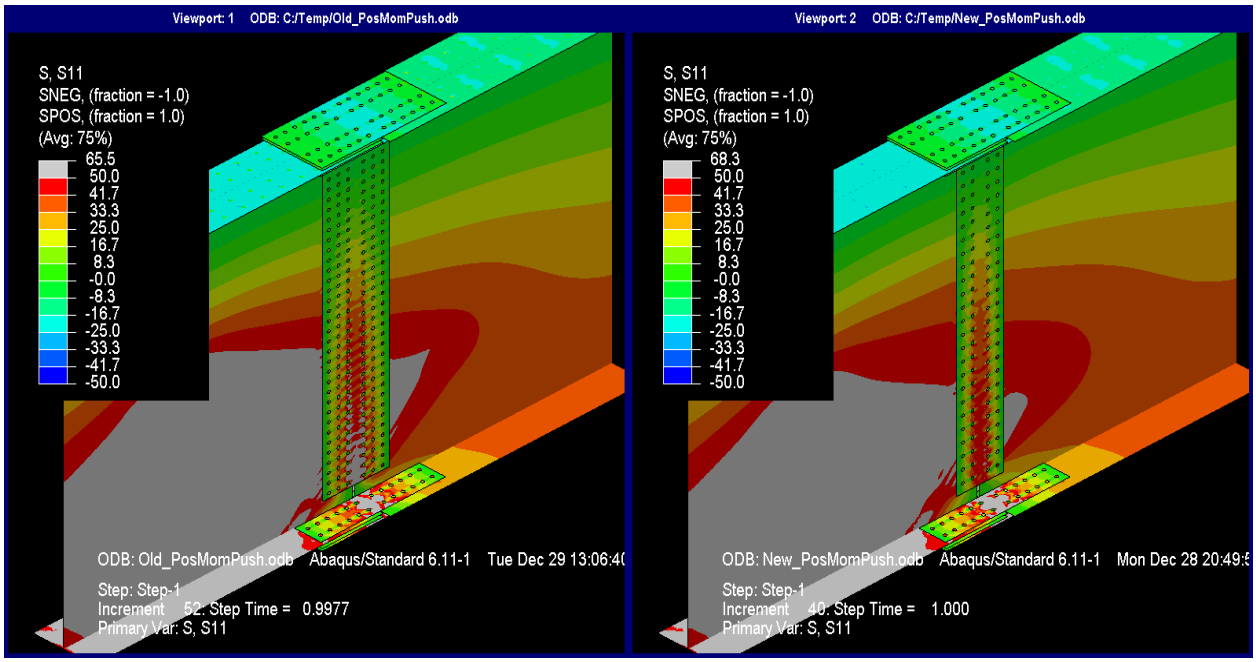

Source: FHWA

Figure 24. Illustration. Longitudinal stresses at last step of pure positive moment (deck not shown for clarity).

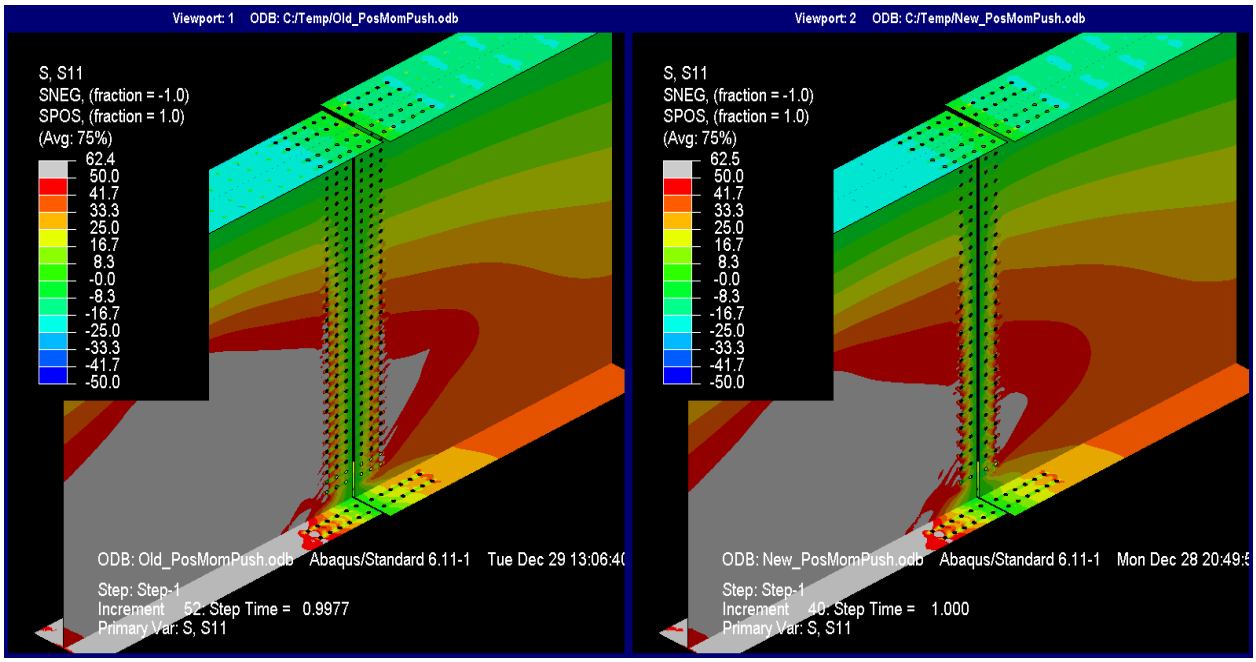

Source: FHWA

Figure 25. Illustration. Longitudinal stresses at last step of pure positive moment (splice plates and deck not shown for clarity).

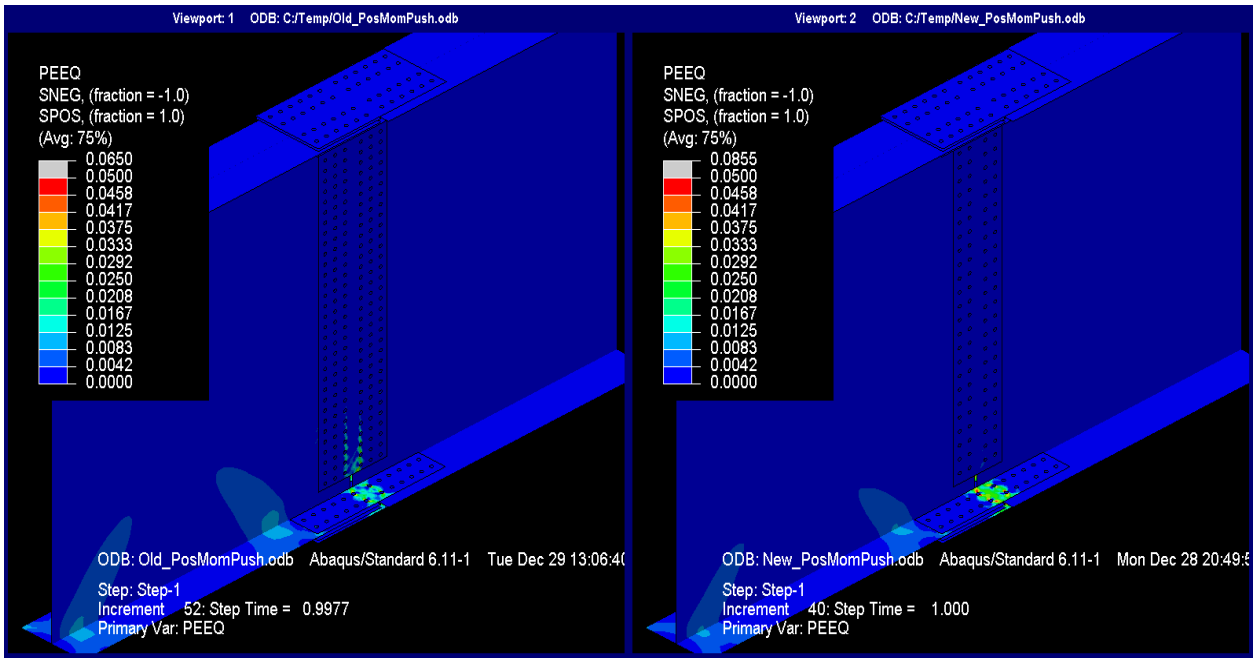

Source: FHWA

Figure 26. Illustration. PEEQ at last step of pure positive moment (deck not shown for clarity).

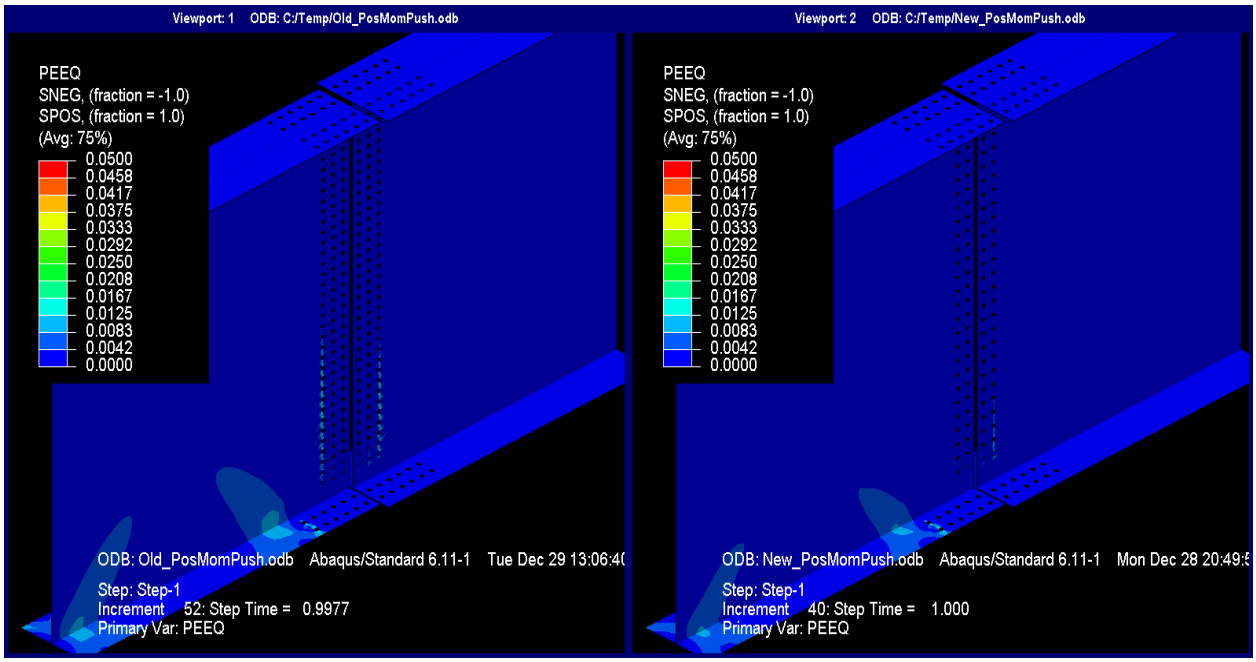

Source: FHWA

Figure 27. Illustration. PEEQ at last step of pure positive moment (splice plates and deck not shown for clarity).

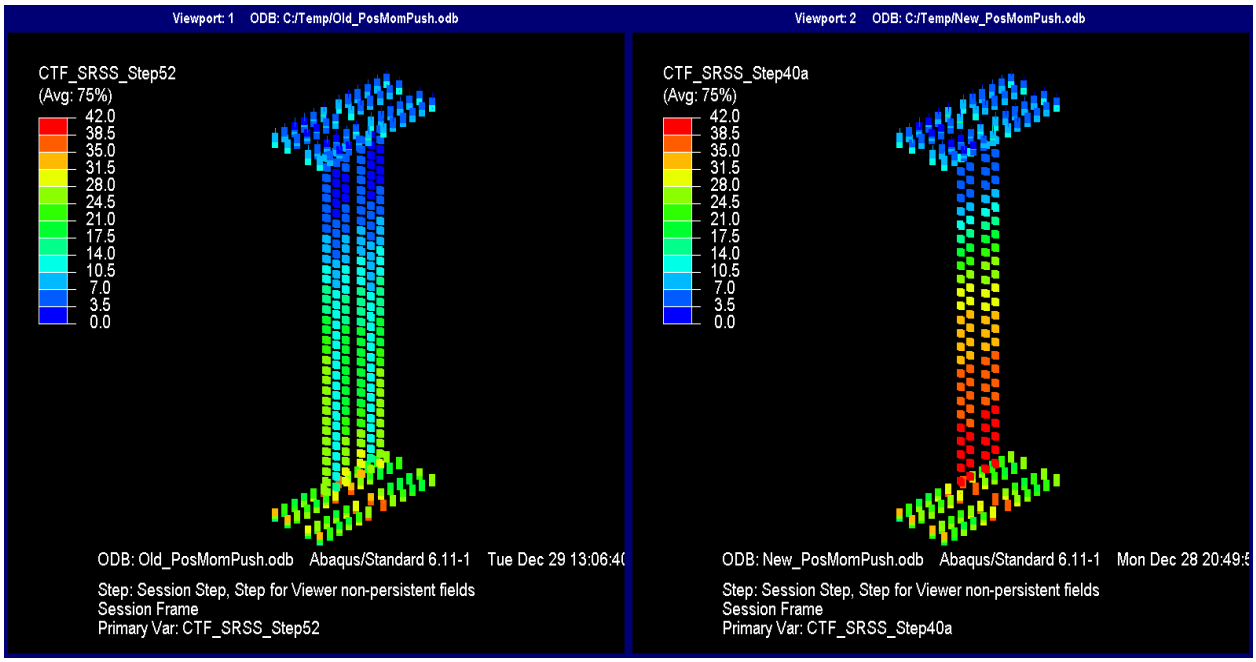

Source: FHWA

Figure 28. Illustration. Resultant forces on bolt shear planes at last step of pure positive moment.

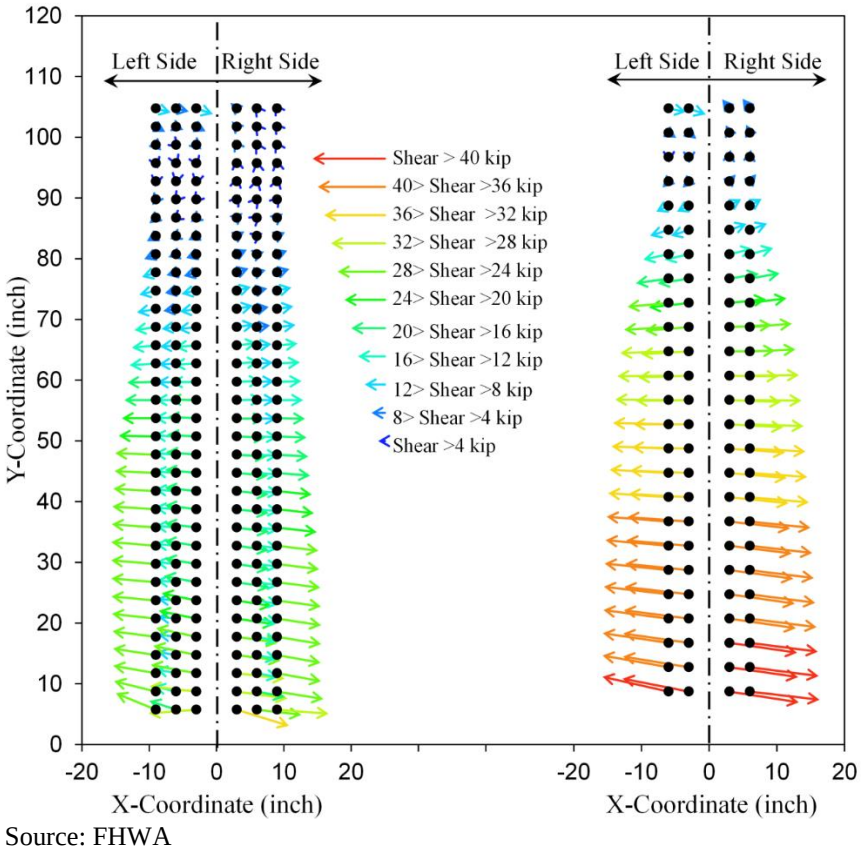

Source: FHWA

Figure 29. Graph. Web splice bolt shear vectors at last step of pure positive moment.

At the design moment, the results in terms of Mises and longitudinal stresses (see 0 though 0) do not differ much between the two methods. The only noticeable difference is that the splice designed by the new method had fewer bolts in the web, which resulted in a higher demand over the splice designed by the current method. However, the shear forces were well within the limits of the bolts (see 0 and 0).

Analysis of the plots from the last step show that the rounding over of the moment/rotation curve presented in 0 was due to plastic hinging of the left girder section. At 0.01 radians of rotation, about half the depth of the left girder has yielded at this point (see 0 through 0). The larger web splice in the splice designed by the current method also transferred more moment than the web splice designed by the new method, as is evident from the increased yielding in the left girder section (see 0). The PEEQ also shows that the splice designed by the current method attracted more plasticity into the web splice, although the splice designed by the new method led to flange splices with a higher demand (see 0 and 0). However, the web bolt demands were also higher for splice designed by the new method
(see 0 and 0), with the largest bolt force being 41.5 kip. It is likely that any additional moment would effectively start fracturing bolts in the splice designed by the new method. However, the limit state of bolt fracture occurred at three times the design moment,
and this would not have controlled the design. The vector plots in 0 show the web's participation in transferring moment because the vectors are horizontal (i.e., no shear in web) with a linear variation in magnitude increasing toward the tension flange.

PURE NEGATIVE MOMENT

0 shows the moment versus rotation plot for the left support with the current method results plotted with circular data points and the new method results plotted with square data points. The overall responses of the two models are nearly equal, and it is obvious that negative moment controlled the design of this connection because the connection did not have a tremendous reserve in strength beyond the design negative moment. Contour plots are presented for the step with approximately M_u = 15,185 kip-ft applied (see 0 through 0) and for the last step in each analysis (see 0 through 0).

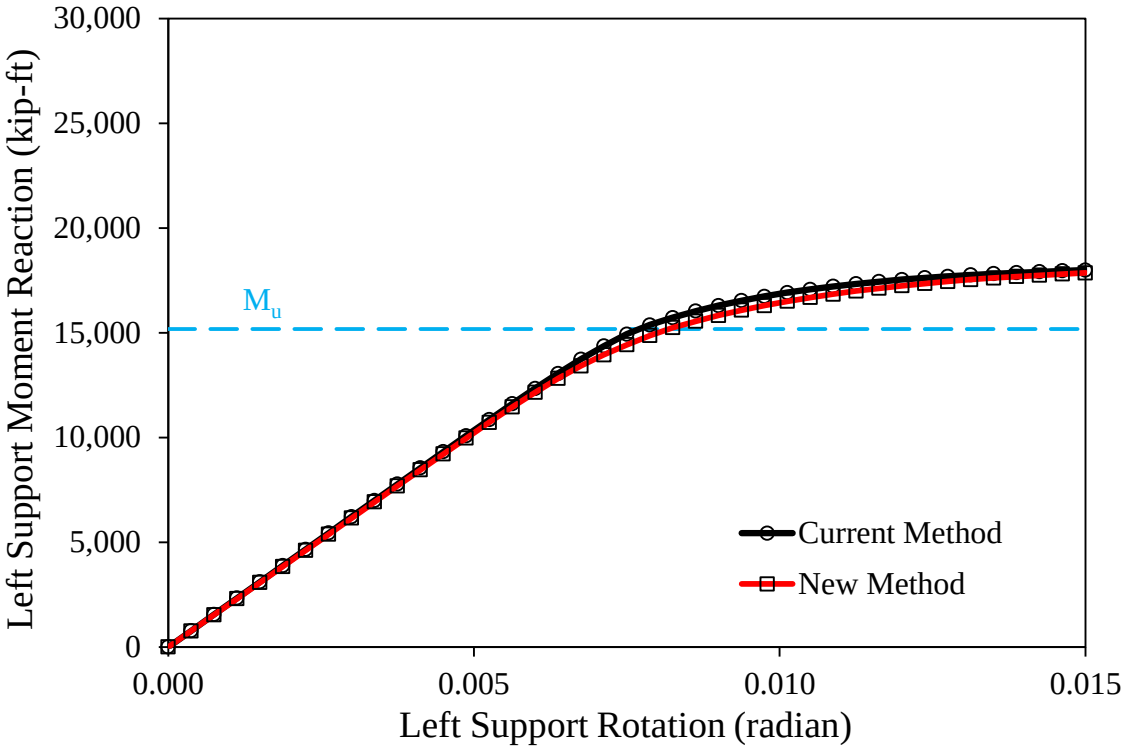

Source: FHWA

Figure 30. Graph. Moment versus rotation of the left support under pure negative moment for the splice designed using the current and new methods.

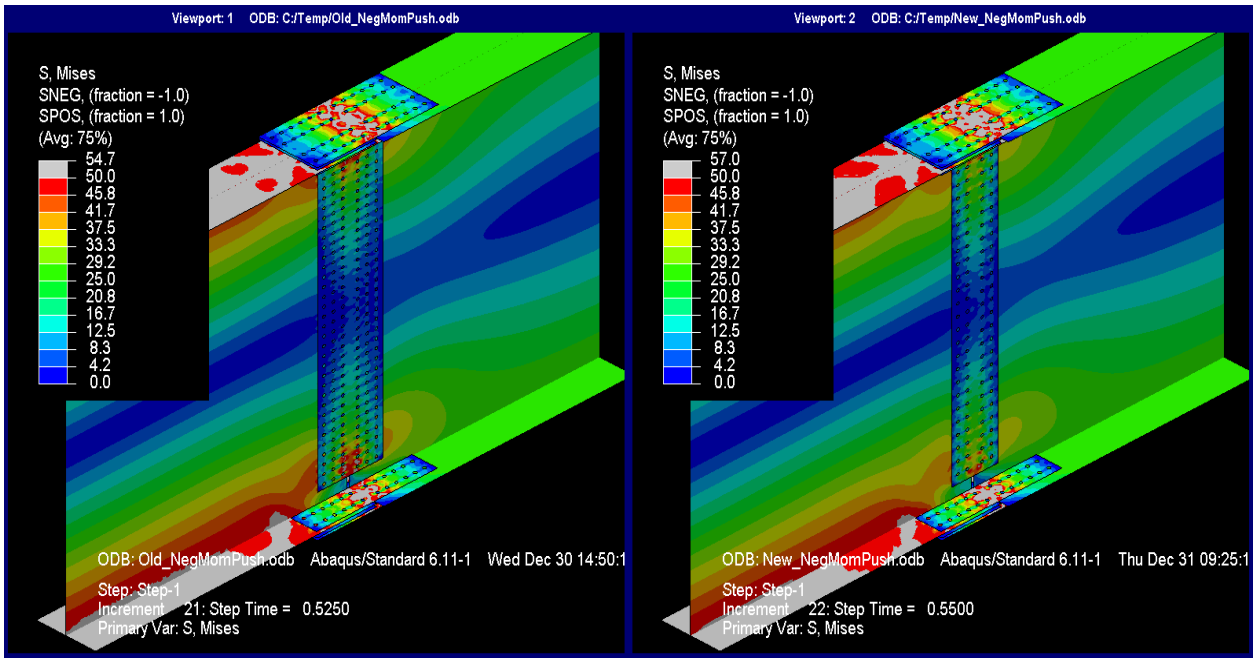

Source: FHWA

Figure 31. Illustration. Mises stresses at pure negative M_u.

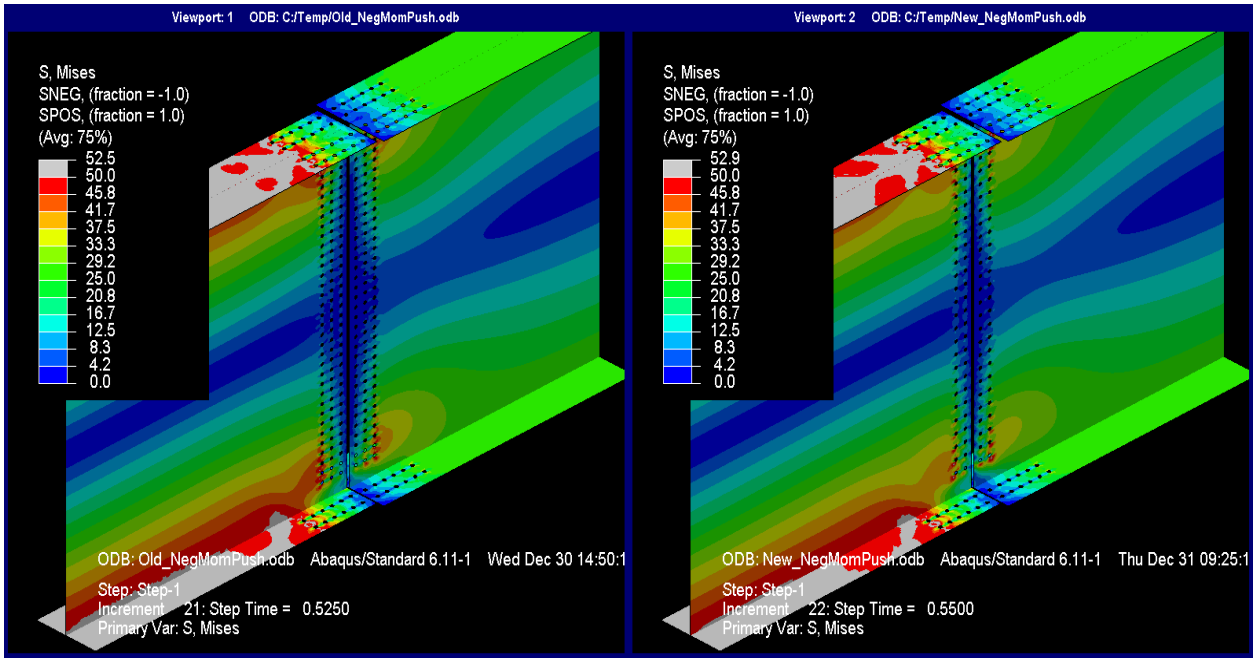

Source: FHWA

Figure 32. Illustration. Mises stresses at pure negative M_u (splice plates not shown for clarity).

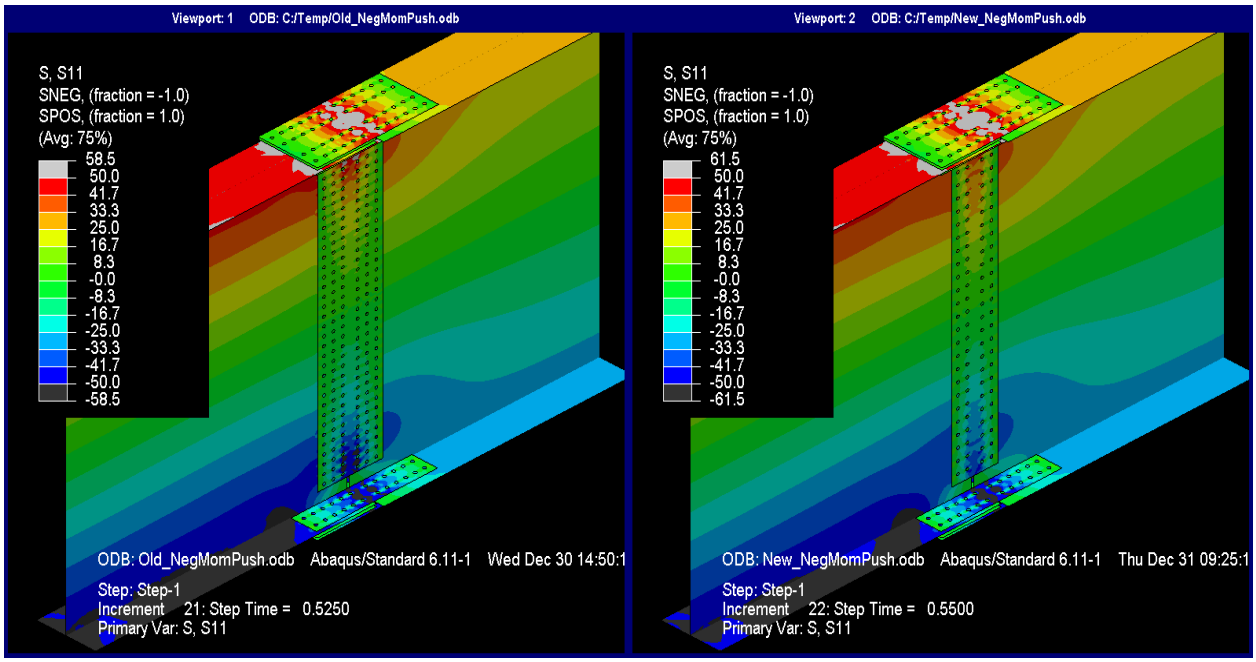

Source: FHWA

Figure 33. Illustration. Longitudinal stresses at pure negative M_u.

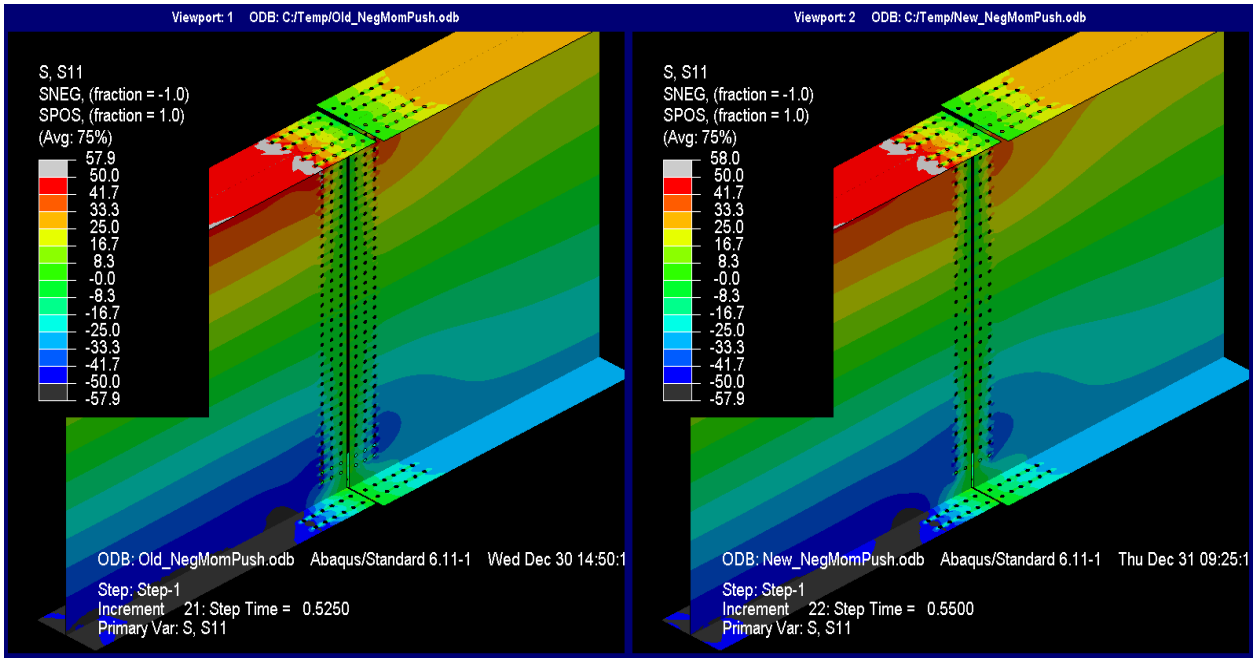

Source: FHWA

Figure 34. Illustration. Longitudinal stresses at pure negative M_u (splice plates not shown for clarity).

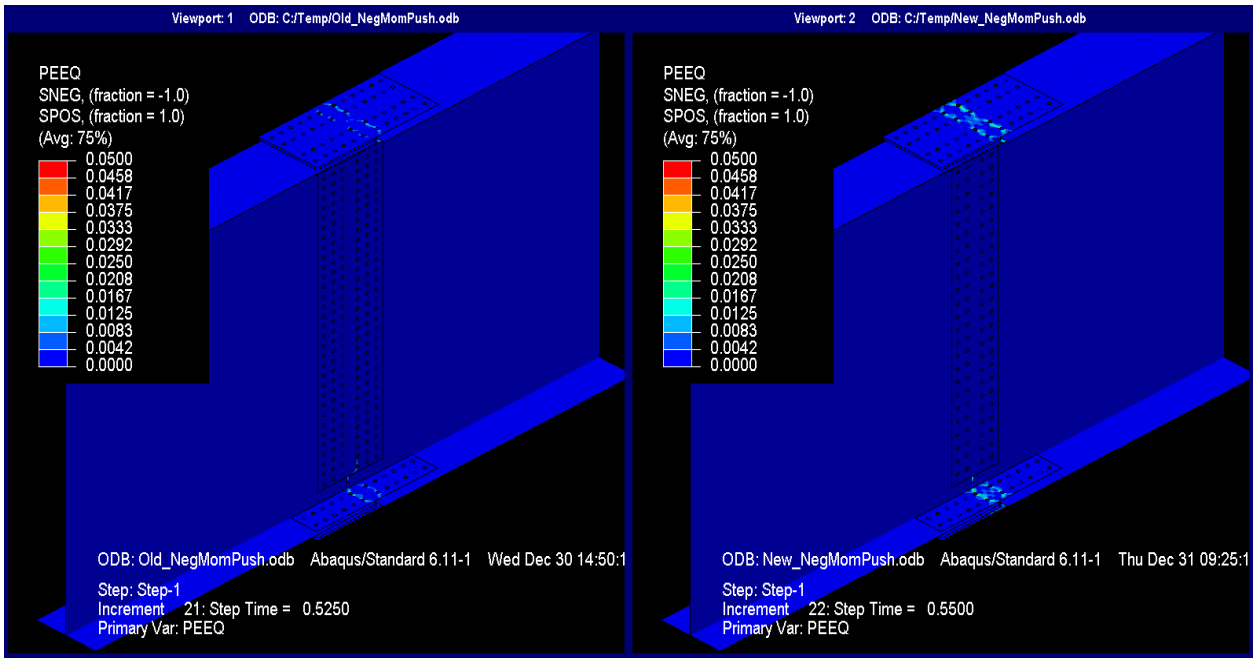

Source: FHWA

Figure 35. Illustration. PEEQ at pure negative M_u.

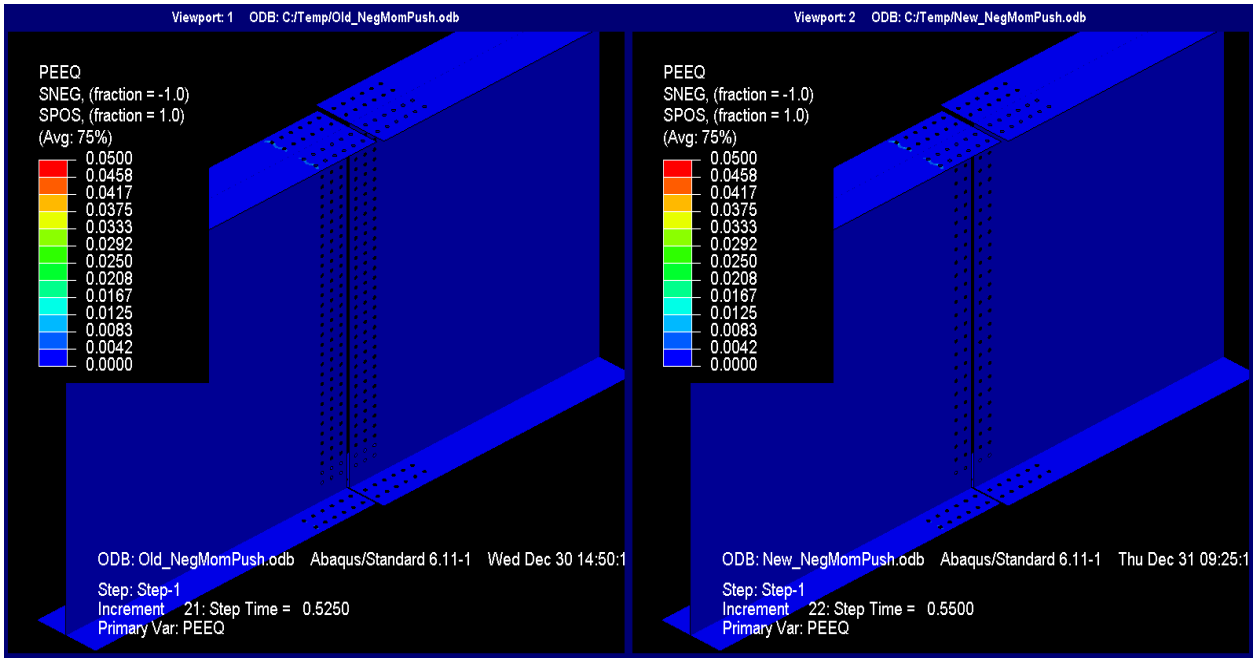

Source: FHWA

Figure 36. Illustration. PEEQ at pure negative M_u (splice plates not shown for clarity).

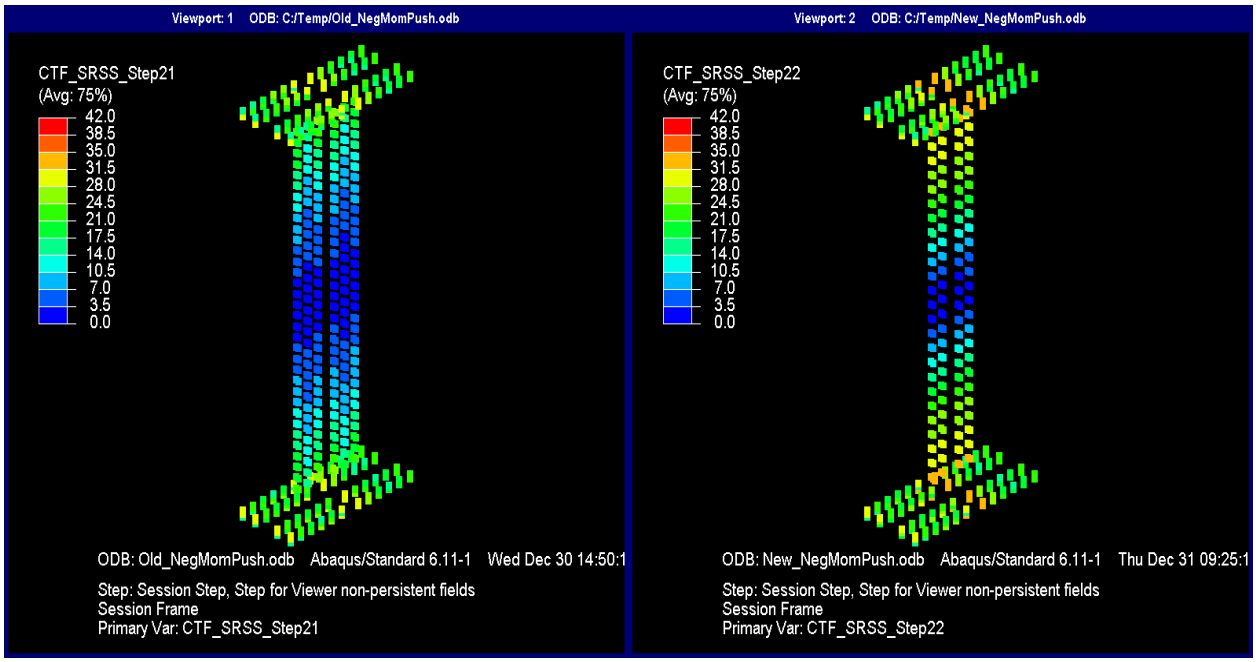

Source: FHWA

Figure 37. Illustration. Resultant forces on bolt shear planes at pure negative M_u.

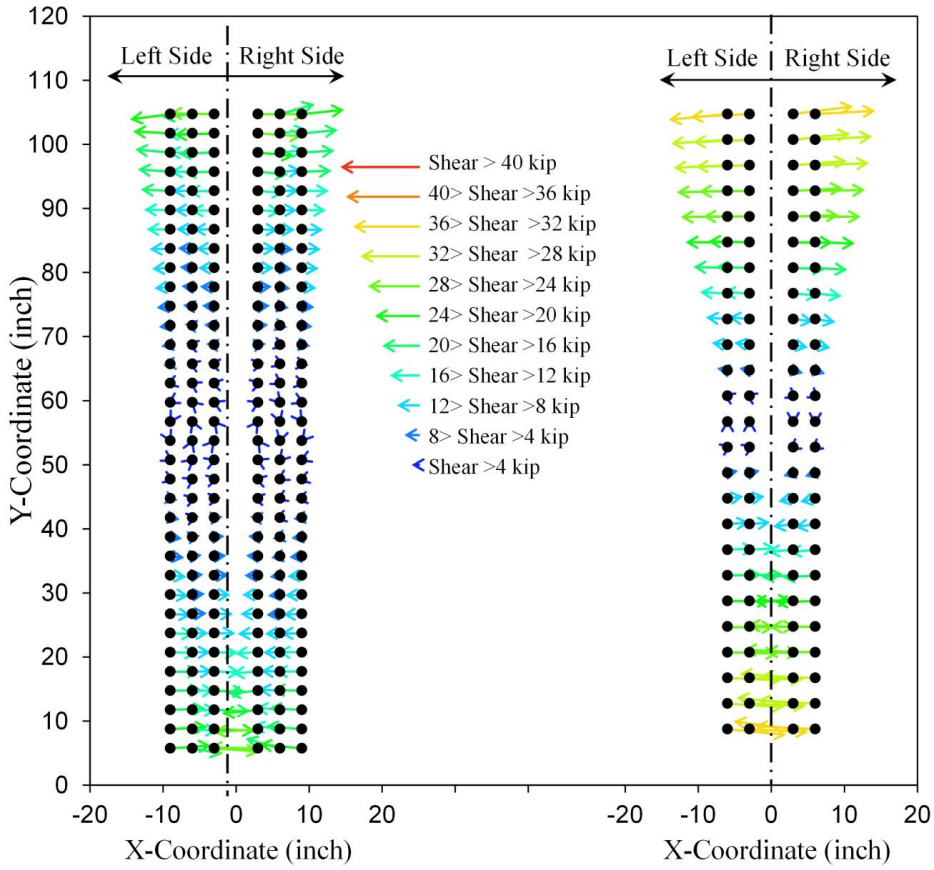

Source: FHWA

Figure 38. Graph. Web splice bolt shear vectors at pure negative M_u.

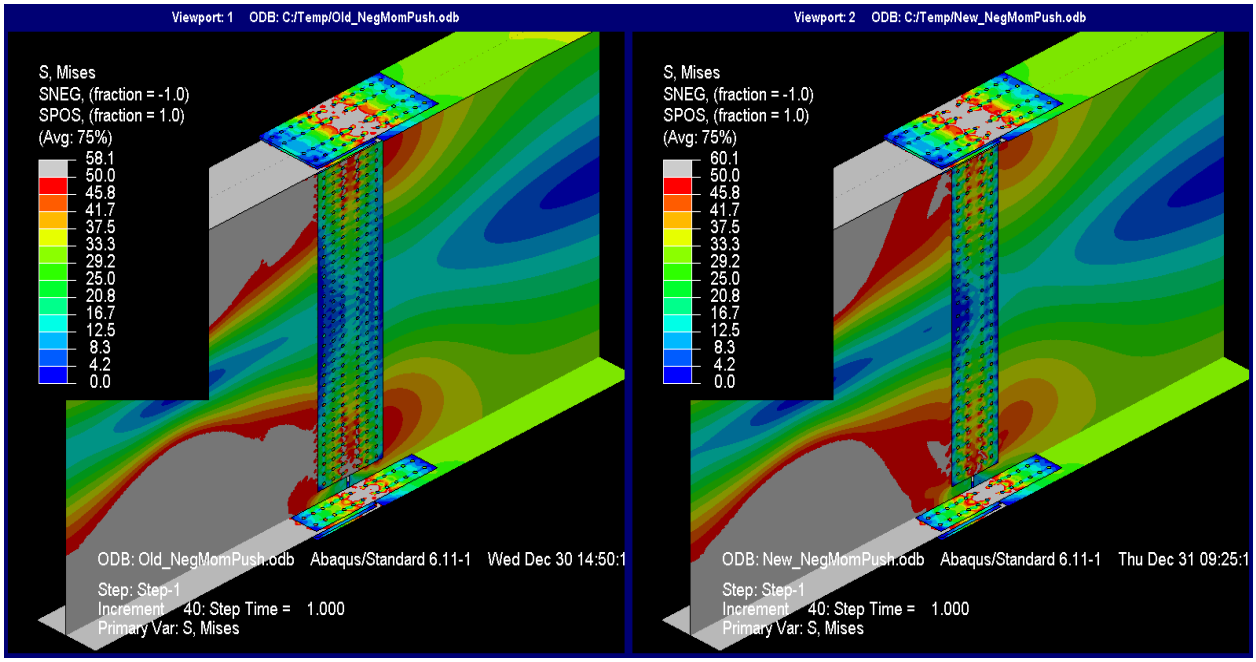

Source: FHWA

Figure 39. Illustration. Mises stresses at last step of pure negative moment.

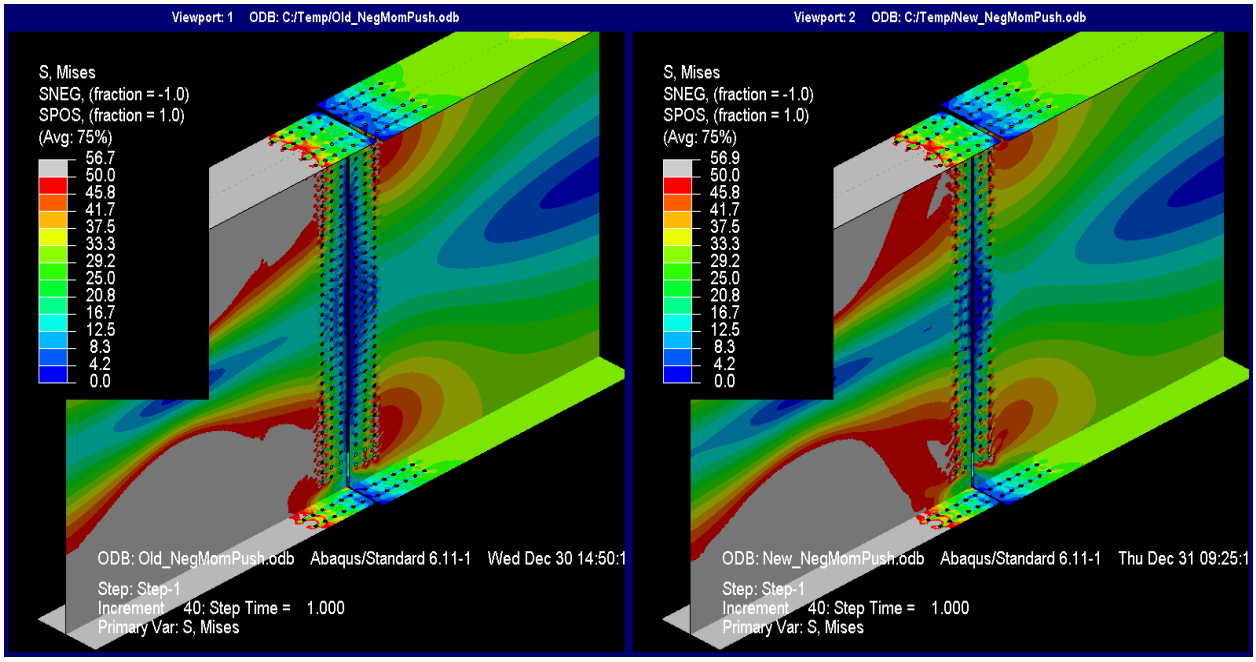

Source: FHWA

Figure 40. Illustration. Mises stresses at last step of pure negative moment (splice plates not shown for clarity).

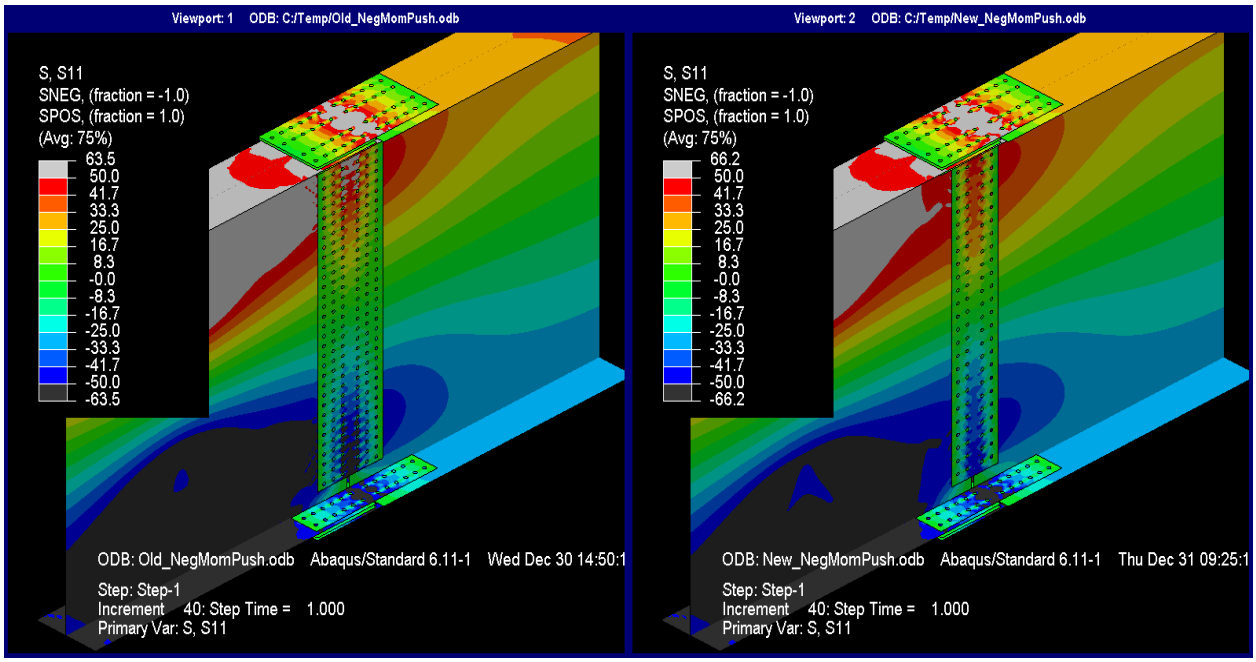

Source: FHWA

Figure 41. Illustration. Longitudinal stresses at last step of pure negative moment.

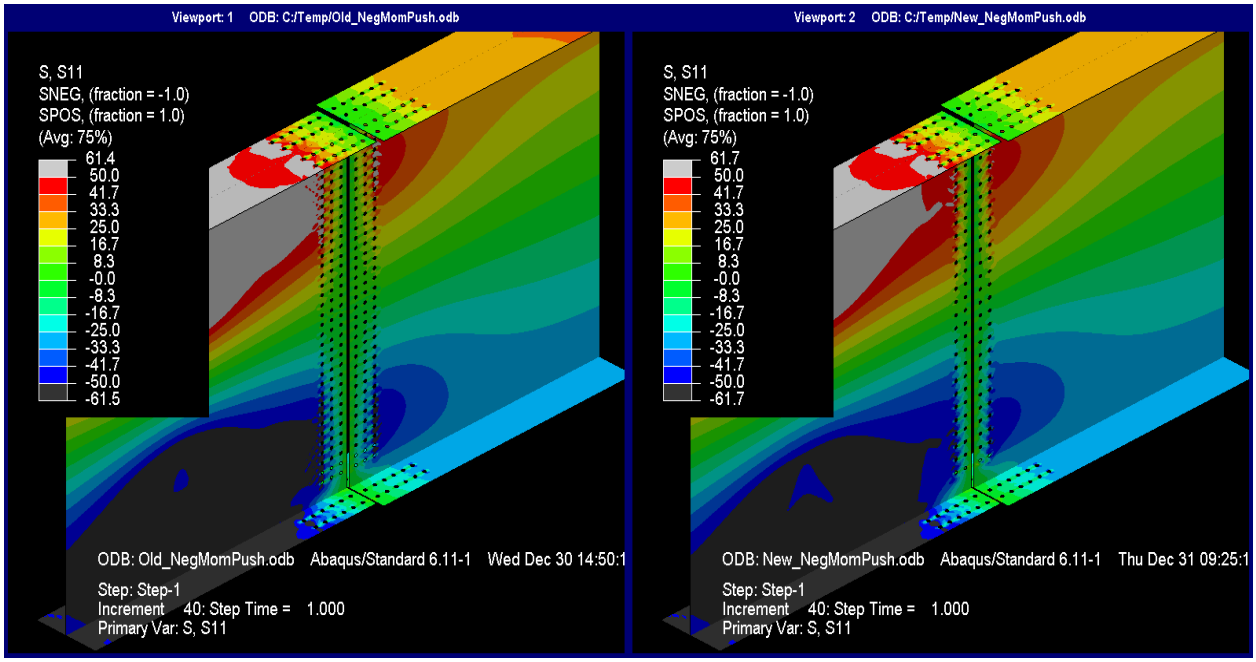

Source: FHWA

Figure 42. Illustration. Longitudinal stresses at last step of pure negative moment (splice plates not shown for clarity).

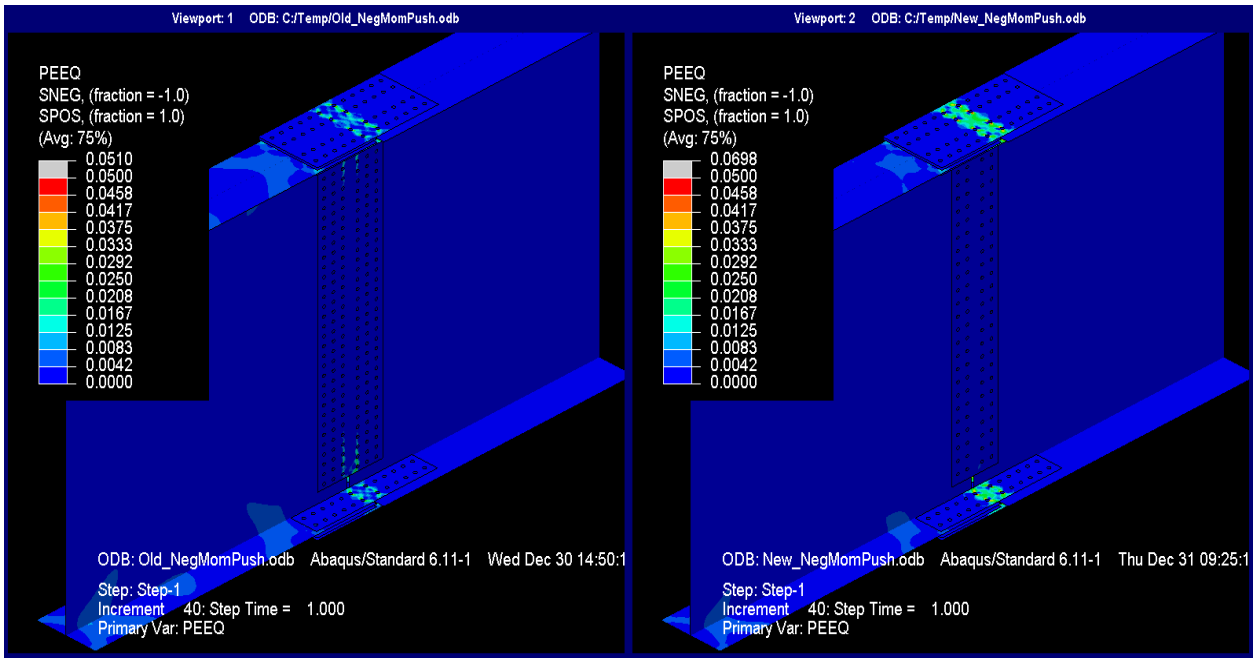

Source: FHWA

Figure 43. Illustration. PEEQ at last step of pure negative moment.

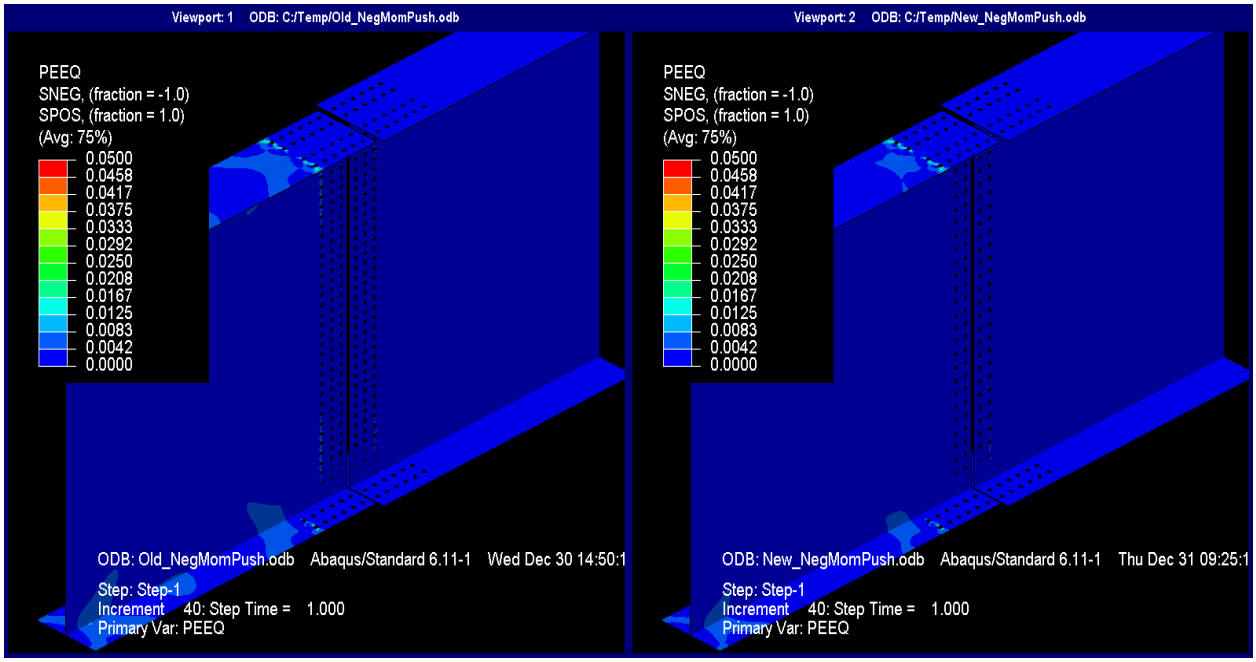

Source: FHWA

Figure 44. Illustration. PEEQ at last step of pure negative moment (splice plates not shown for clarity).

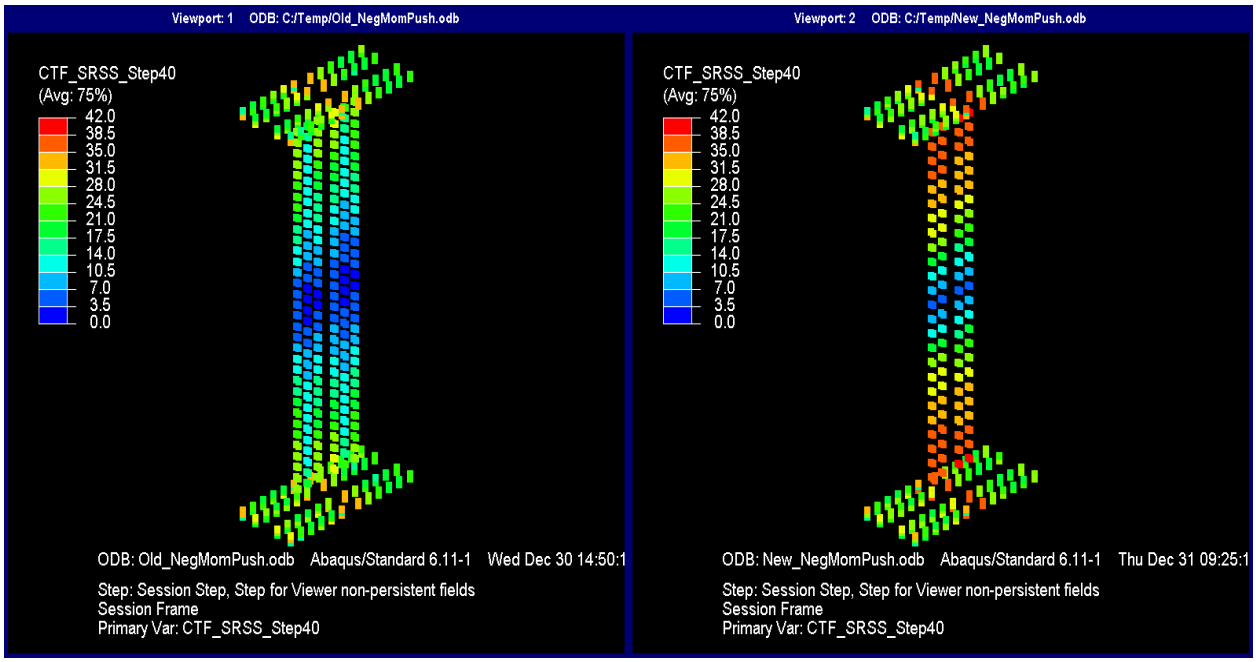

Source: FHWA

Figure 45. Illustration. Resultant forces on bolt shear planes at last step of pure negative moment.

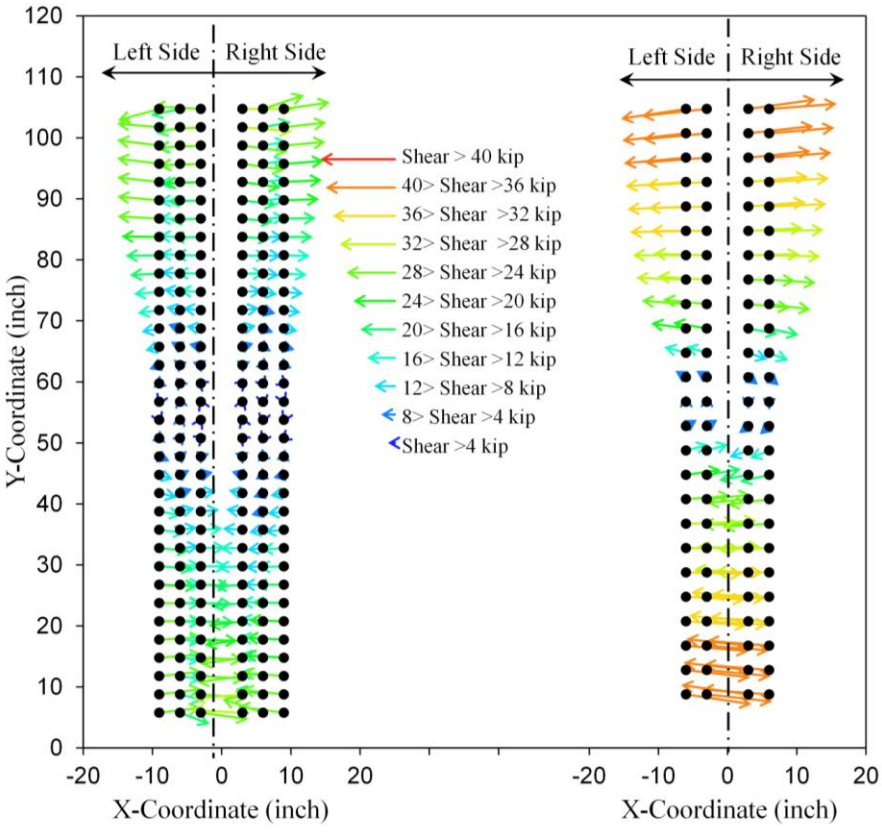

Source: FHWA

Figure 46. Graph. Web splice bolt shear vectors at last step of pure negative moment.

At the design moment, the Mises stresses show that the flanges of the left girder have just yielded along with the flange splice plates (see 0 and 0). The same can be said for the longitudinal stresses (see 0 and 0), which indicate, not surprisingly, that these stresses dominated the Mises failure criterion. The PEEQ plot in 0 shows that the splice designed by the new method had a slightly higher demand on the flange splice plates than the splice designed by the current method. Though the demands on the flange bolts were nearly the same between the two methods, there was an expected higher demand on the web bolts in the splice designed with the new method (see 0 and 0).

Analysis of the plots from the last step shows that the rounding over of the moment/rotation curve presented in 0 was from plastic hinging of the left girder section (see 0 and 0). At 0.015 radians of rotation, nearly the entire depth of the left girder had yielded. The stress contours between the two scenarios only differed in regards to the splice designed by the current method, which transferred more stress across the web splice than the splice designed by the new method. There was more yielding in the girder webs and web splice in the splice designed by the current method. However, the demands on the flange splices in the splice designed by the new method were higher (mostly evident on the PEEQ plot in 0). This resulted in higher demands on the bolts in the flange splices designed by the new method (with the highest shear forces being 39.4 kip) approaching their fracture strength (see 0 and 0). The vector plots in 0 show the web's participation in transferring moment as the vectors were horizontal (i.e., no shear in web) with a linear variation in magnitude increasing away from the girder centroid.

HIGH SHEAR LOADING

0 shows a force versus displacement plot for the left support with the circular data points indicating the results from the current method and the square data points indicating the results from the new method. The plots are identical, which is the first indication that the design method is insensitive to shear loading. The plateau response of each of the curves in 0 is primarily from hinging in the left girder section at the interface between the elastic and inelastic elements.

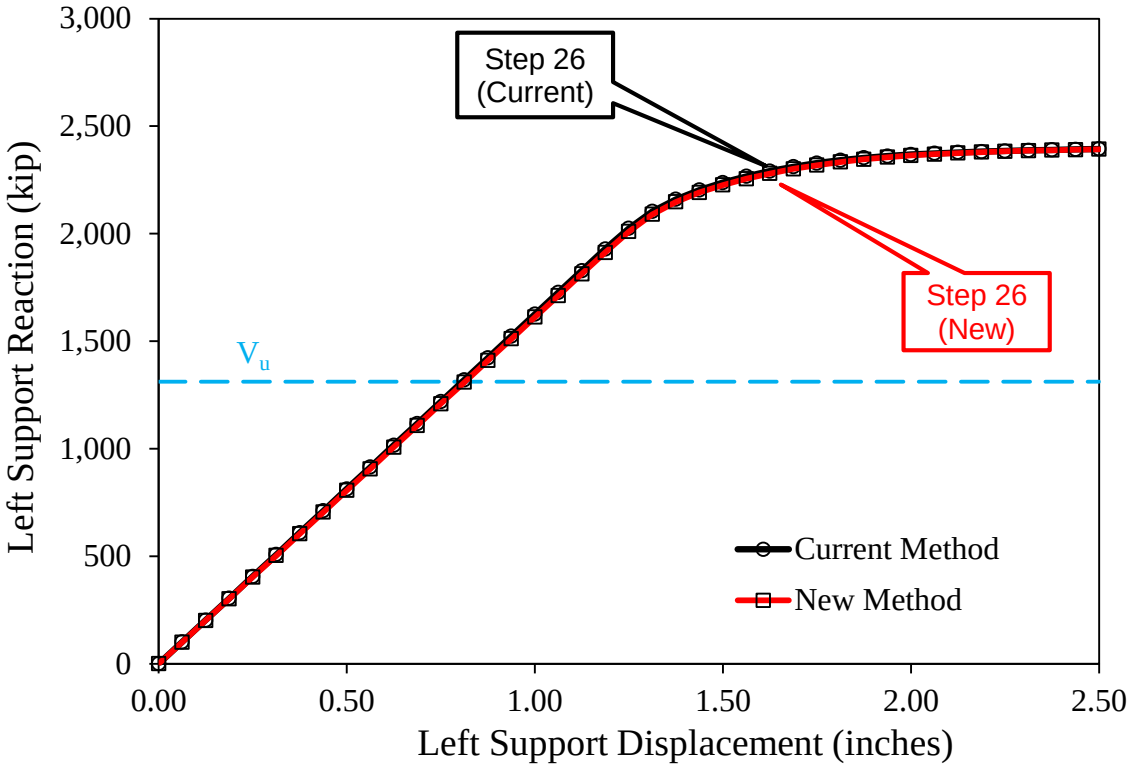

Source: FHWA

Figure 47. Graph. Force versus displacement at the left support under high shear loading for the splice designed using the current and new methods.

Contour plots are presented for the step with V_u = 1,312 kip (see 0 through 0). The system is still elastic (see 0 and 0), although the shear stresses were at about 80 percent of their yield value (see 0 and 0). The bolt demands were low; the bolts were only at about one-third of their design capacity although slightly higher in the splice designed by the new method (see 0 and 0).

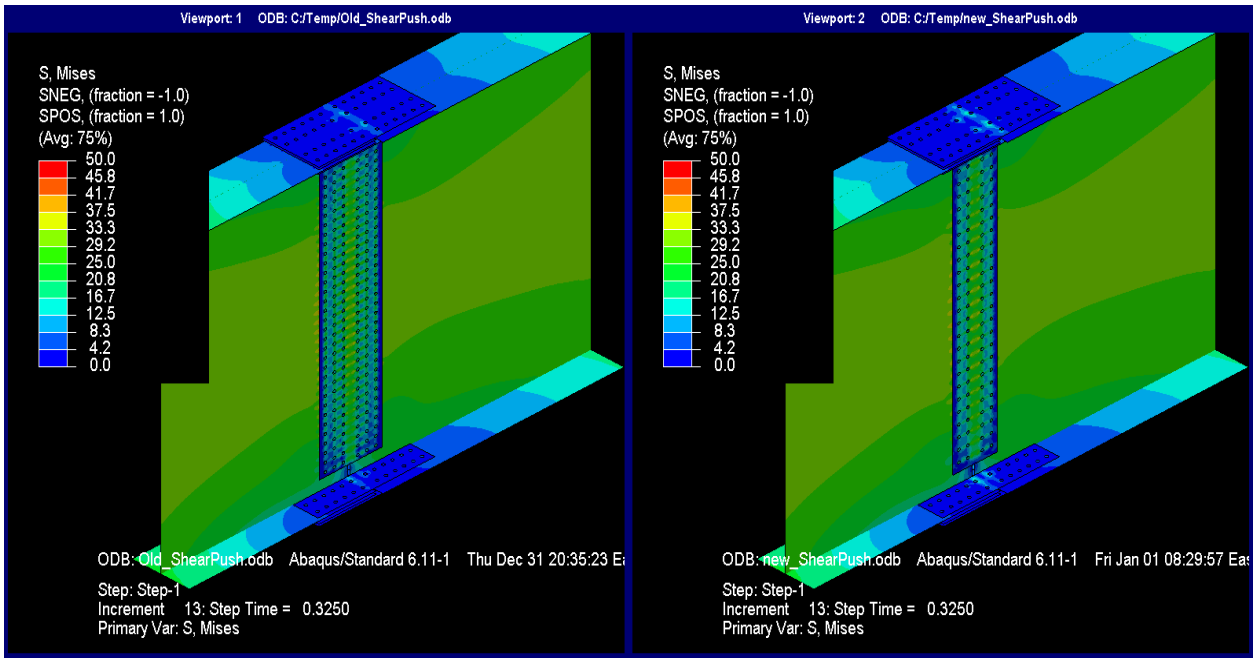

Source: FHWA

Figure 48. Illustration. Mises stresses at V_u.

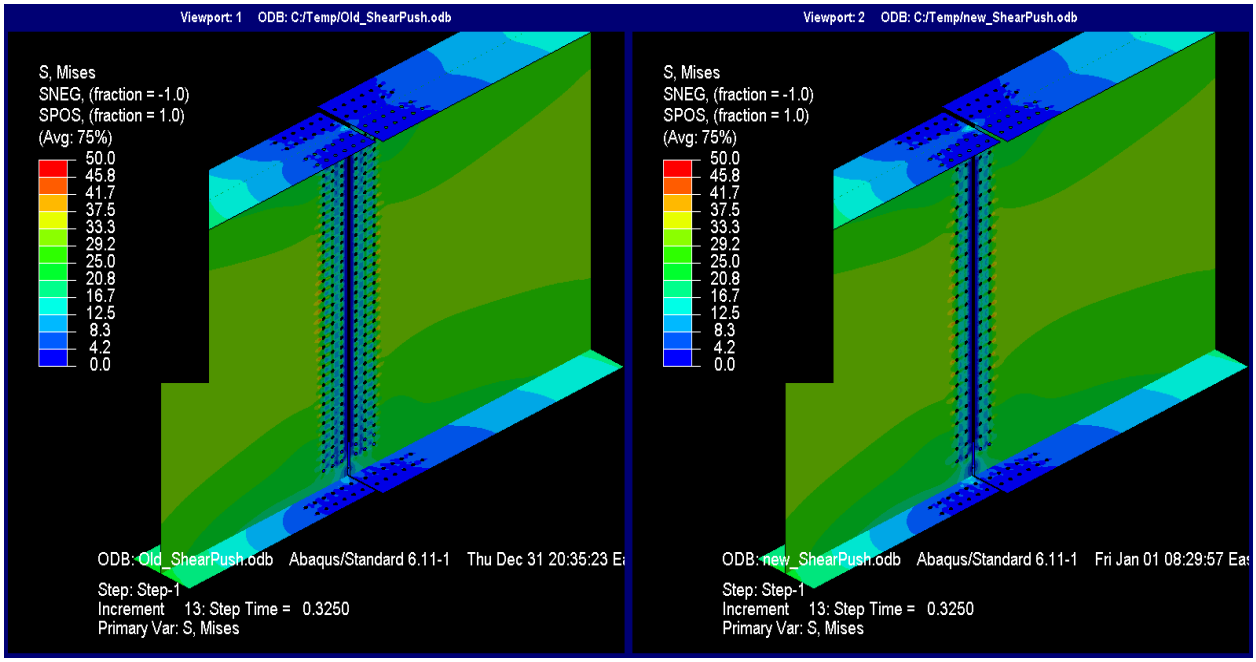

Source: FHWA

Figure 49. Illustration. Mises stresses at V_u (splice plates not shown for clarity).

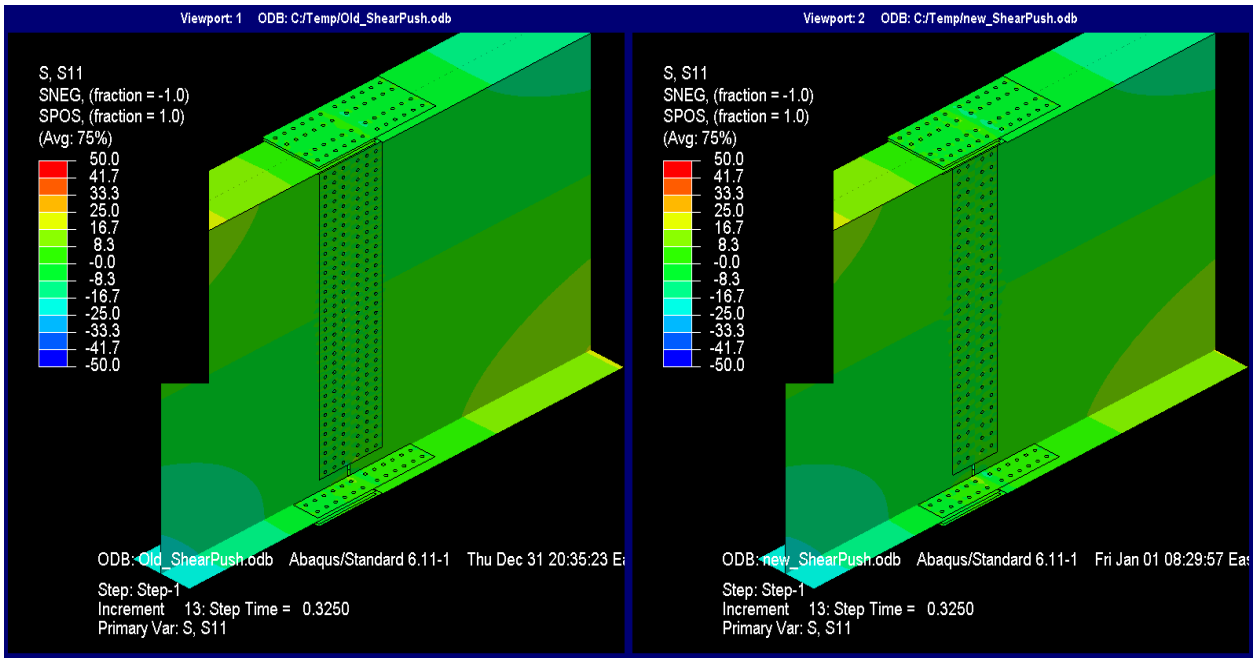

Source: FHWA

Figure 50. Illustration. Longitudinal stresses at V_u.

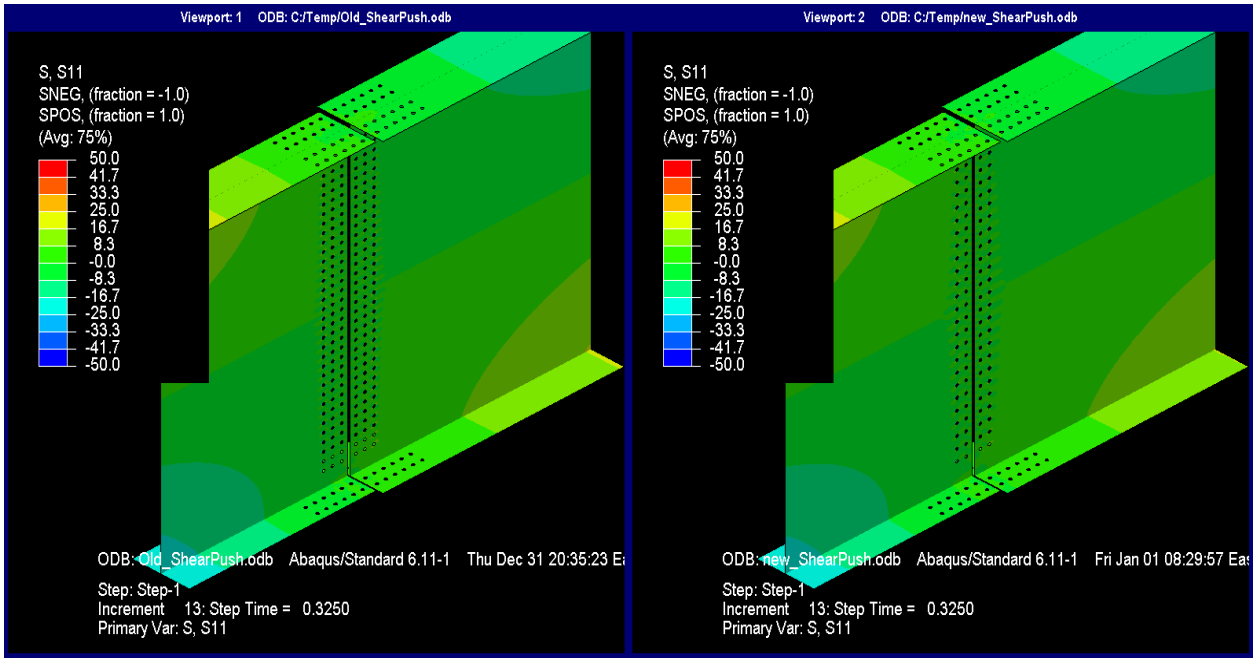

Source: FHWA

Figure 51. Illustration. Longitudinal stresses at V_u (splice plates not shown for clarity).

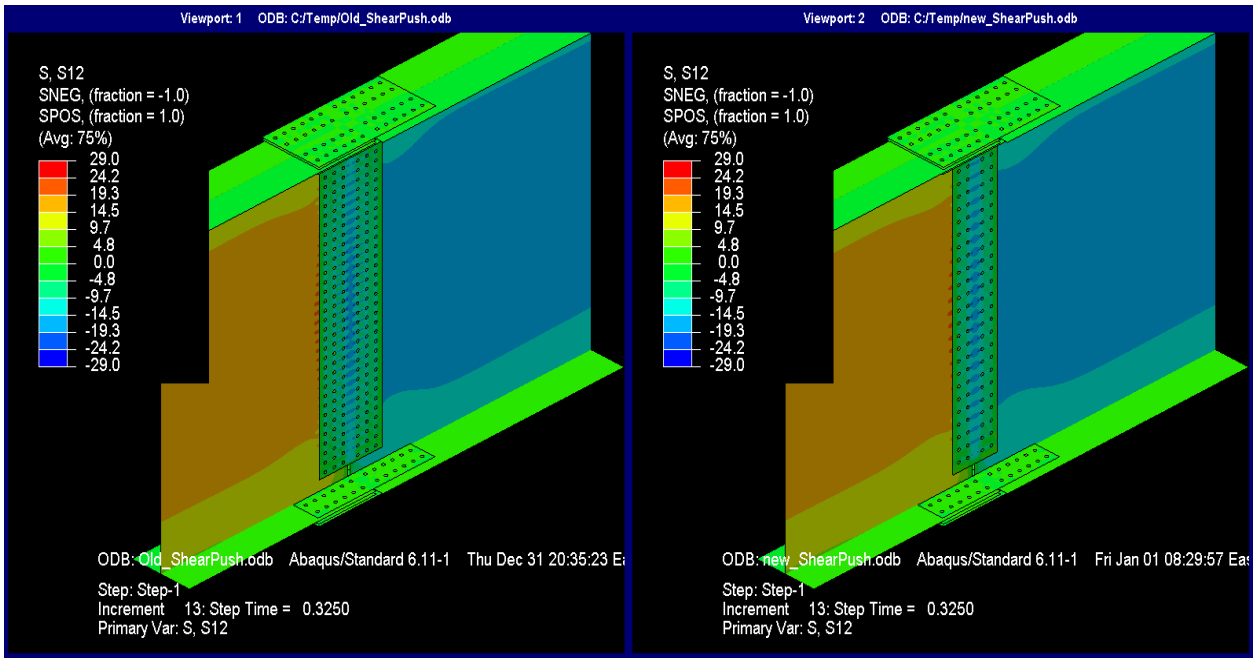

Source: FHWA

Figure 52. Illustration. Shear stresses at V_u.

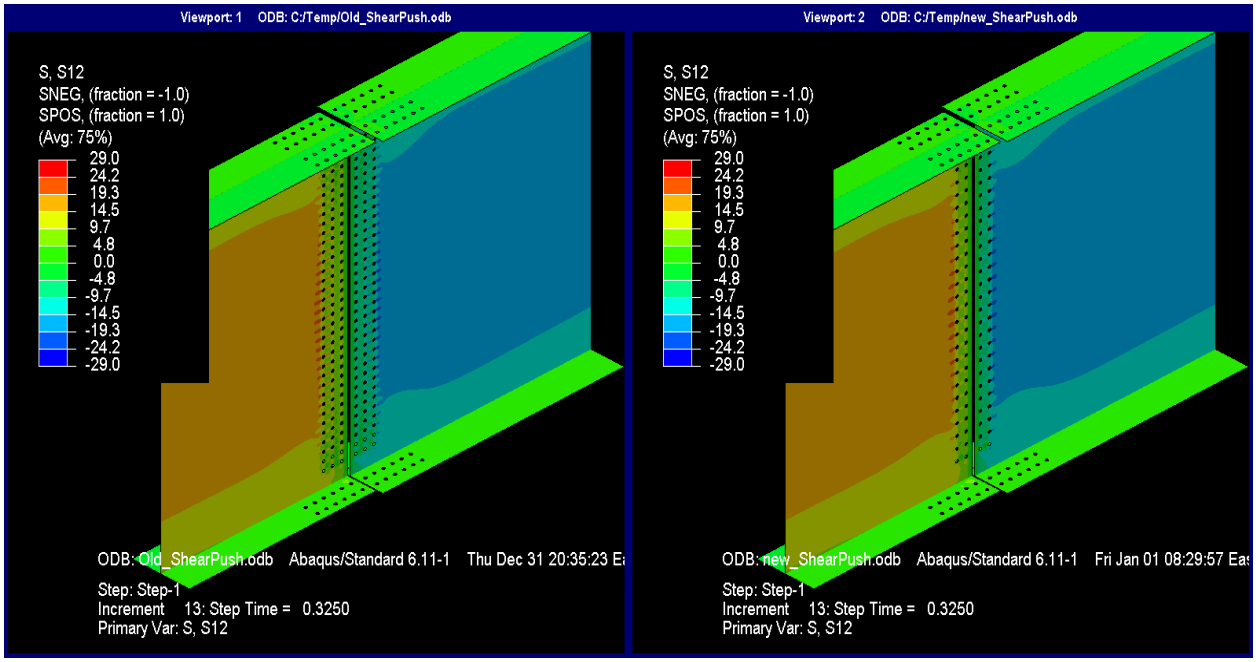

Source: FHWA

Figure 53. Illustration. Shear stresses at V_u (splice plates not shown for clarity).

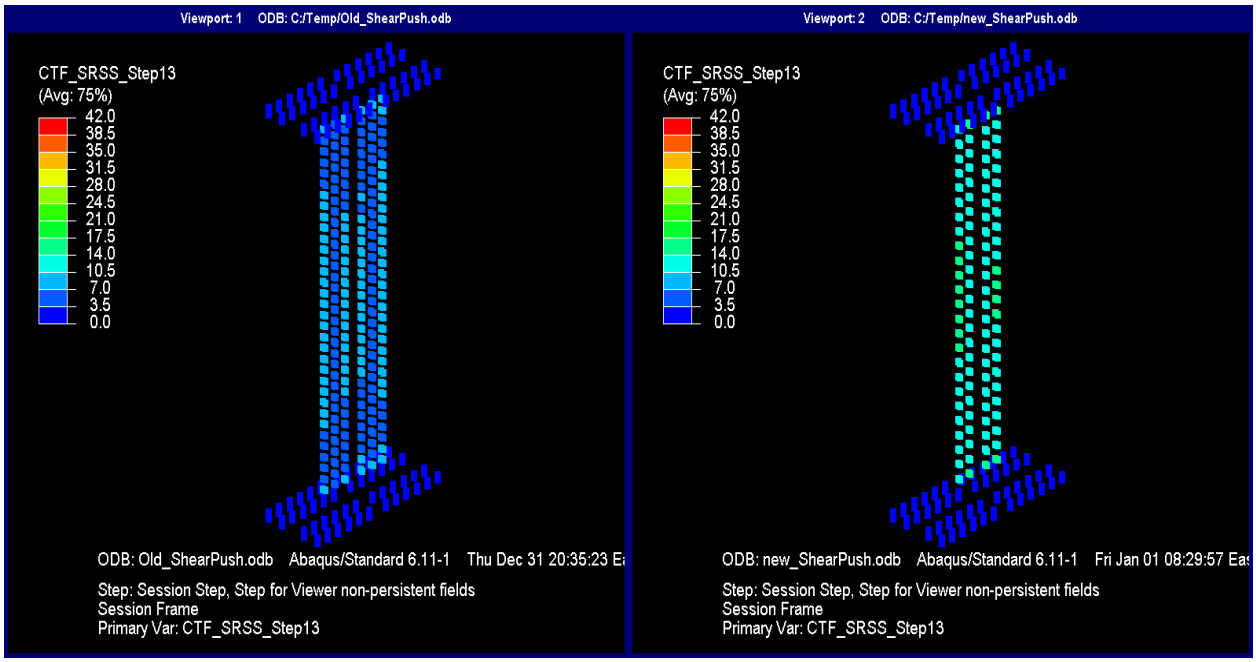

Source: FHWA

Figure 54. Illustration. Resultant forces on bolt shear planes at V_u.

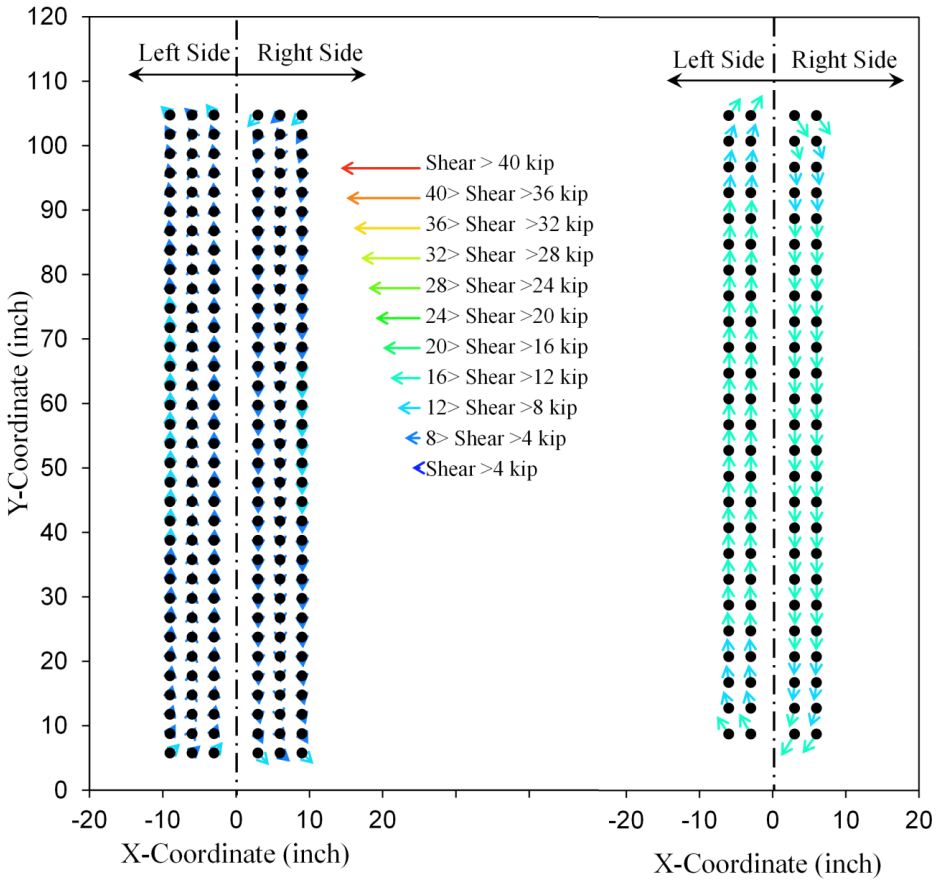

Source: FHWA

Figure 55. Graph. Web splice bolt shear vectors at V_u.

Step 26 was chosen as the second interrogation level because it began just after yielding had started. Contour plots are shown in 0 through 0. The subsequent steps resulted in excessive straining at the plastic hinge in the left girder, not within the spliced region. In both models, the majority of both webs were yielding, and the middle portion of the web splice plates was also approaching yield (see 0 and 0). Not surprisingly, the yielding response was dominated by the shear stresses as the contour plot showed most of the web at or approaching 29 ksi (see 0 and 0). The most telling plots were the PEEQ contours in 0 and 0, which were each plotted with a maximum strain of 0.015. The differences were minor between the splices created via the two design methods; each showed a nearly equal level of plastic straining, which indicates that the design method was insensitive to shear response. The resultant bolt forces (0 and 0) were uniform under shear (though expectedly larger in the splice designed via the new method because of lesser bolts) but still well within their design limits. The vectors in 0 were mostly vertical under this scenario of primarily shear loading; however, the corner bolts were slightly rotated, which indicates that some effect of moment was being taken by those bolts.

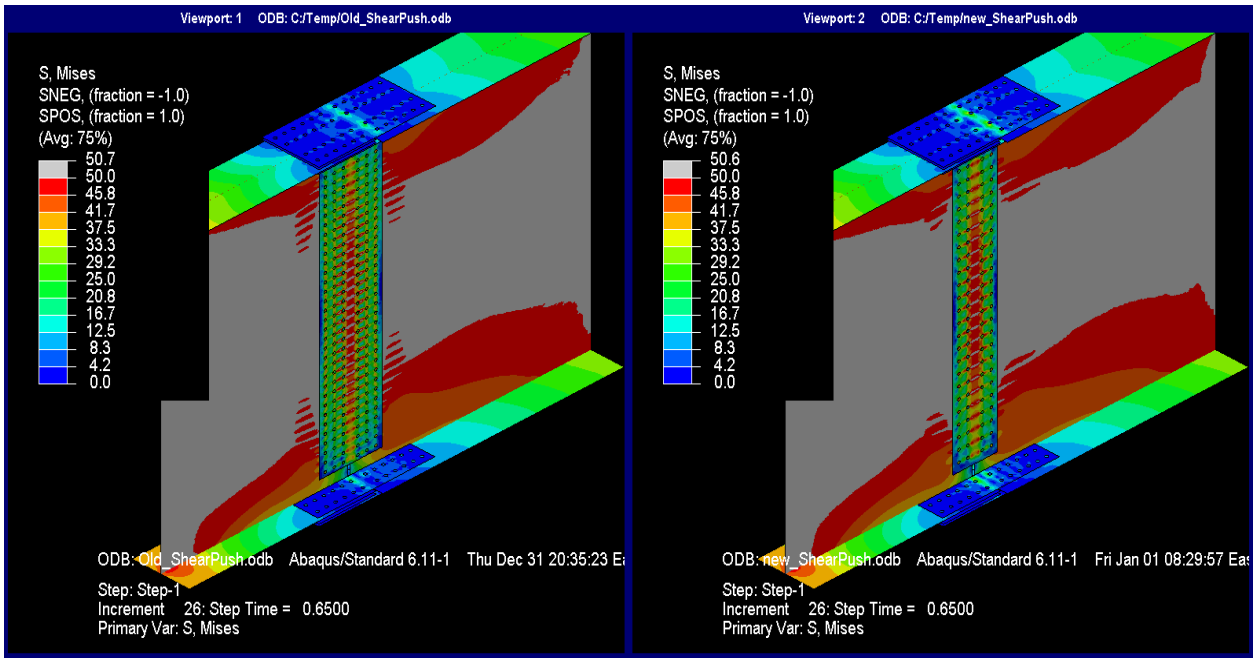

Source: FHWA

Figure 56. Illustration. Mises stresses at step 26.

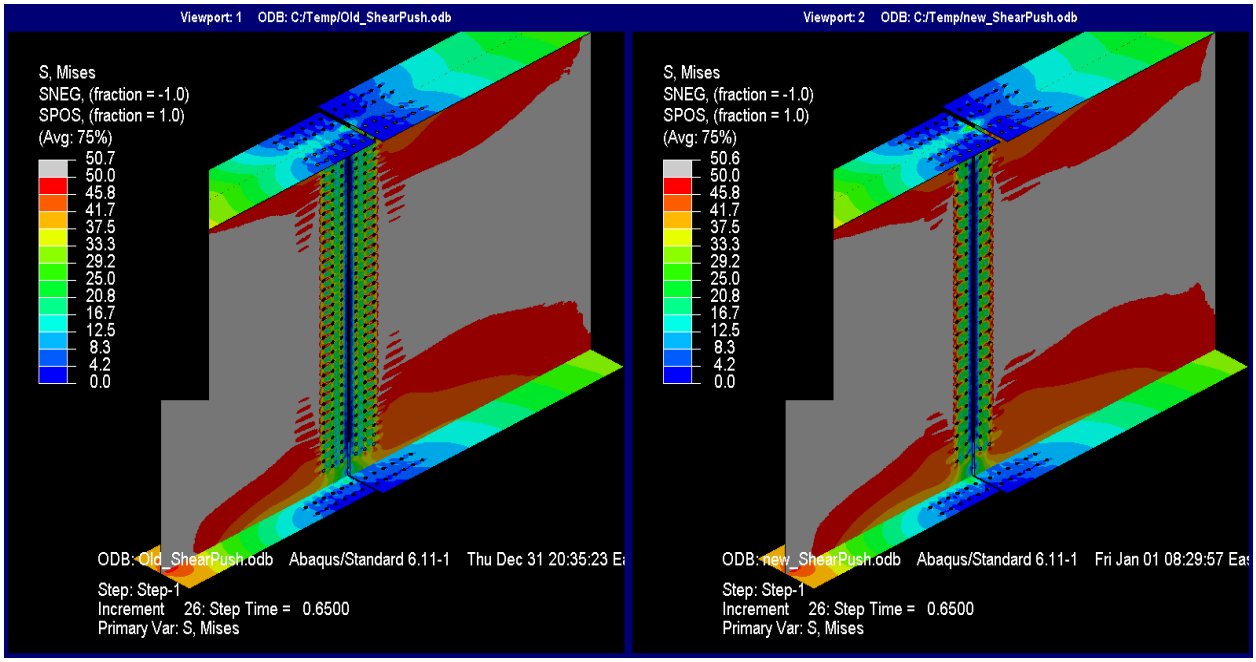

Source: FHWA

Figure 57. Illustration. Mises stresses at step 26 (splice plates not shown for clarity).

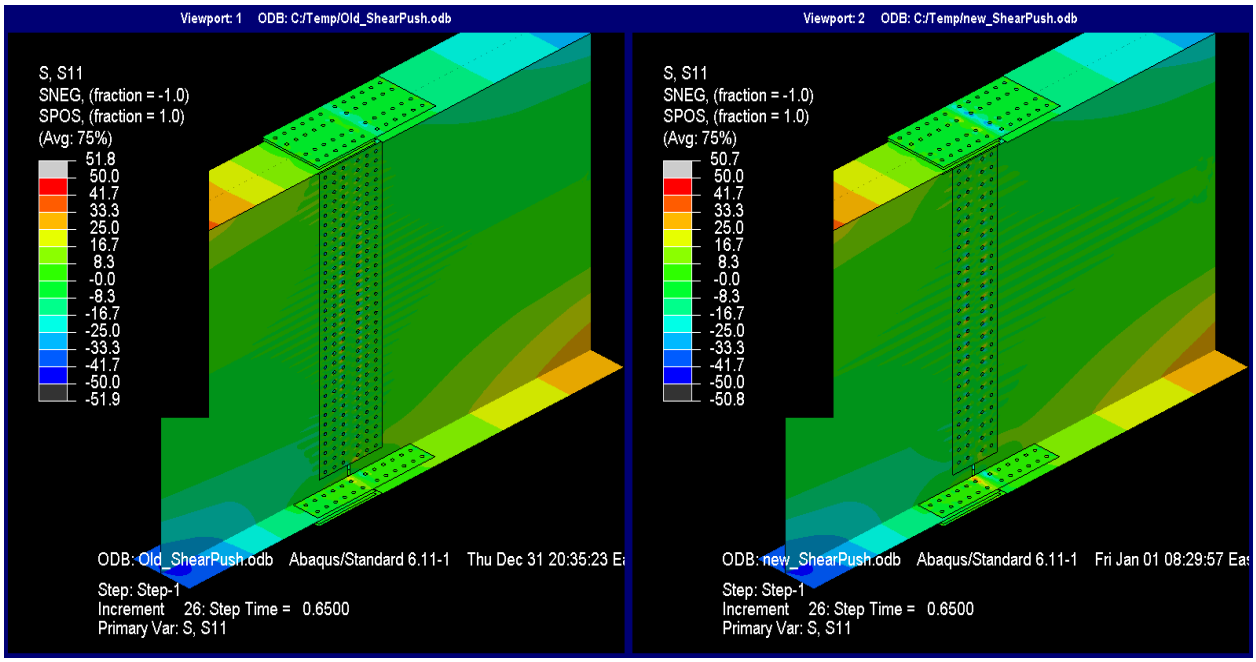

Source: FHWA

Figure 58. Illustration. Longitudinal stresses at step 26.

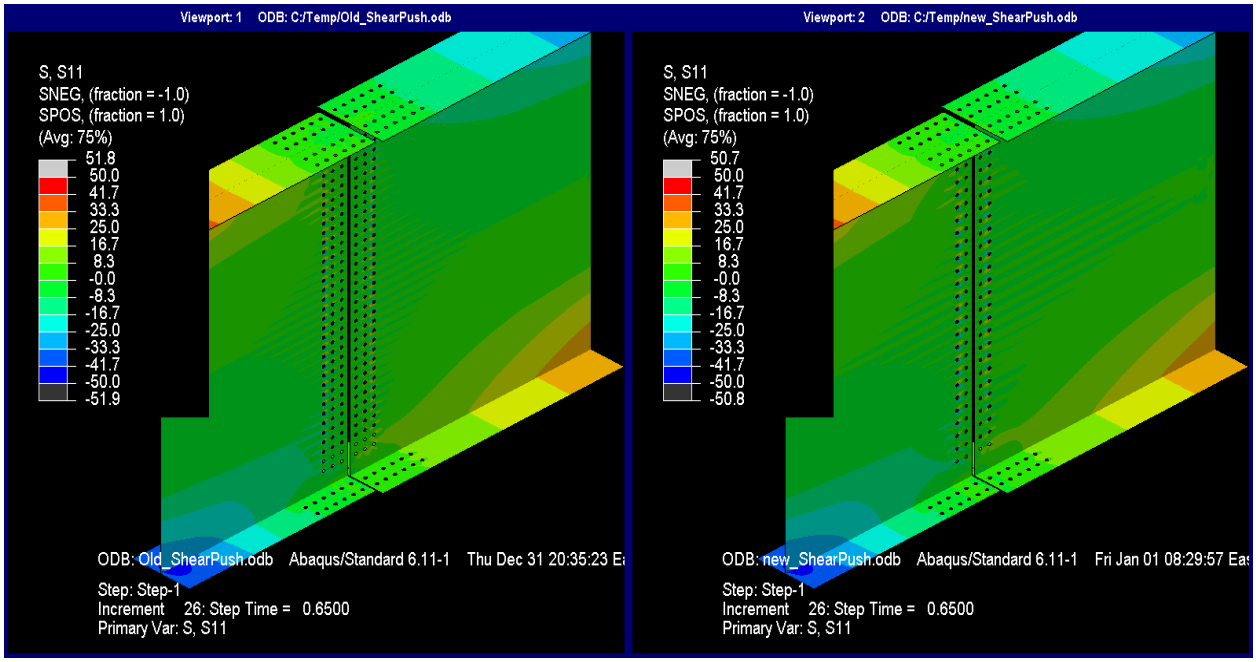

Source: FHWA

Figure 59. Illustration. Longitudinal stresses at step 26 (splice plates not shown for clarity).

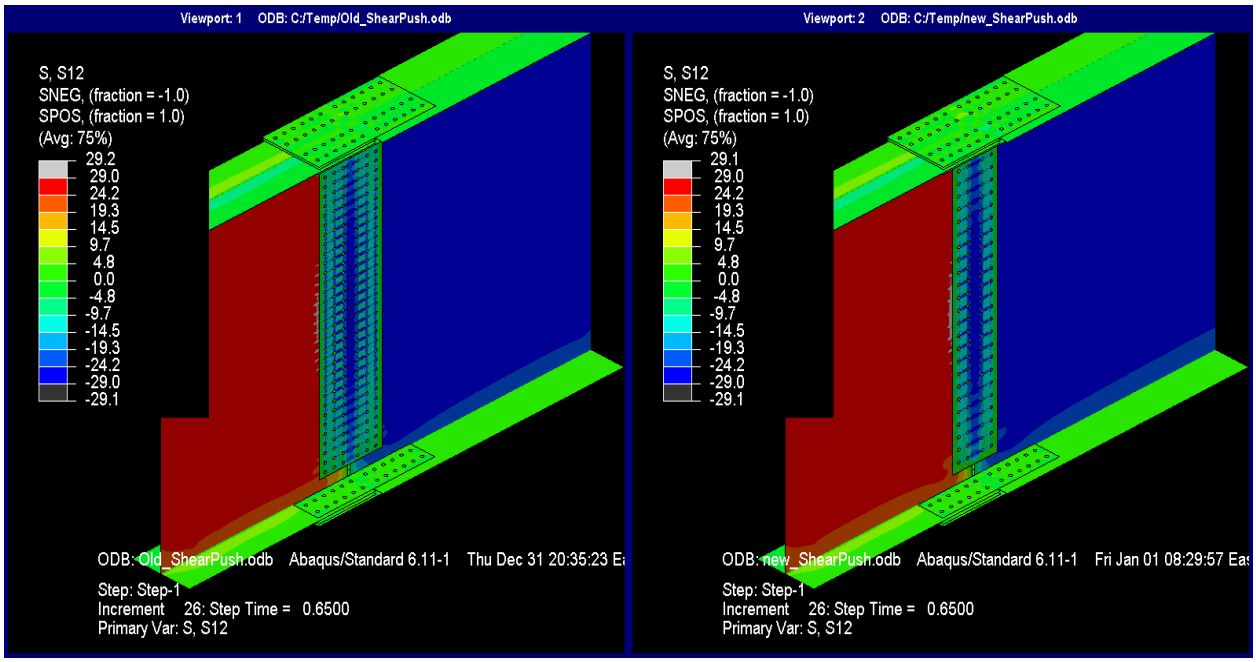

Source: FHWA

Figure 60. Illustration. Shear stresses at step 26.

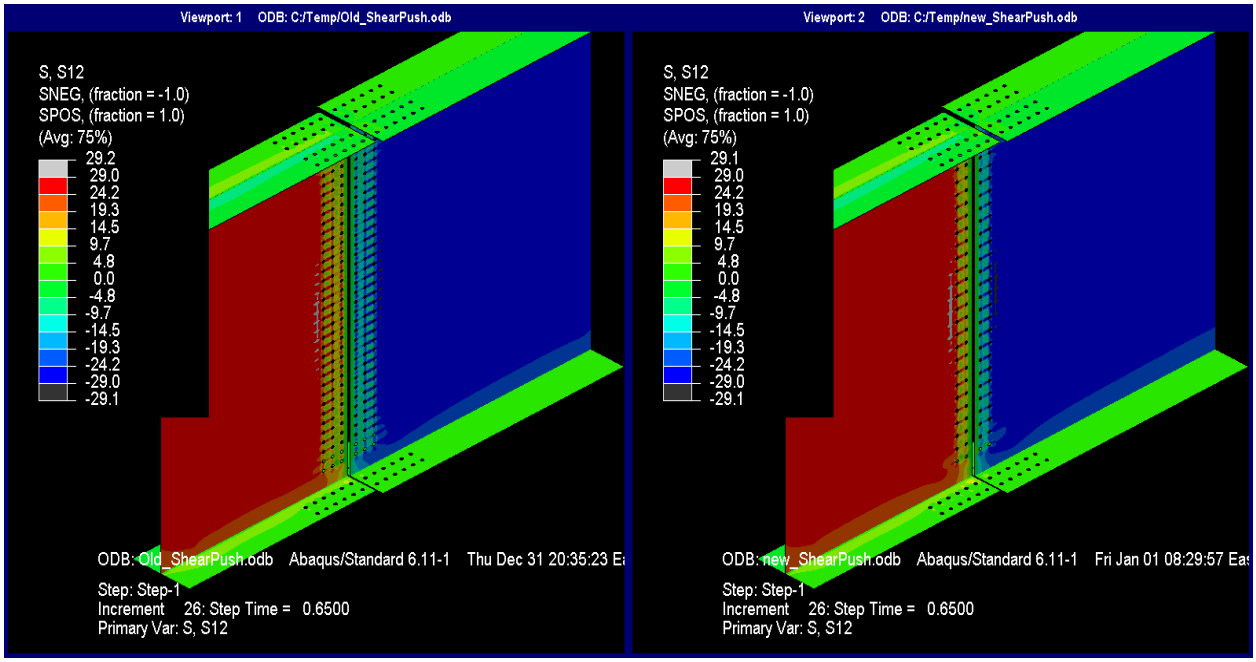

Source: FHWA

Figure 61. Illustration. Shear stresses at step 26 (splice plates not shown for clarity).

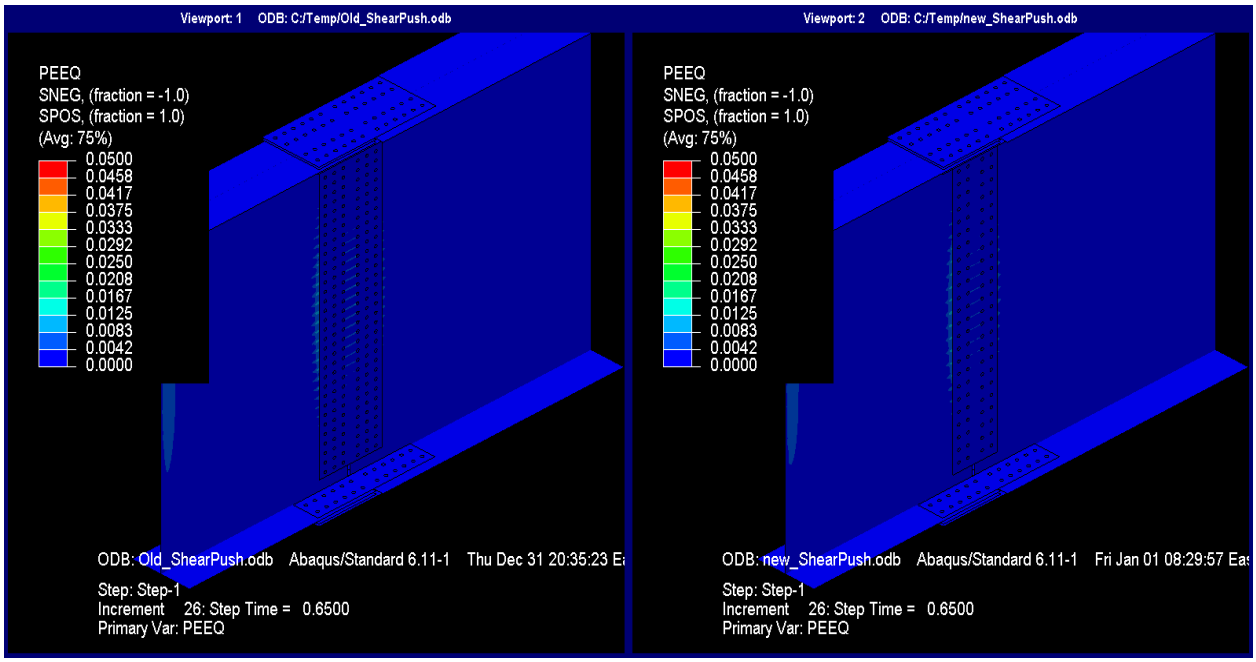

Source: FHWA

Figure 62. Illustration. PEEQ at step 26 (plotted with maximum of 0.05).

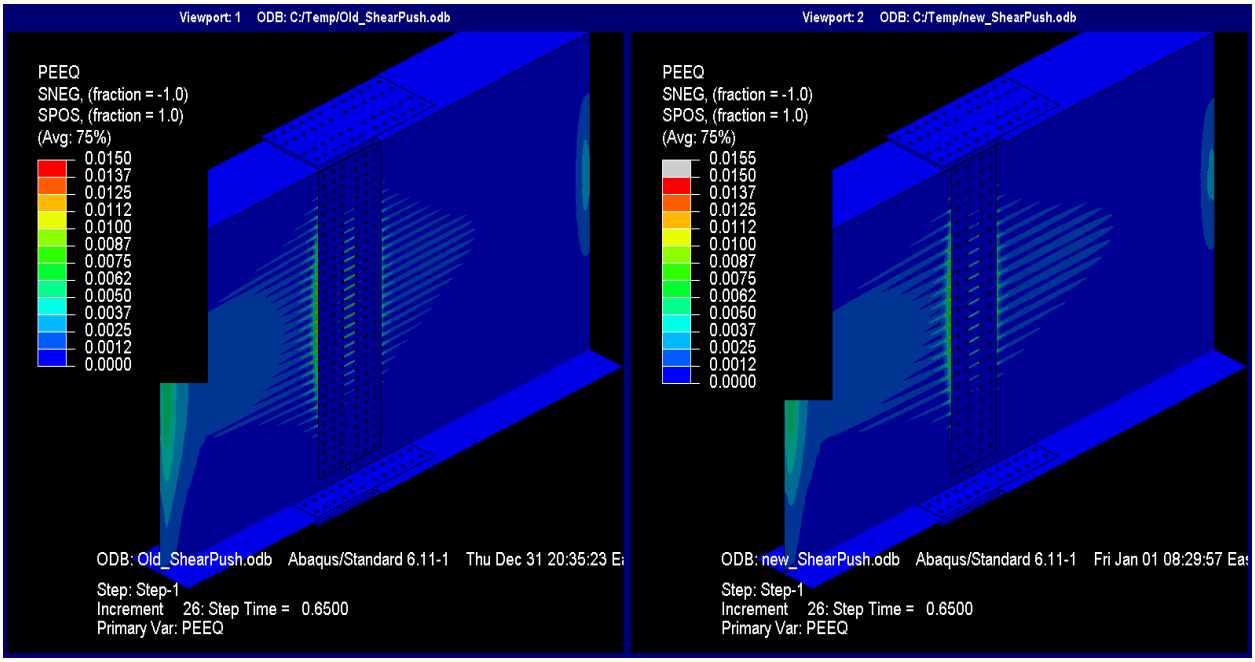

Source: FHWA

Figure 63. Illustration. PEEQ at step 26 (plotted with maximum of 0.015).

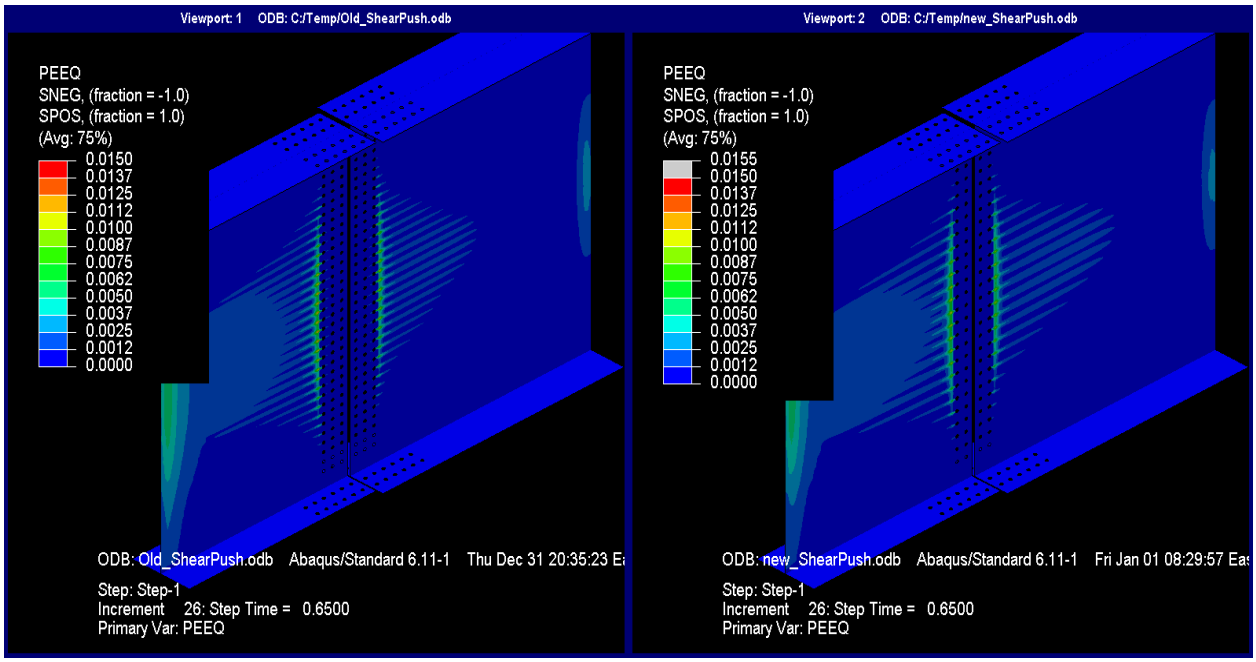

Source: FHWA

Figure 64. Illustration. PEEQ at step 26 (plotted with maximum of 0.015; splice plates not shown for clarity).

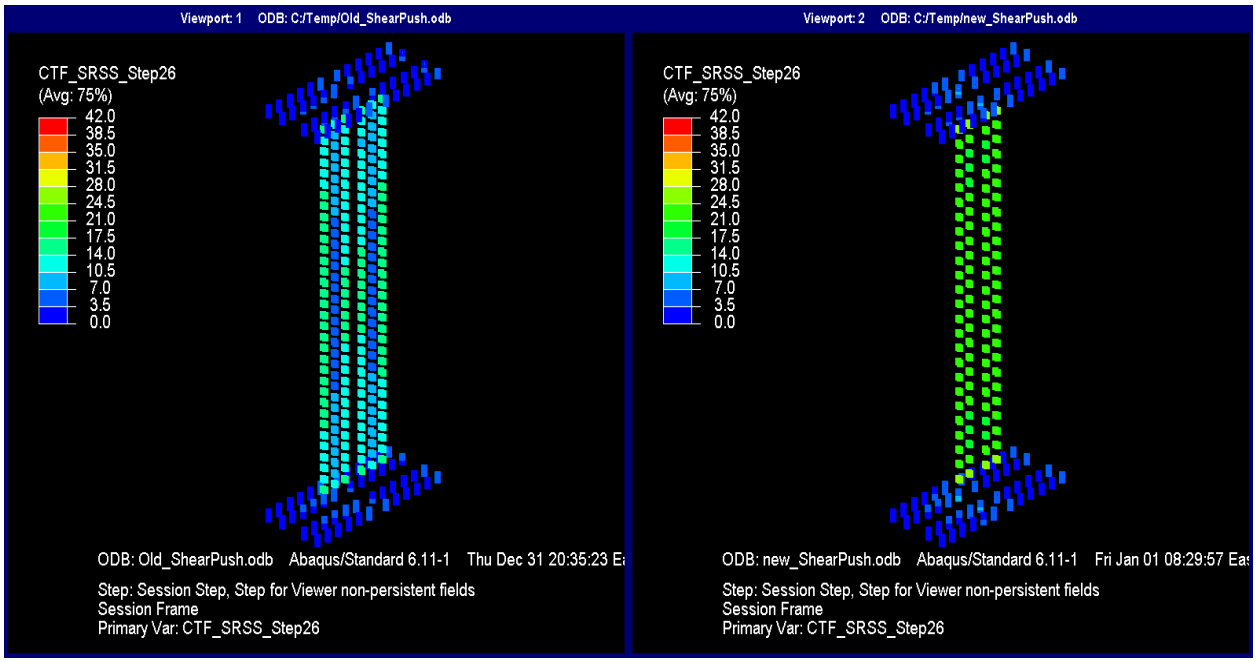

Source: FHWA

Figure 65. Illustration. Resultant forces on bolt shear planes at step 26.

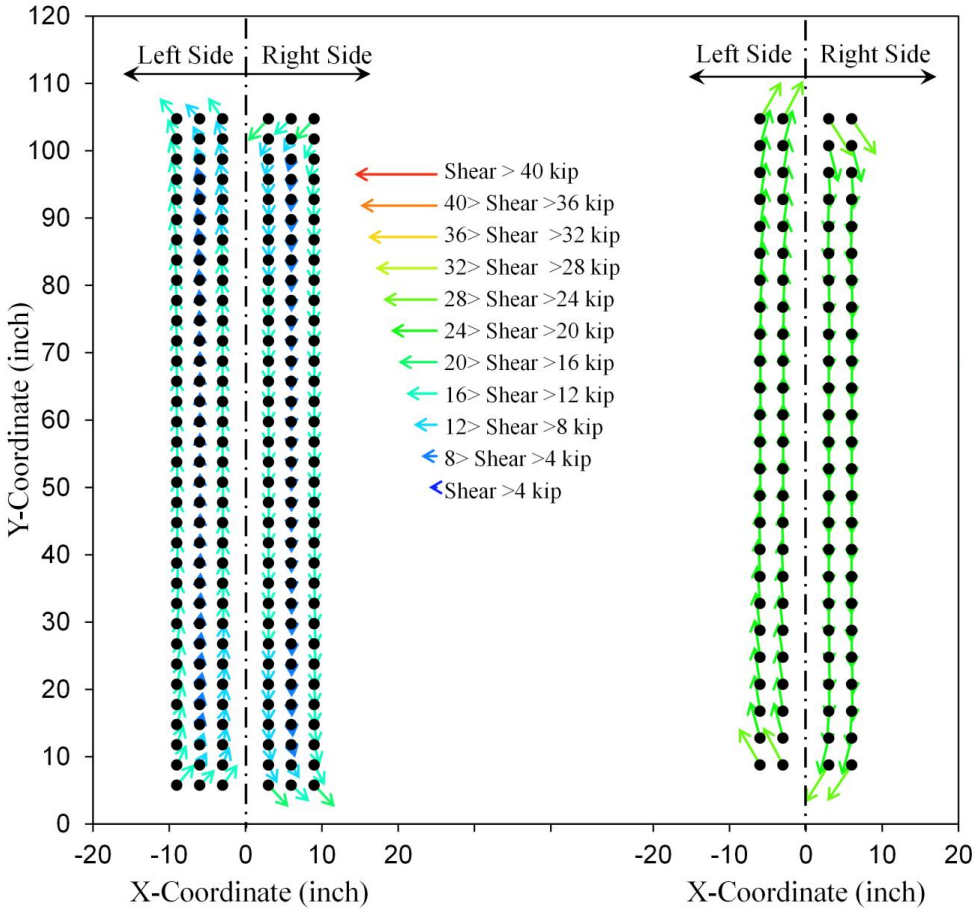

Source: FHWA

Figure 66. Graph. Web splice bolt shear vectors at step 26.

PROPORTIONAL POSITIVE MOMENT AND SHEAR

0 shows a force versus displacement plot for the left support. Circular data points indicate the results from the current method, and square data points indicate the results from the new method. In this scenario, the load was applied to a cantilever beam, so the plateau response demonstrated in each of the methods was not representative of behavior in the bolted connection. The response was due to hinging at the interface between the elastic and inelastic elements in the right girder. However, throughout the loading, the responses were identical. Results in 0 through 0 are presented for step 20, in which V_u = 1,312 kip, while results in 0 through 0 are presented for step 34 just before the plastic hinge formed in the
right girder.

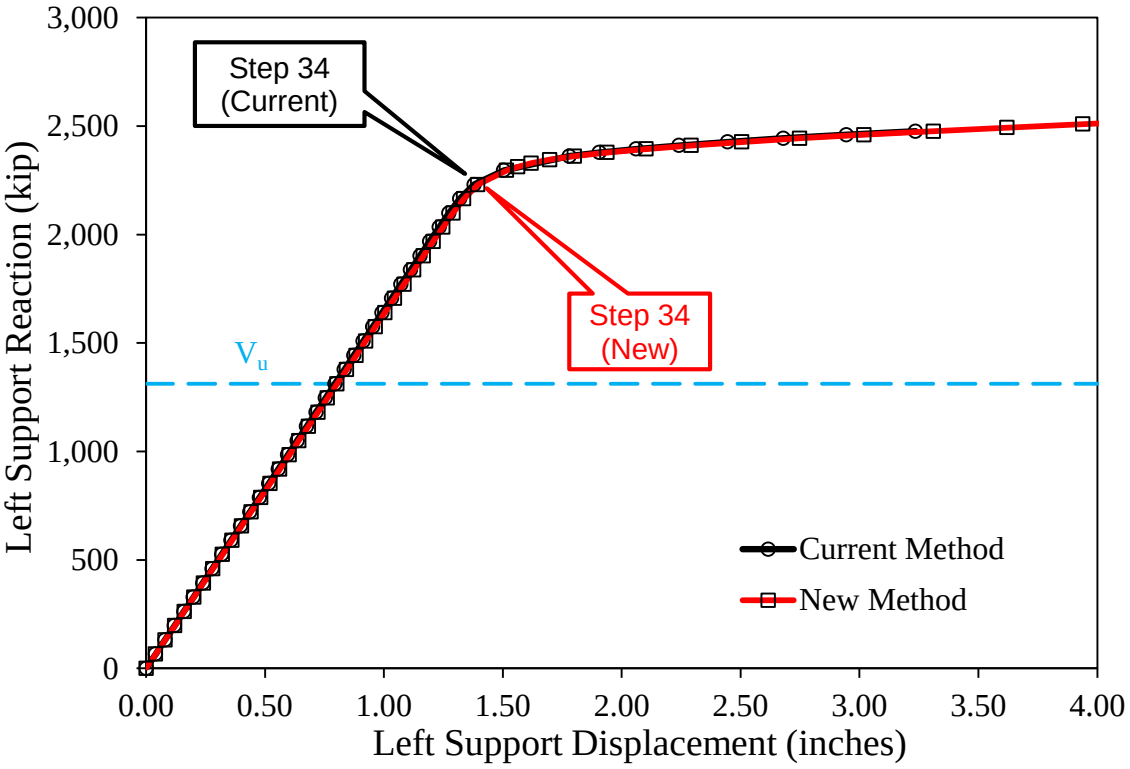

Source: FHWA

Figure 67. Graph. Force versus displacement at left support under proportional positive moment for the splice designed using the current and new methods.

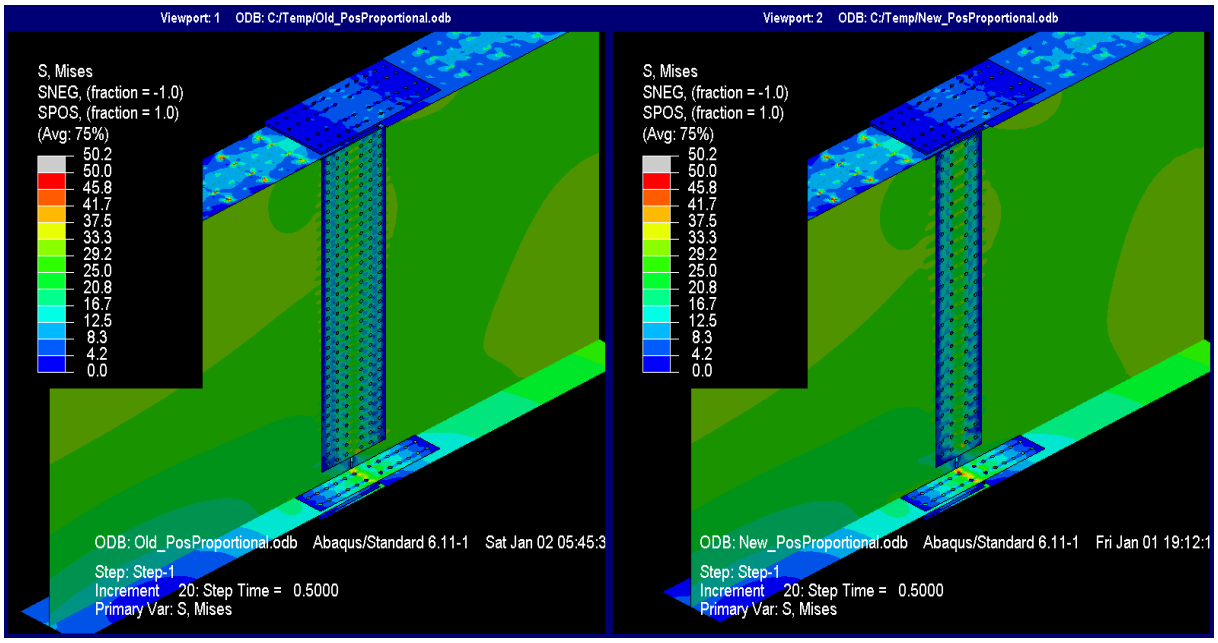

Source: FHWA

Figure 68. Illustration. Mises stresses at proportional positive moment loading at V_u (deck not shown for clarity).

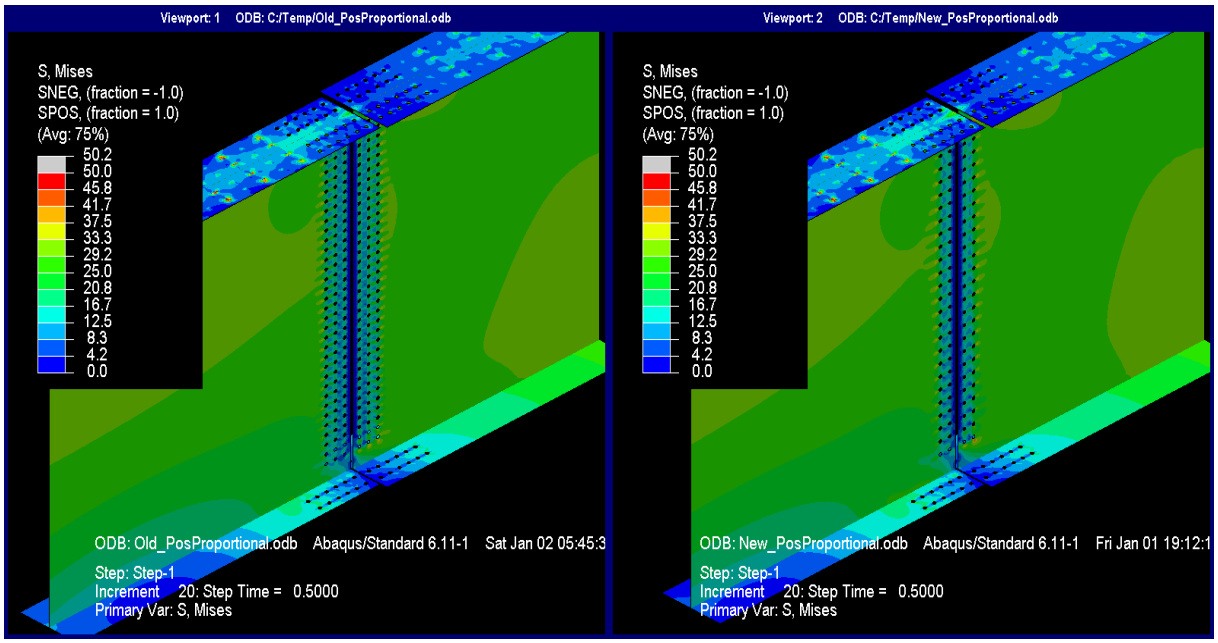

Source: FHWA

Figure 69. Illustration. Mises stresses at proportional positive moment loading at V_u (splice plates and deck not shown for clarity).

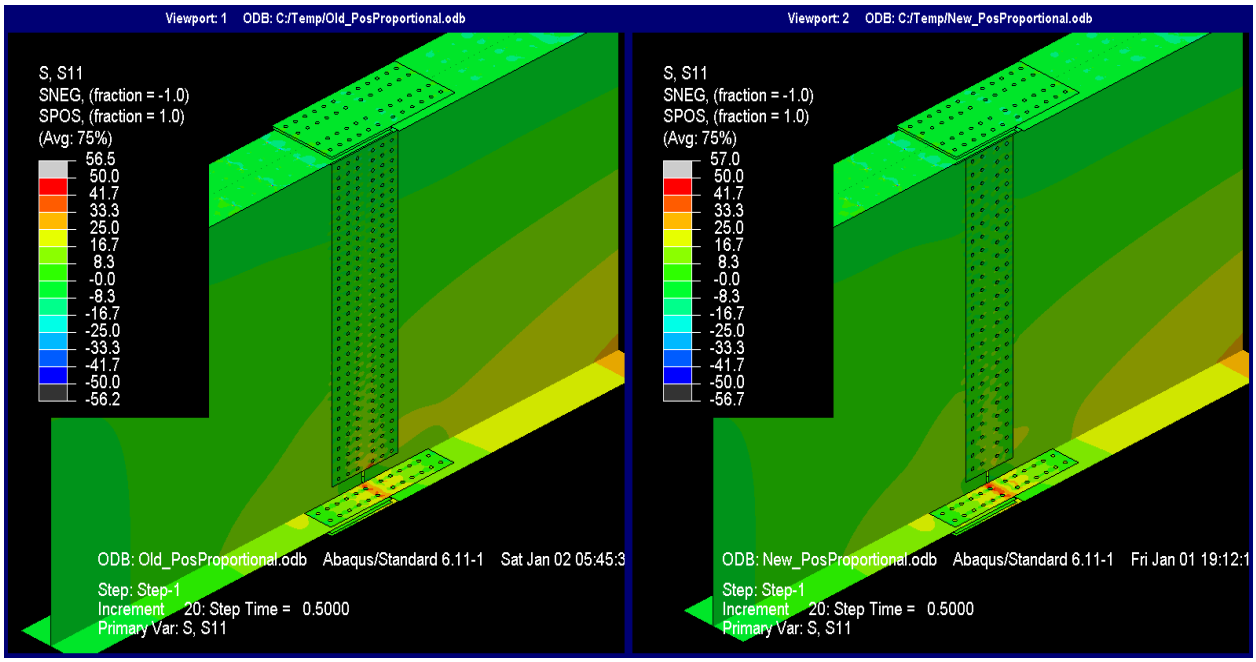

Source: FHWA

Figure 70. Illustration. Longitudinal stresses at proportional positive moment loading at V_u (deck not shown for clarity).

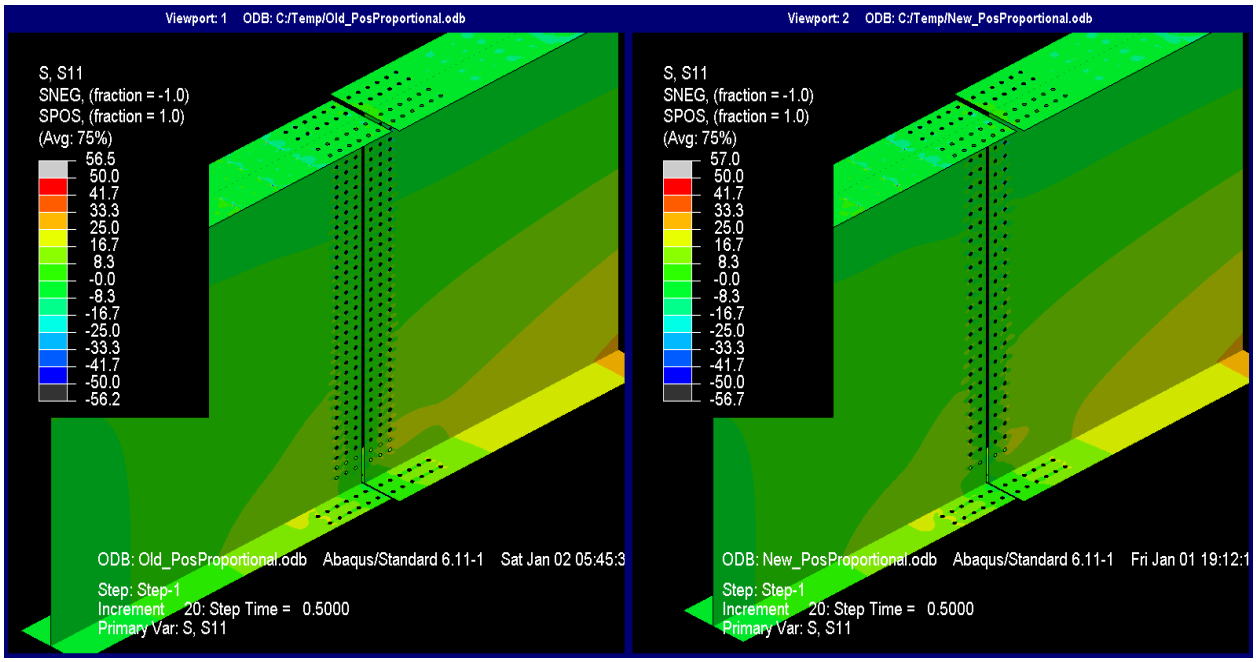

Source: FHWA

Figure 71. Illustration. Longitudinal stresses at proportional positive moment loading at V_u (splice plates and deck not shown for clarity).

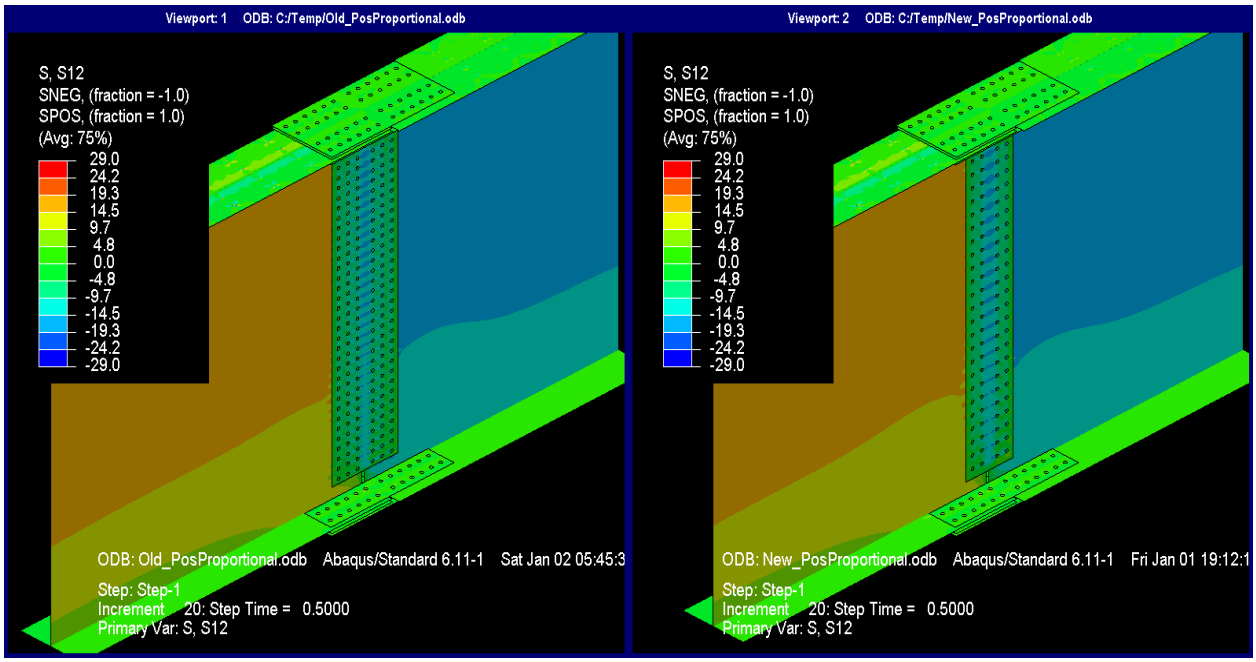

Source: FHWA

Figure 72. Illustration. Shear stresses at proportional positive moment loading at V_u (deck not shown for clarity).

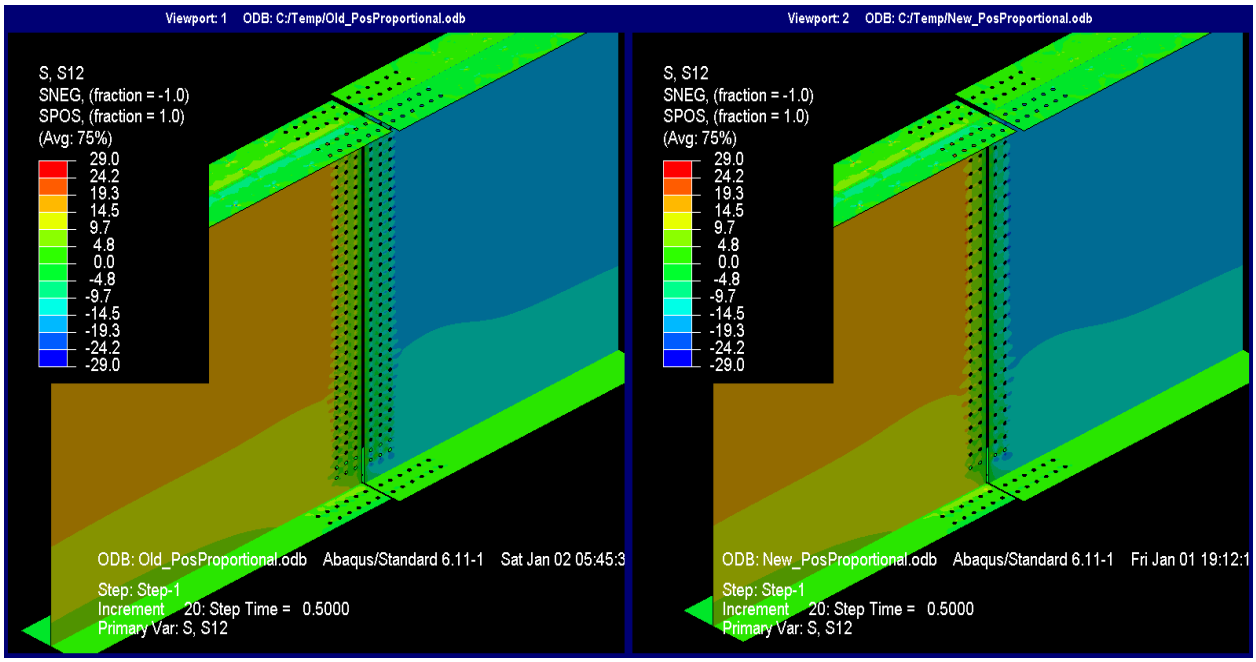

Source: FHWA

Figure 73. Illustration. Shear stresses at proportional positive moment loading at V_u (splice plates and deck not shown for clarity).

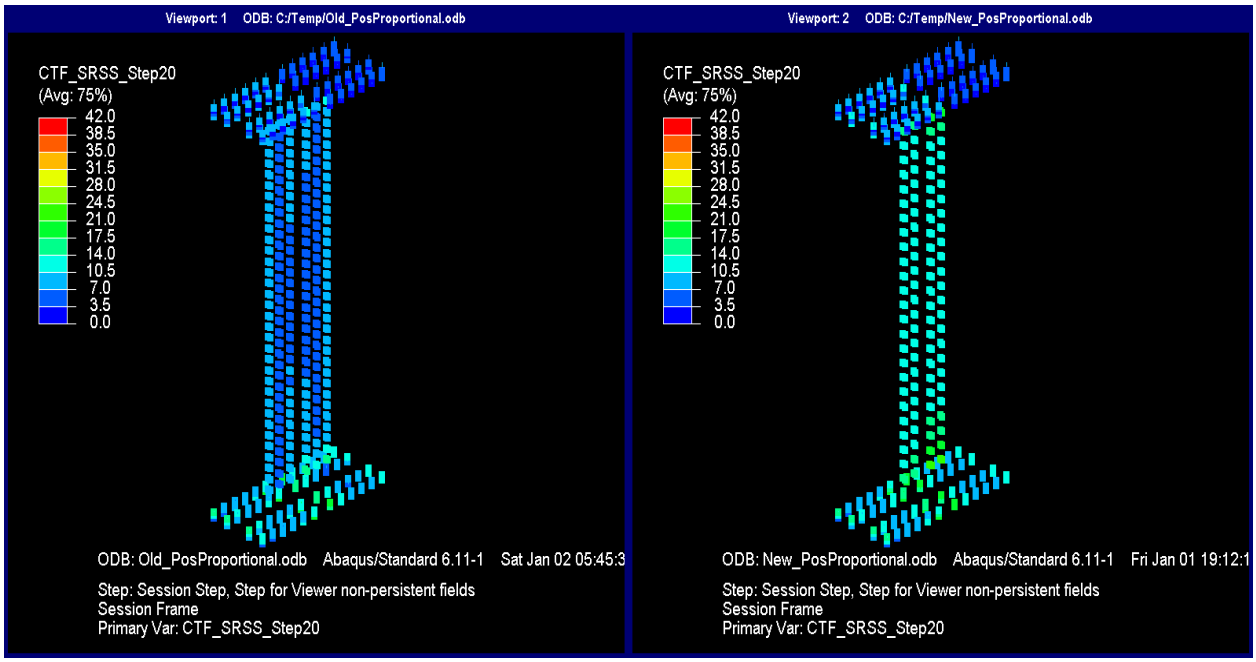

Source: FHWA

Figure 74. Illustration. Resultant forces on bolt shear planes at proportional positive moment loading at V_u.

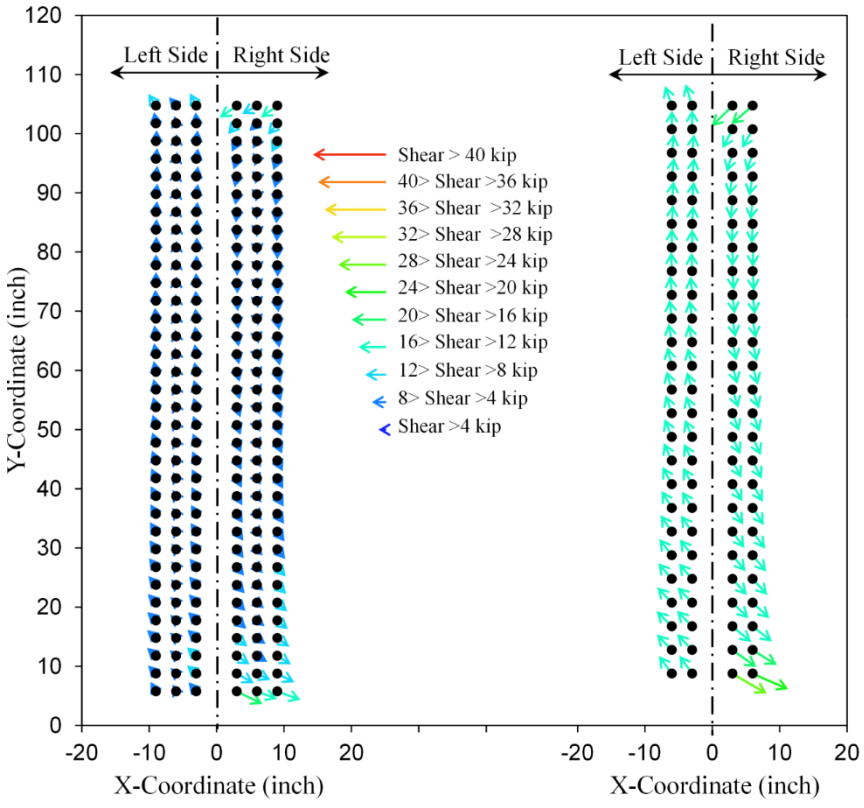

Source: FHWA

Figure 75. Graph. Web splice bolt shear vectors at proportional positive moment loading at V_u.

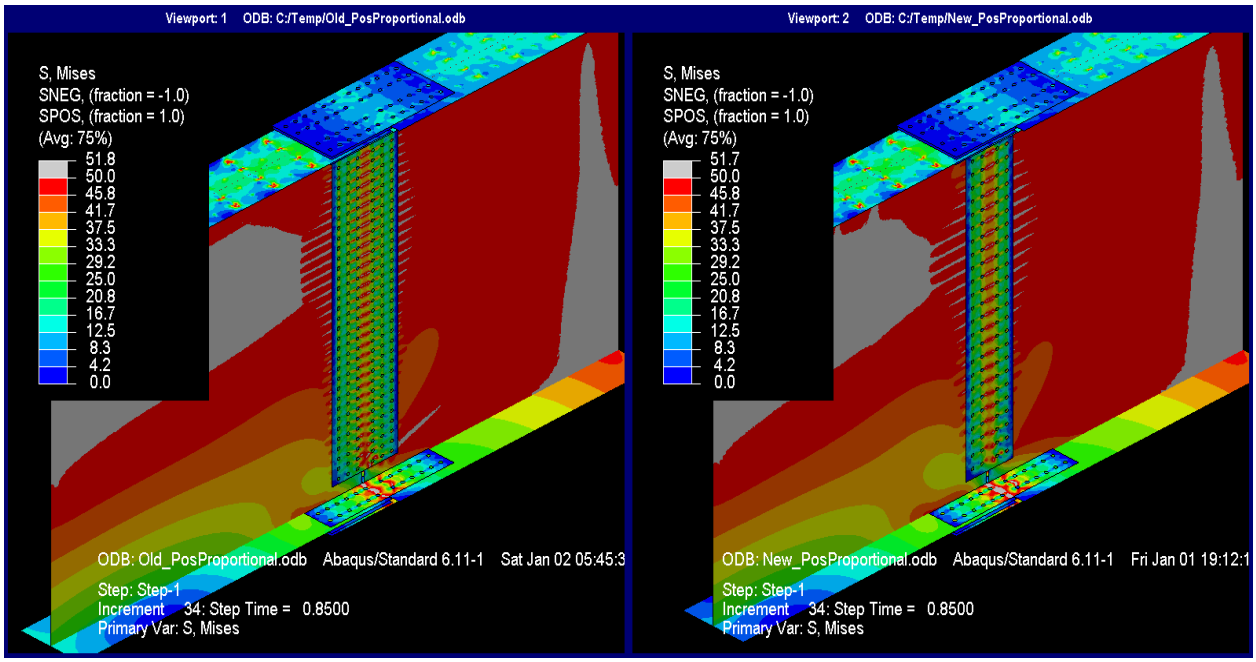

Source: FHWA

Figure 76. Illustration. Mises stresses at step 34 (deck not shown for clarity).

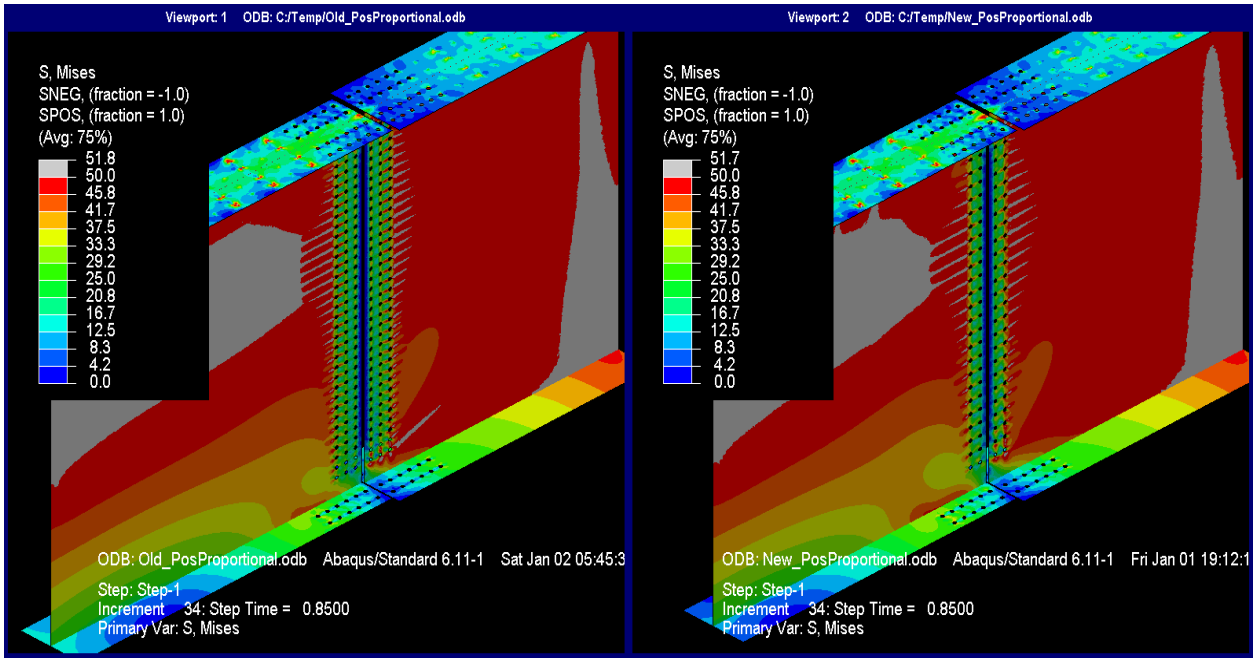

Source: FHWA

Figure 77. Illustration. Mises stresses at step 34 (splice plates and deck not shown for clarity).

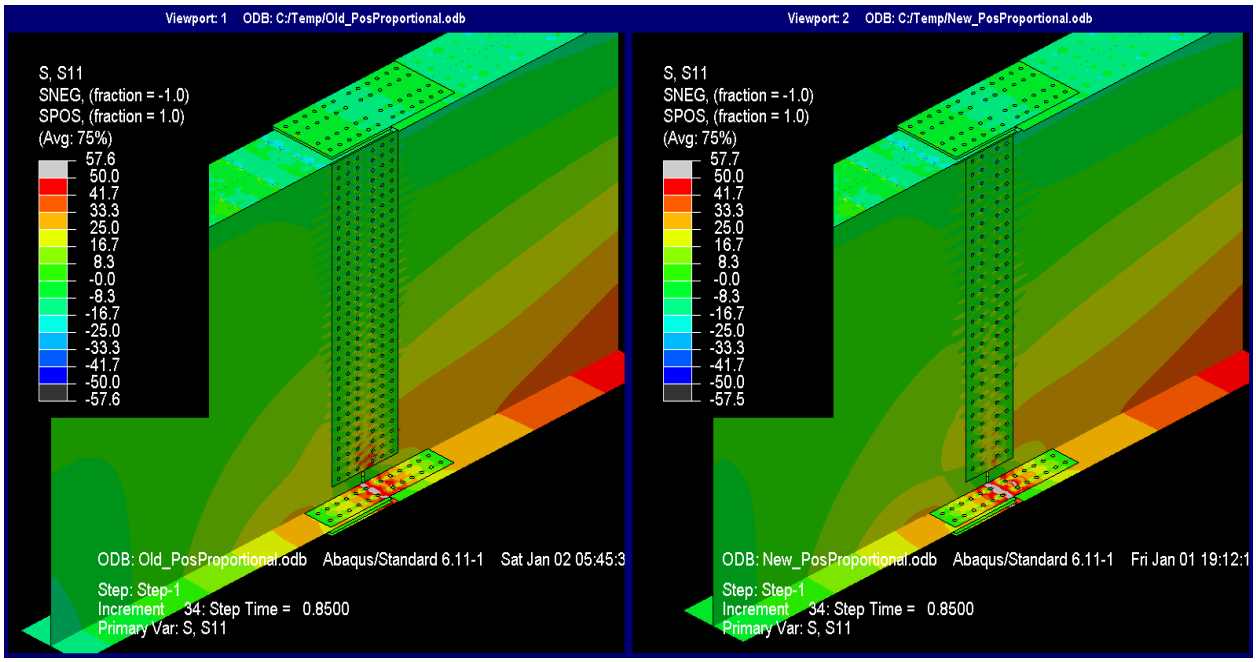

Source: FHWA

Figure 78. Illustration. Longitudinal stresses at step 34 (deck not shown for clarity).

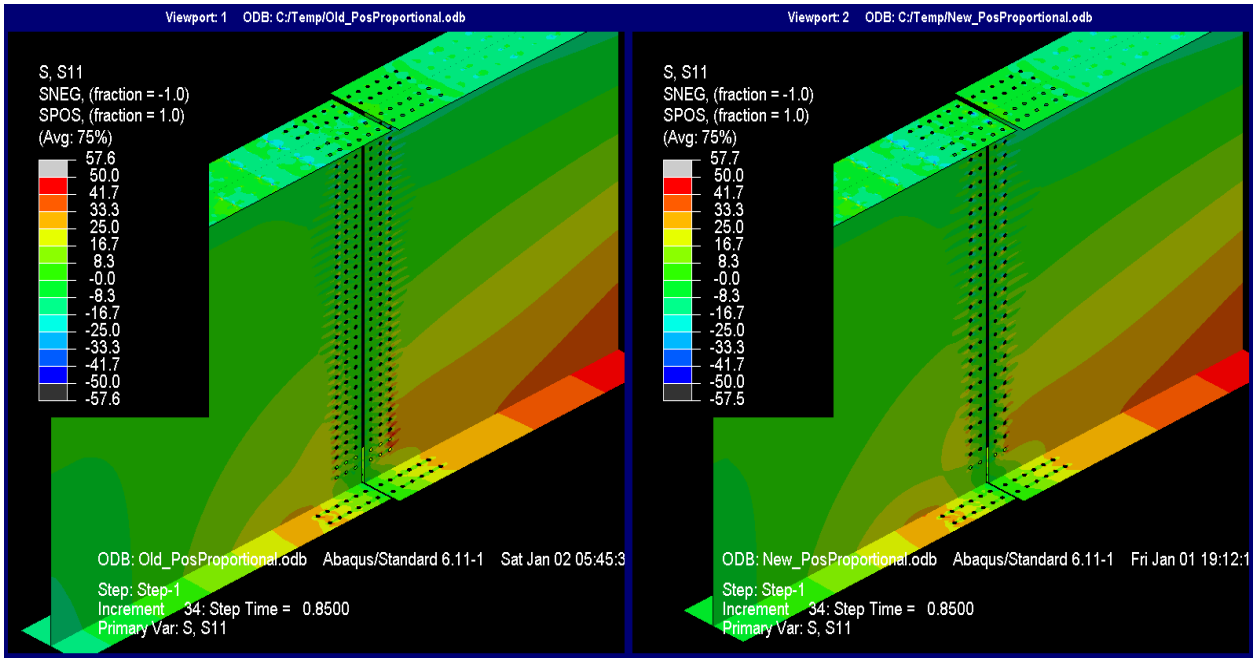

Source: FHWA

Figure 79. Illustration. Longitudinal stresses at step 34 (splice plates and deck not shown for clarity).

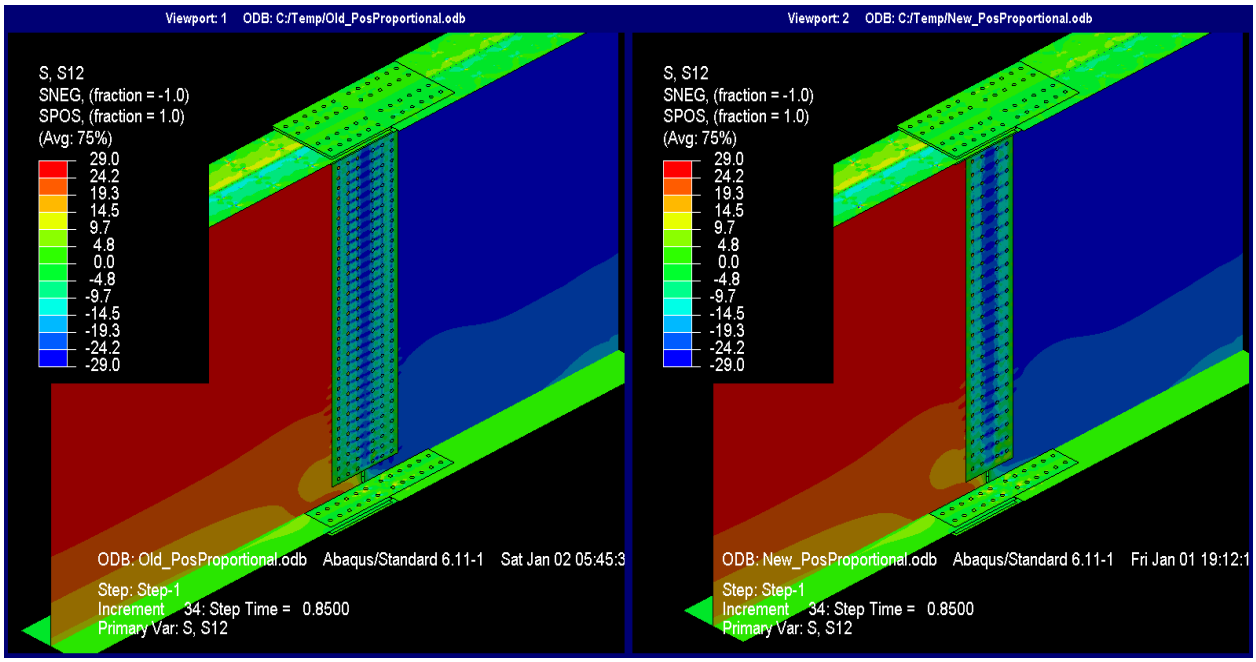

Source: FHWA

Figure 80. Illustration. Shear stresses at step 34 (deck not shown for clarity).

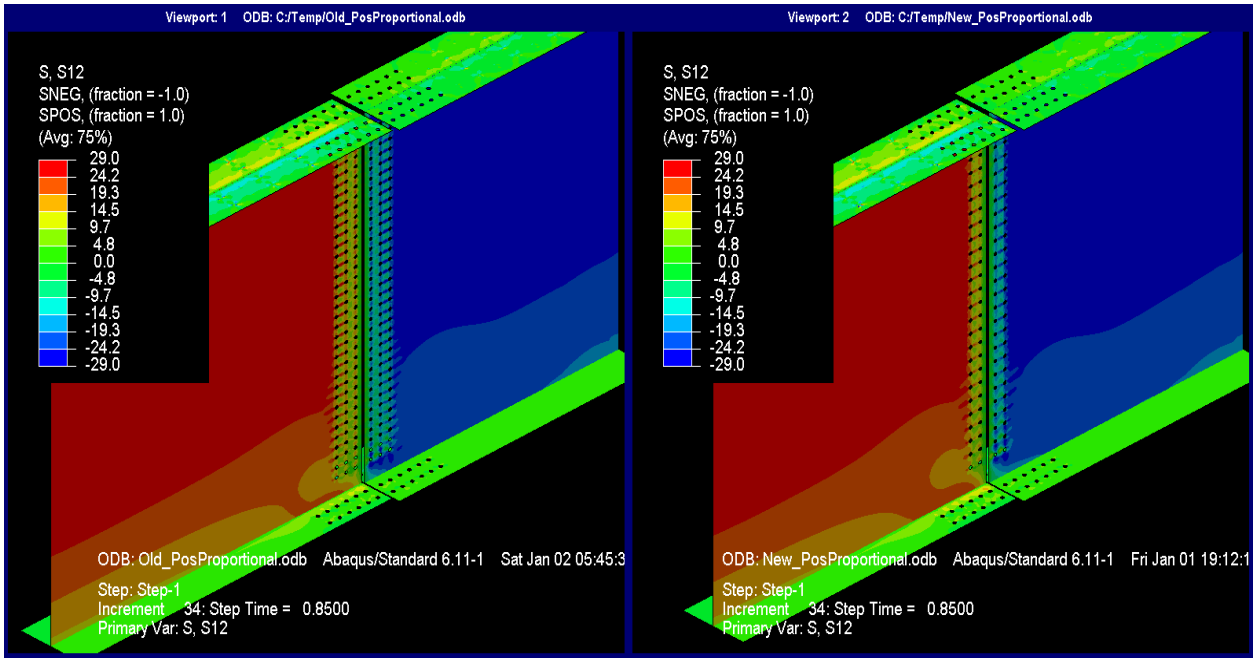

Source: FHWA

Figure 81. Illustration. Shear stresses at step 34 (splice plates and deck not shown for clarity).

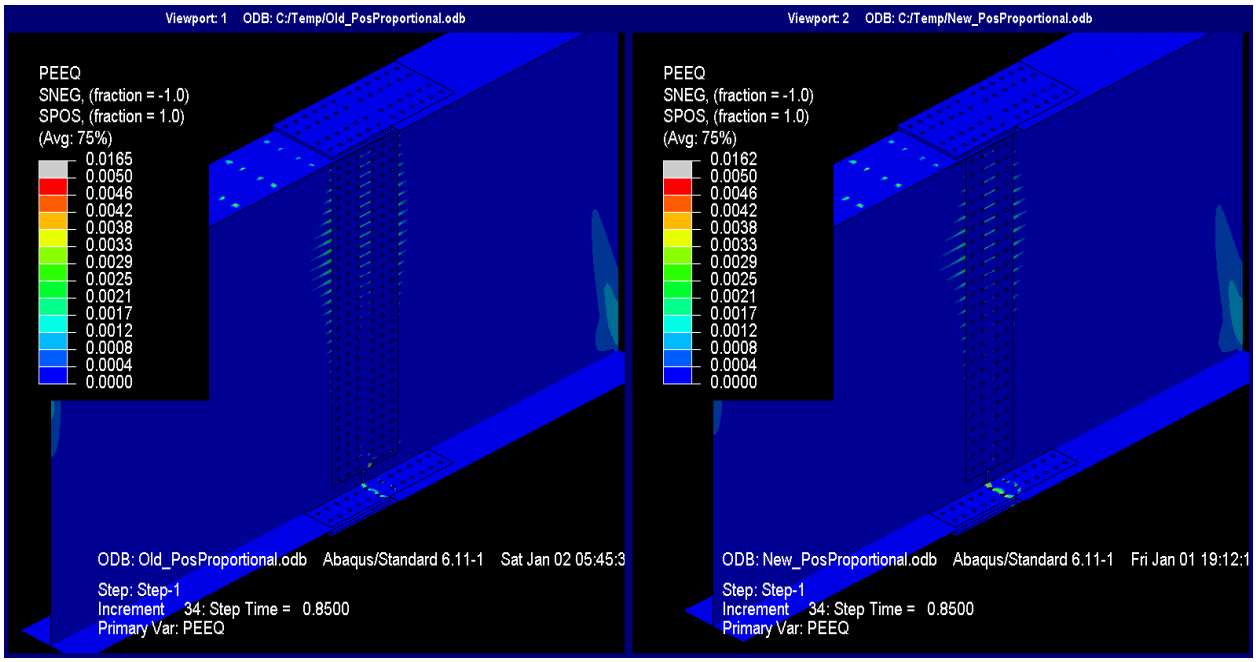

Source: FHWA

Figure 82. Illustration. PEEQ at step 34 (deck not shown for clarity).

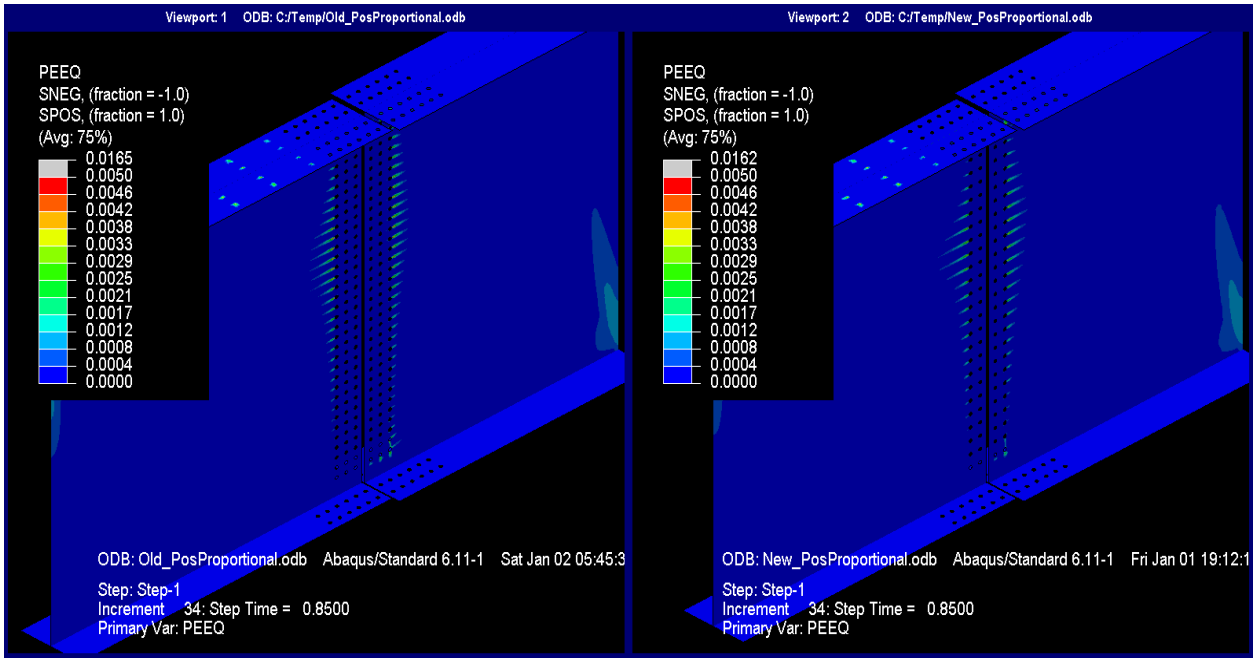

Source: FHWA

Figure 83. Illustration. PEEQ at step 34 (splice plates and deck not shown for clarity).

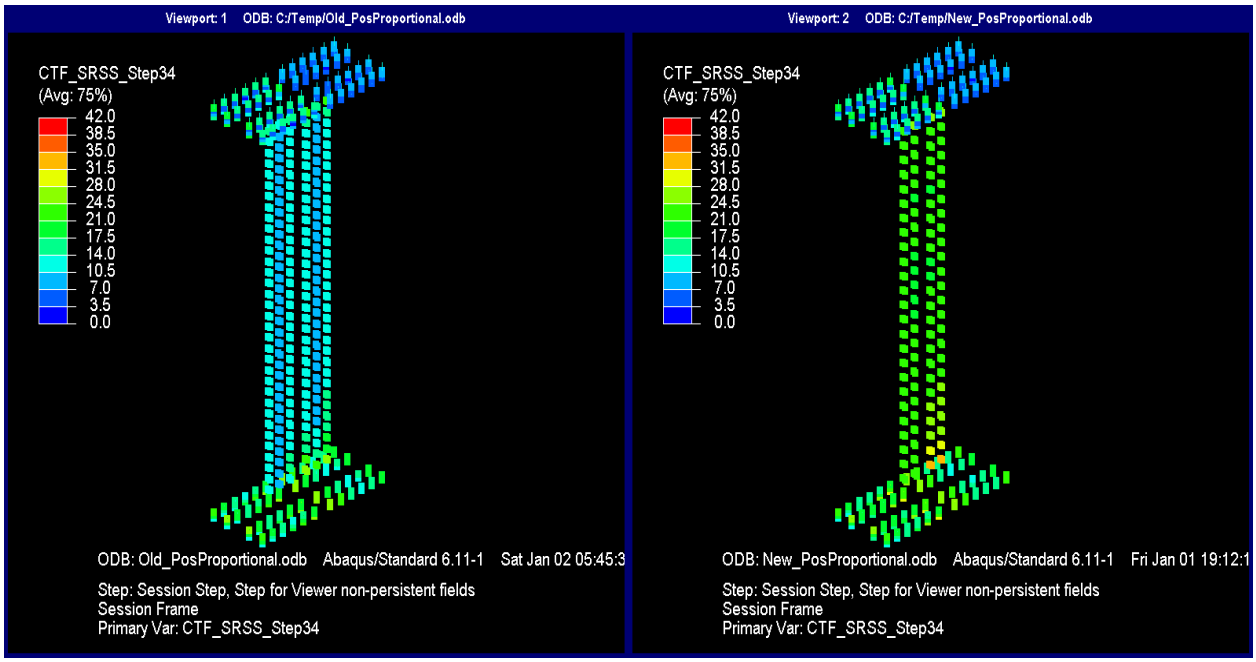

Source: FHWA

Figure 84. Illustration. Resultant forces on bolt shear planes at step 34.

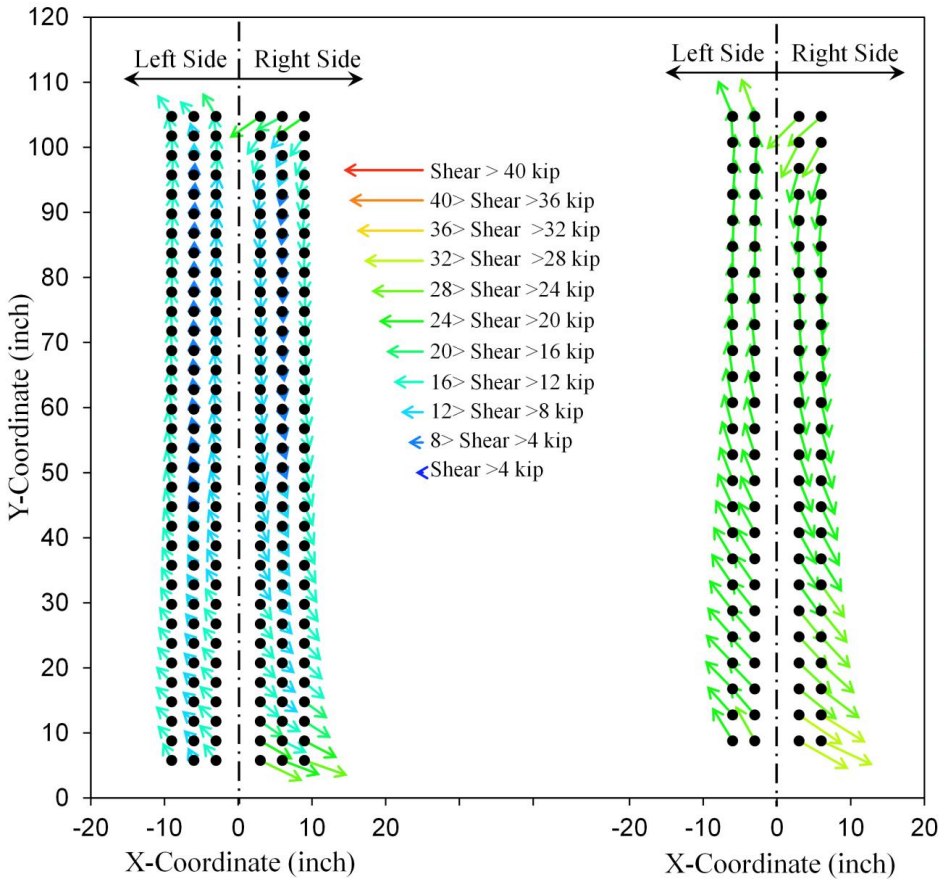

Source: FHWA

Figure 85. Graph. Web splice bolt shear vectors step 34.

At the design force level, the system was elastic (see 0 and 0). Bolt forces were slightly higher for the splice designed using the new method but were well within their design limits (see 0 and 0).

At step 34, the applied shear was 2,230 kip, which was 70 percent higher than the design shear. The Mises stresses showed yielding in the upper portion of the left girder and yielding over nearly the full depth at the interface between the elastic and inelastic elements on the right girder (see 0 and 0). It may seem odd to see the left girder yield near the top flange in a positive proportional moment scenario; however, as seen in 0, in this scenario, a negative moment had to be applied at the left support to attain a positive design moment at the bolted splice. Further analysis of the longitudinal and shear stress plots showed that the yielding was dominated by the shear stresses as they were closest to their yielding limit (see 0 and 0). The PEEQ plots in 0 and 0 showed similar response in the web, although slightly higher demands existed on the flange splice plates in the splice designed using the new design methodology. The bolt forces shown in 0 were within their design limits, although the forces were expectedly larger in the splice designed using the new method. The bolt force vectors in 0 were primarily vertical, indicating that the shear in the girder was dominating the force in the bolts. However, the vectors for bolts closest to the flanges had horizontal components, and there was a characteristic rotation of all the vectors around a point near the girder neutral axis, indicating that the web splice did carry some moment.

PROPORTIONAL NEGATIVE MOMENT AND SHEAR (NO DECK)

0 shows a force versus displacement plot for the left support. Circular data points indicate the results from the current method, and square data points indicate the results from the new method. Elastically, the behaviors were similar, although once inelasticity started, the splice designed using the new method demonstrated slightly lower strength. There was also a difference in where the analysis terminated. For the splice designed by the current method, the analysis was terminated after step 36 because the strength was not appreciably increasing. However, for the splice designed by the new method, the analysis could not converge to a solution beyond step 32, which was a result of some bolts reaching their capacity.

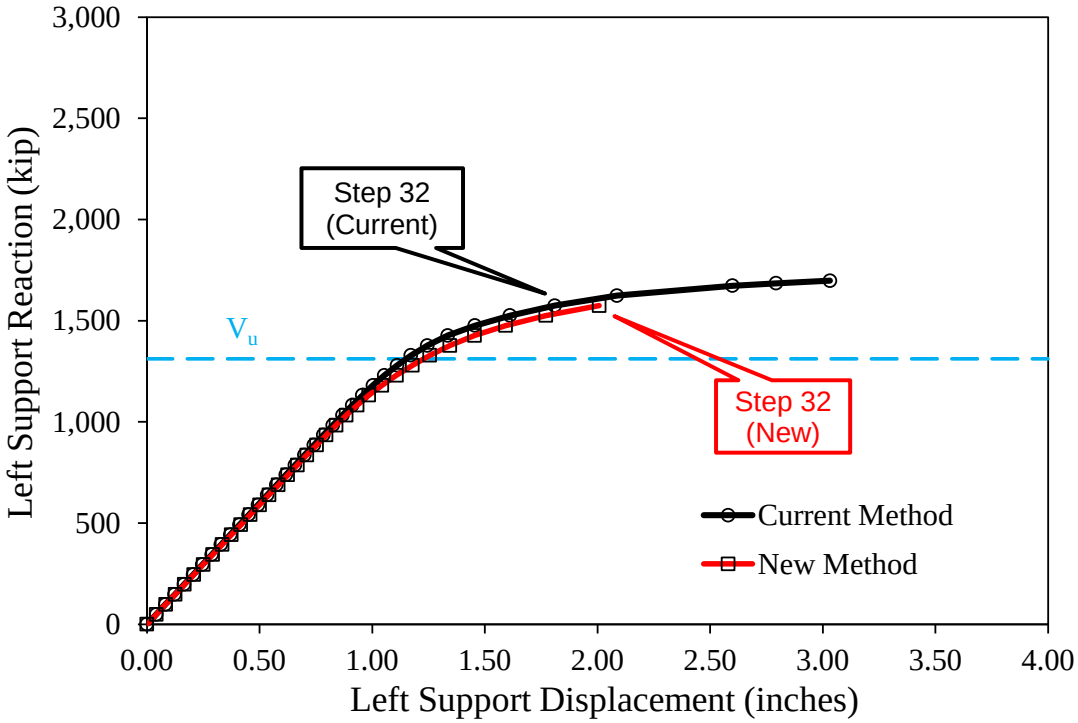

Source: FHWA

Figure 86. Graph. Force versus displacement at the left support under proportional negative moment for the splice designed using the current and new methods.

Contour plot data are presented in 0 through 0 at the design loading (i.e., step 27 in 0). The splice plates, a small portion of the right girder web near the top and bottom of the web splice, and the web splice had started to yield in the splice designed with both methods (see 0 and 0). The longitudinal stress plot indicates that most of the yielding was dominated by the longitudinal stresses generated from the moment (see 0 and 0). The PEEQ plots show that any significant yielding was primarily isolated to just the flange splice plates and was slightly greater in the splice designed using the new method (see 0
and 0). The resultant bolt forces show that the lead bolts on the flange splices had shear forces in the low 30-kip range in the splices designed by each method. The corner web bolts
in the splice designed using the new method had bolt forces in the upper 30-kip range (see 0) versus the mid-20 kip for the current design method. This is more easily seen in
0 where the corner bolts on the right girder section were the most highly loaded, and the bolt forces were obviously lower in the splice designed using the current method because twice as many bolts were provided. The bolt vectors were primarily horizontal, indicating that the moment in the girders was controlling the forces in the bolts.

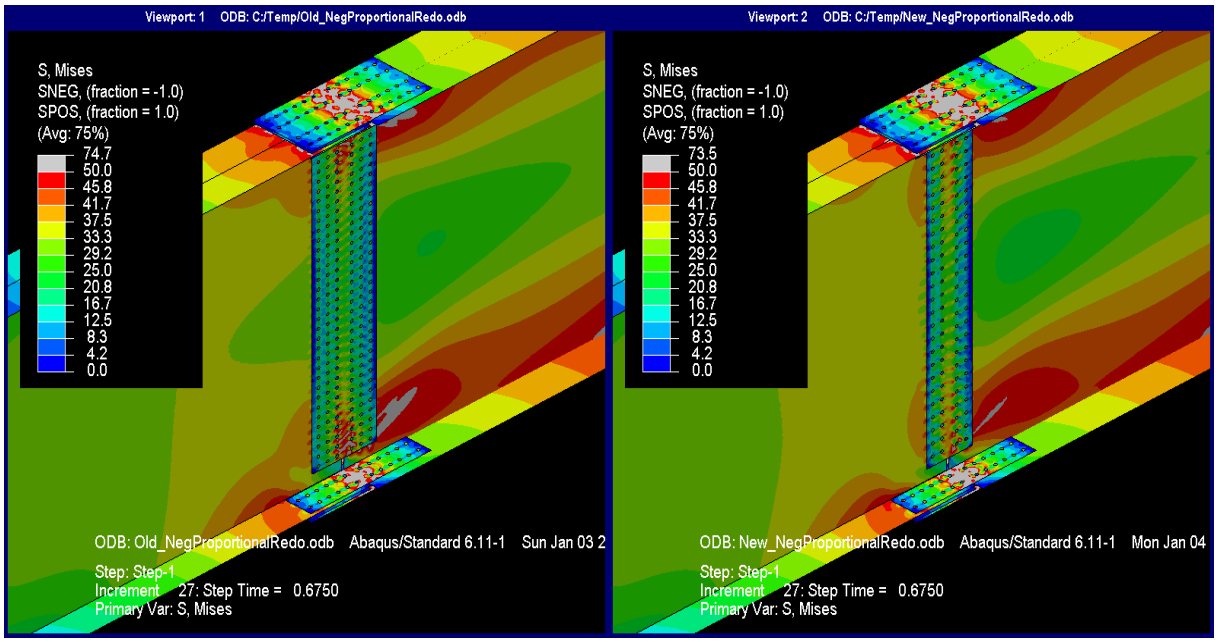

Source: FHWA

Figure 87. Illustration. Mises stresses at proportional negative moment at V_u.

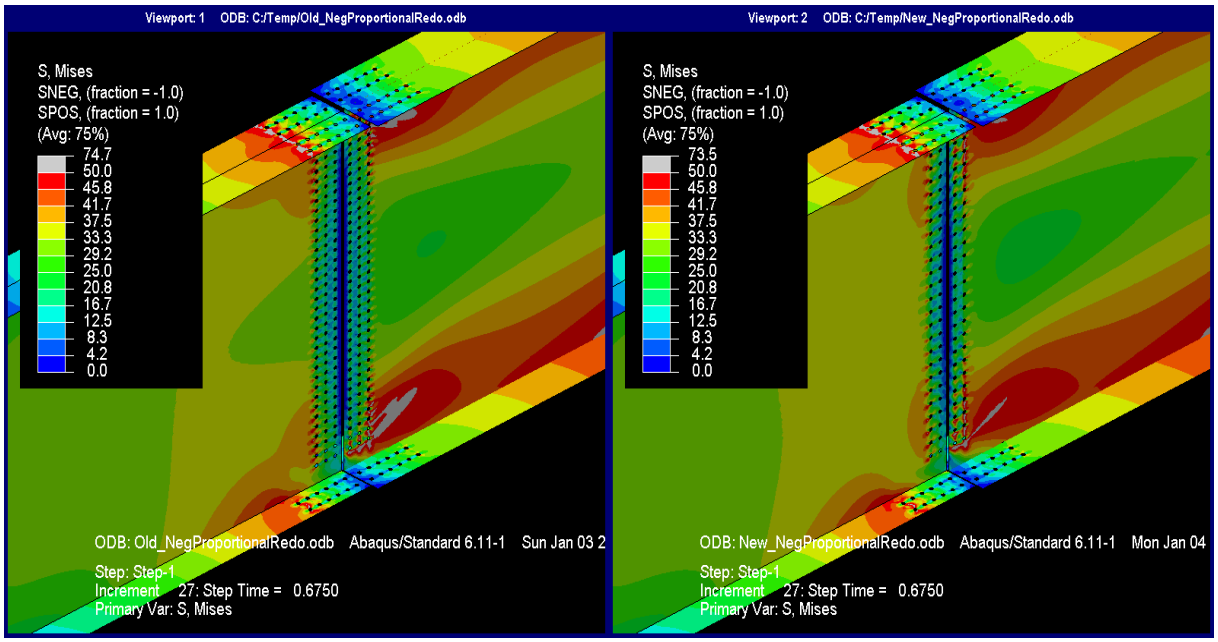

Source: FHWA

Figure 88. Illustration. Mises stresses at proportional negative moment at V_u (splice plates not shown for clarity).

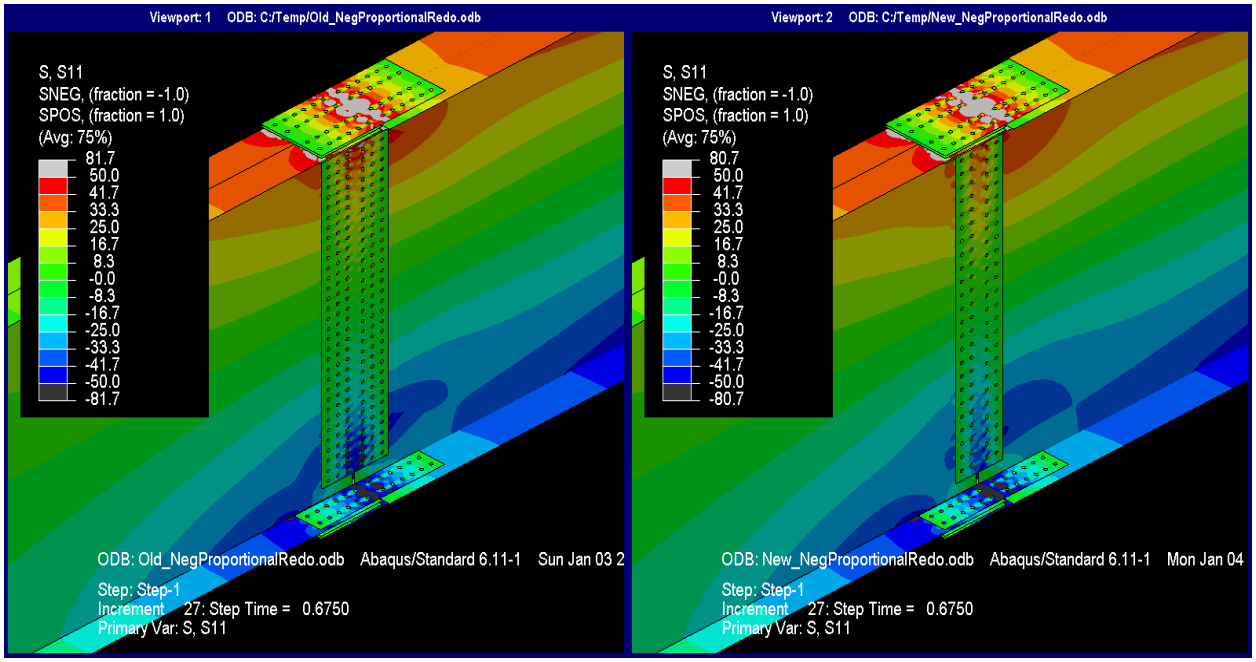

Source: FHWA

Figure 89. Illustration. Longitudinal stresses at proportional negative moment at V_u.

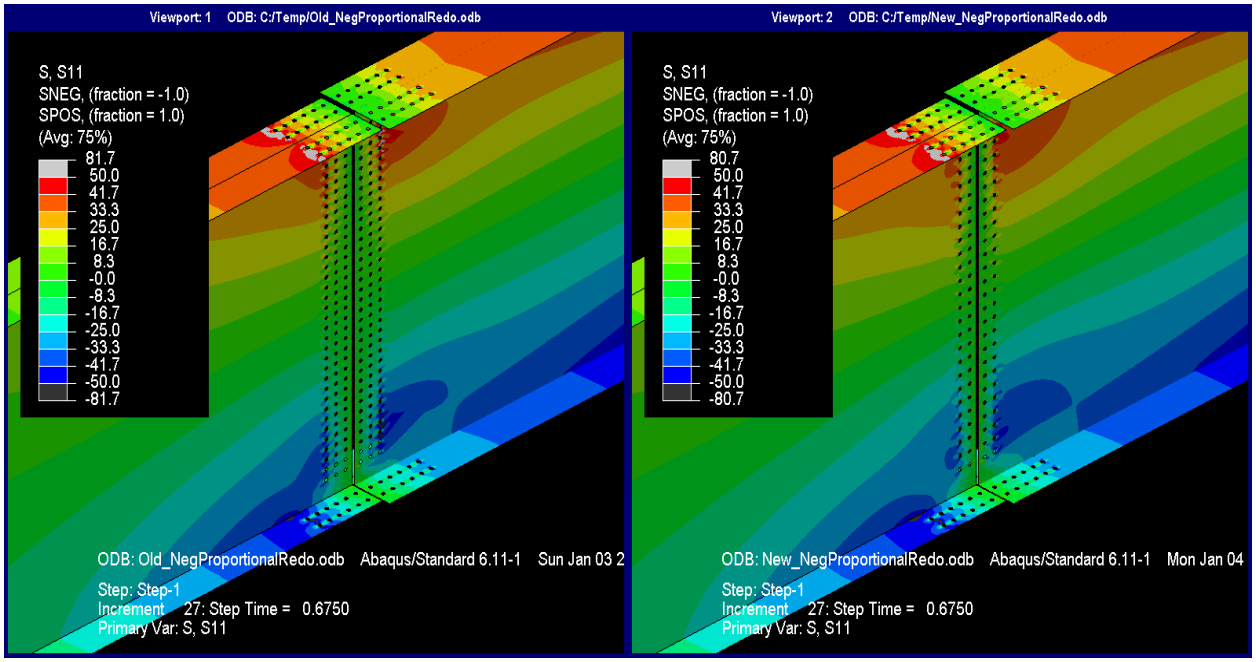

Source: FHWA

Figure 90. Illustration. Longitudinal stresses at proportional negative moment at V_u (splice plates not shown for clarity).

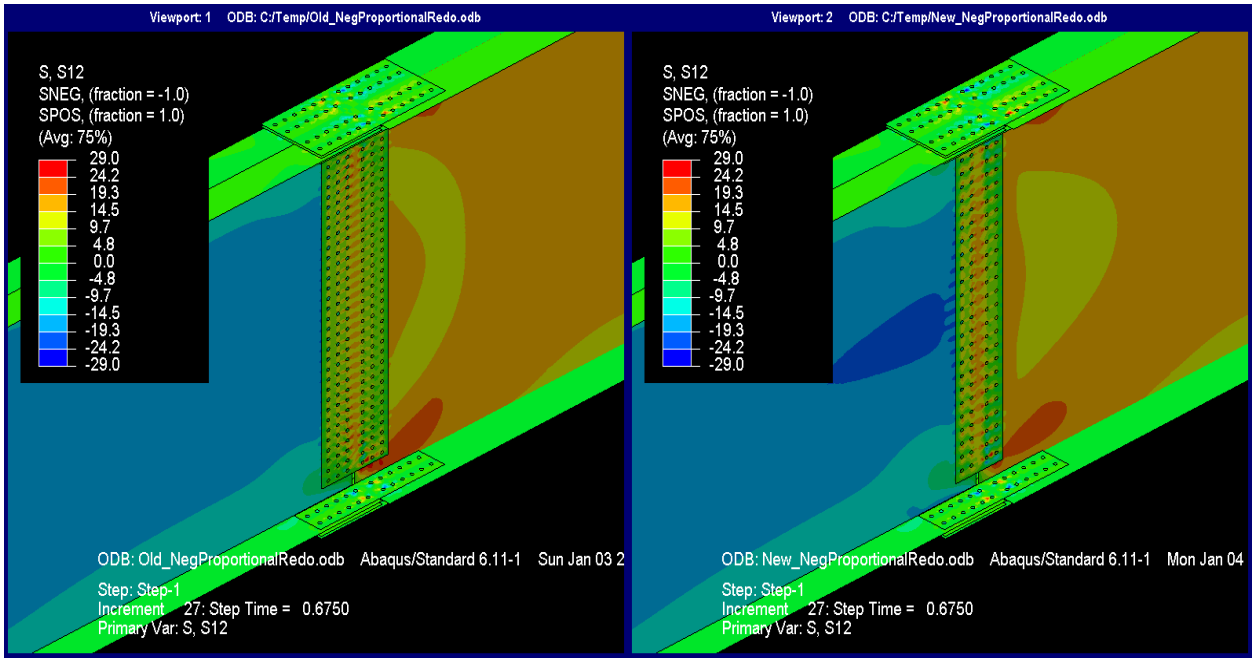

Source: FHWA

Figure 91. Illustration. Shear stresses at proportional negative moment at V_u.

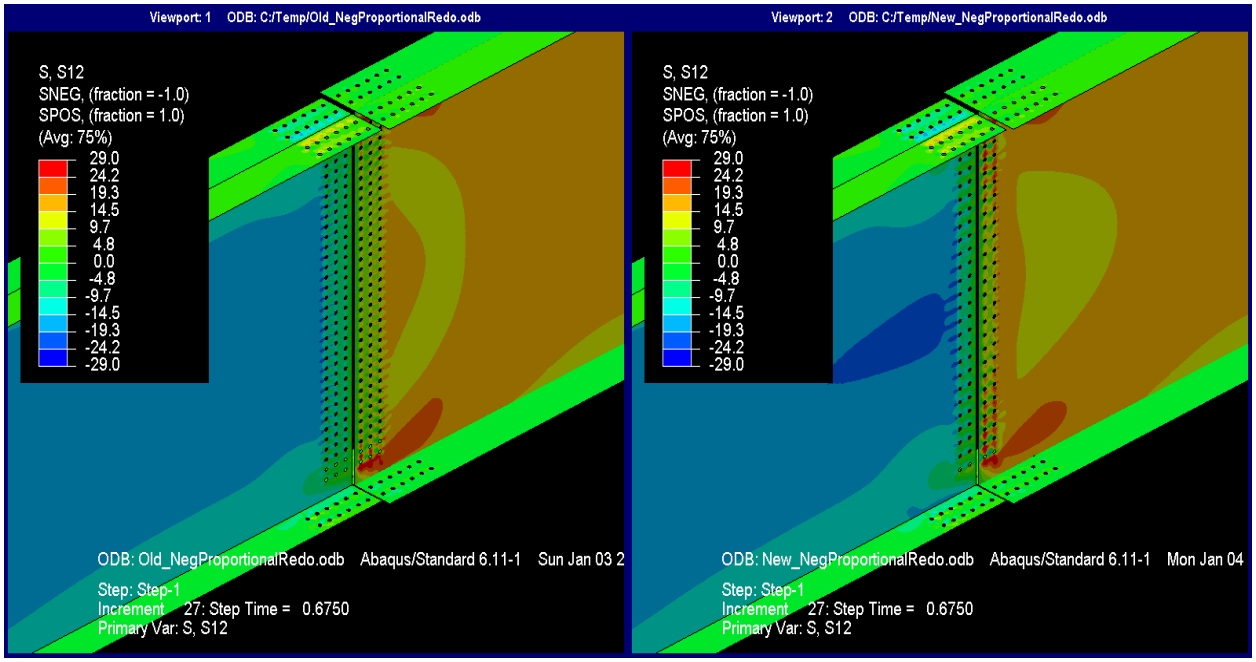

Source: FHWA

Figure 92. Illustration. Shear stresses at proportional negative moment at V_u (splice plates not shown for clarity).

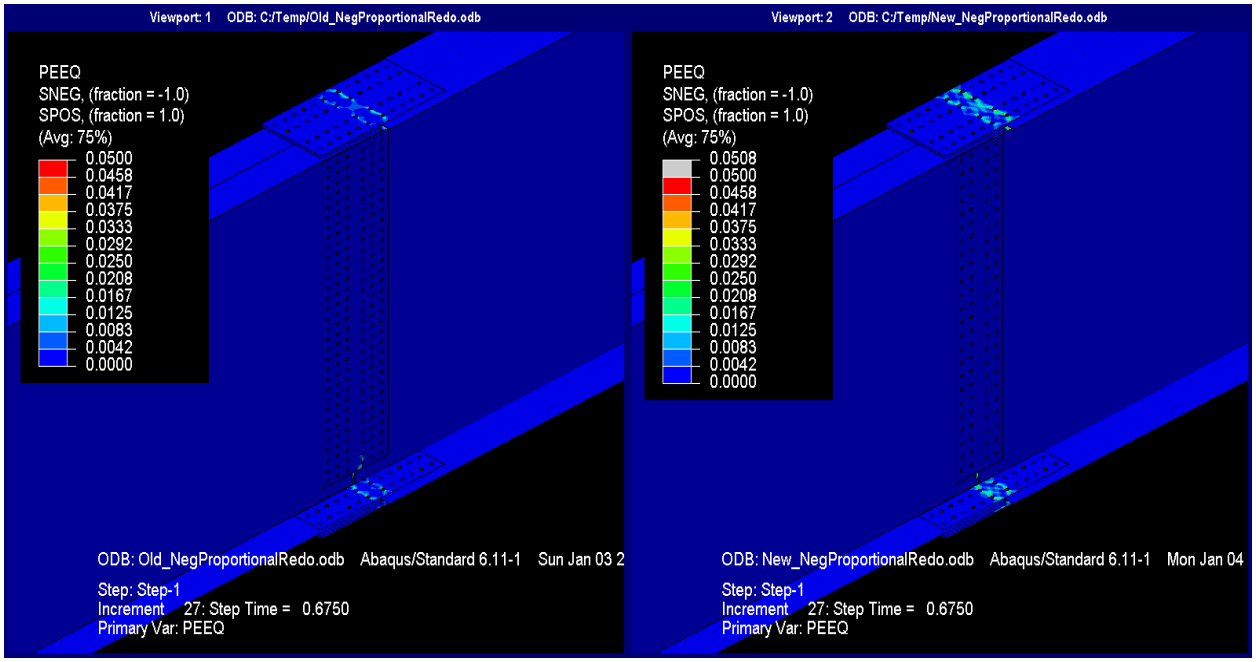

Source: FHWA

Figure 93. Illustration. PEEQ at proportional negative moment at V_u.

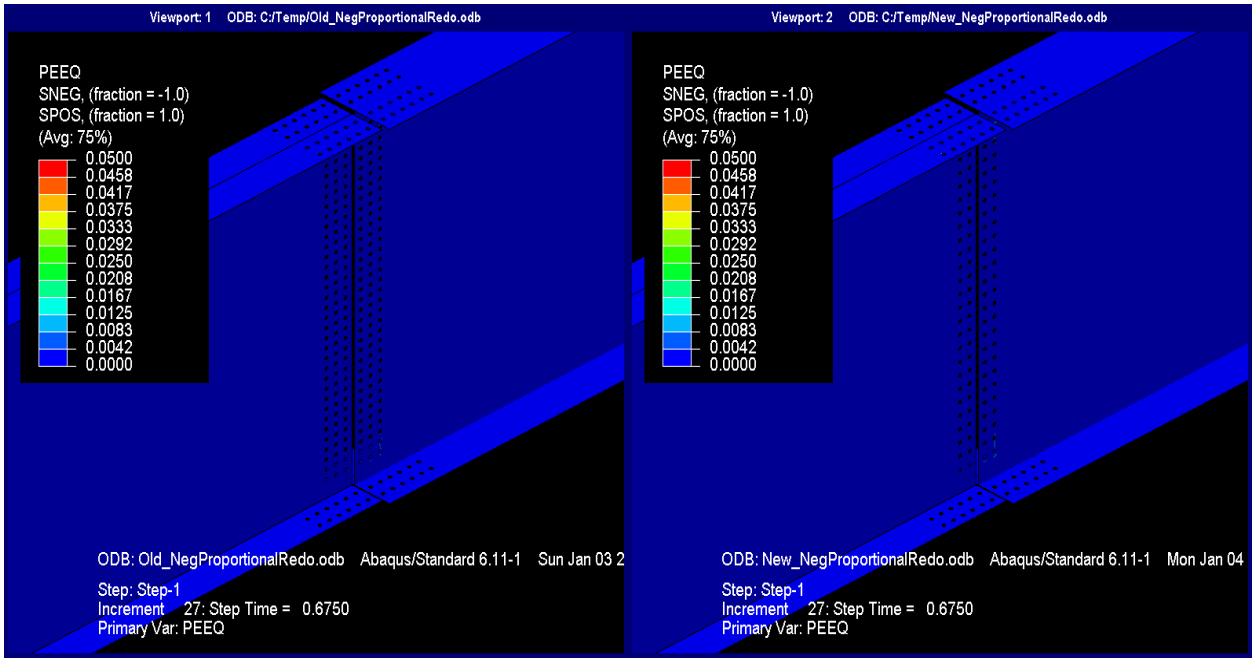

Source: FHWA

Figure 94. Illustration. PEEQ at proportional negative moment at V_u (splice plates not shown for clarity).

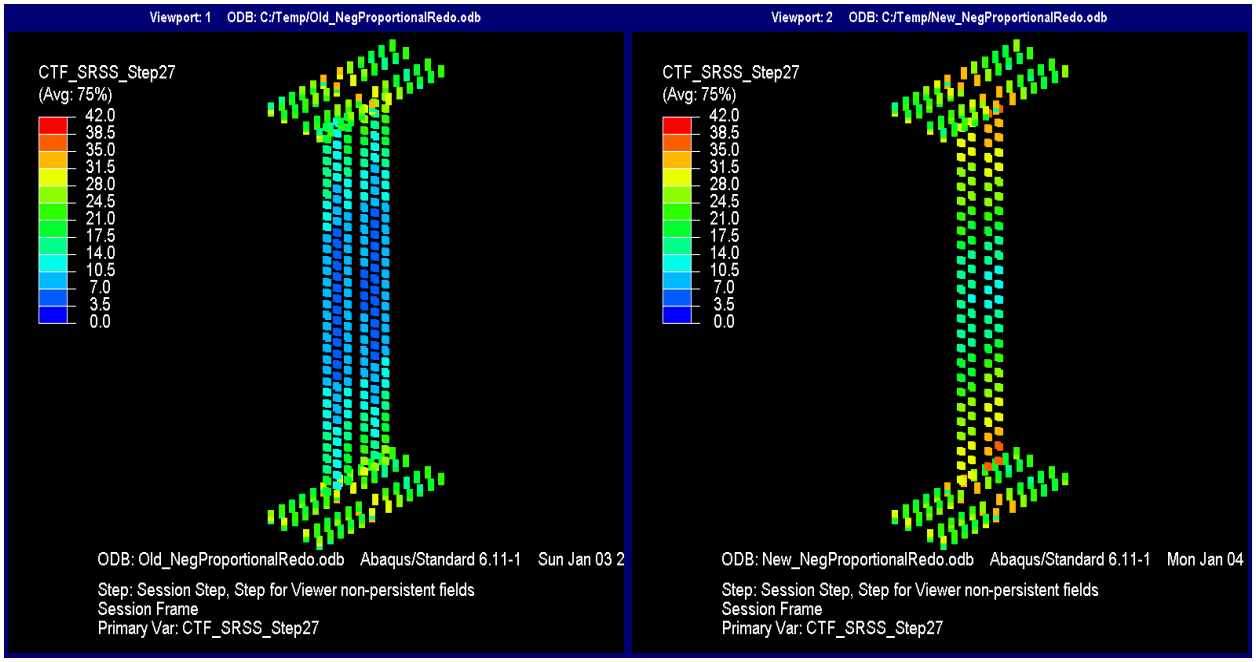

Source: FHWA

Figure 95. Illustration. Resultant forces on bolt shear planes at proportional negative moment at V_u.

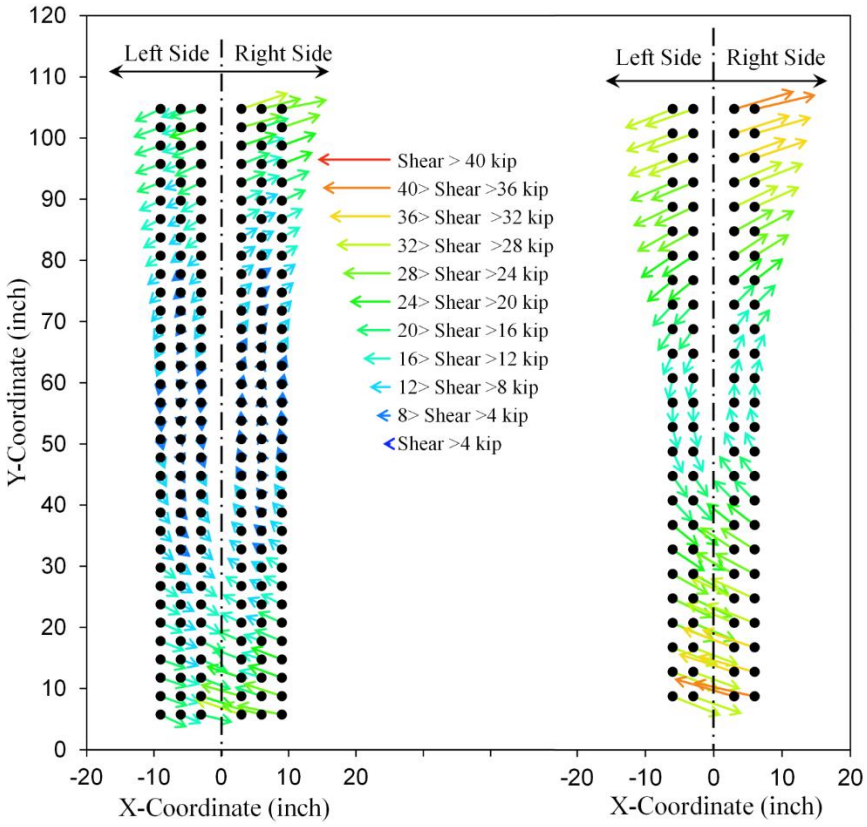

Source: FHWA

Figure 96. Graph. Web splice bolt shear vectors at proportional negative moment at V_u.

At the higher level of interrogation, the response from step 32 was examined for each method, and contour plot data are presented in 0 through 0. At step 32, the shear in the girder was 1,574 kip. The Mises stress plots at this level show that yielding was primarily continuing in the right girder section only as a plastic hinge was developing, which was mainly driven by the longitudinal stresses (see 0 through 0). The PEEQ plots faintly show yielding in the right girder web, although most of the yielding was concentrated in the flange splice plate (see 0 and 0). There was also additional yielding in the web splice in the splice designed using the current method. The largest difference between the
two methods can be seen in the bolt force results. In the splice designed using the new method, the force in the lead bolt in the flange splices varied from 38 to 40 kip depending on the bolt (see 0). This was reduced slightly in the splice designed using the current method, although the forces were in the mid-30 kip range. The web splice bolts were also loaded more heavily in the splice designed using the new method; in fact, the two corner bolts on the right girder section reached the 42-kip limit, which terminated the analysis. The force vectors in the web splice shown in 0 had large horizontal components in bolts closer to the flanges with a characteristic rotation of all vectors around the girder centroid, indicating that the web splice was contributing to moment transfer.

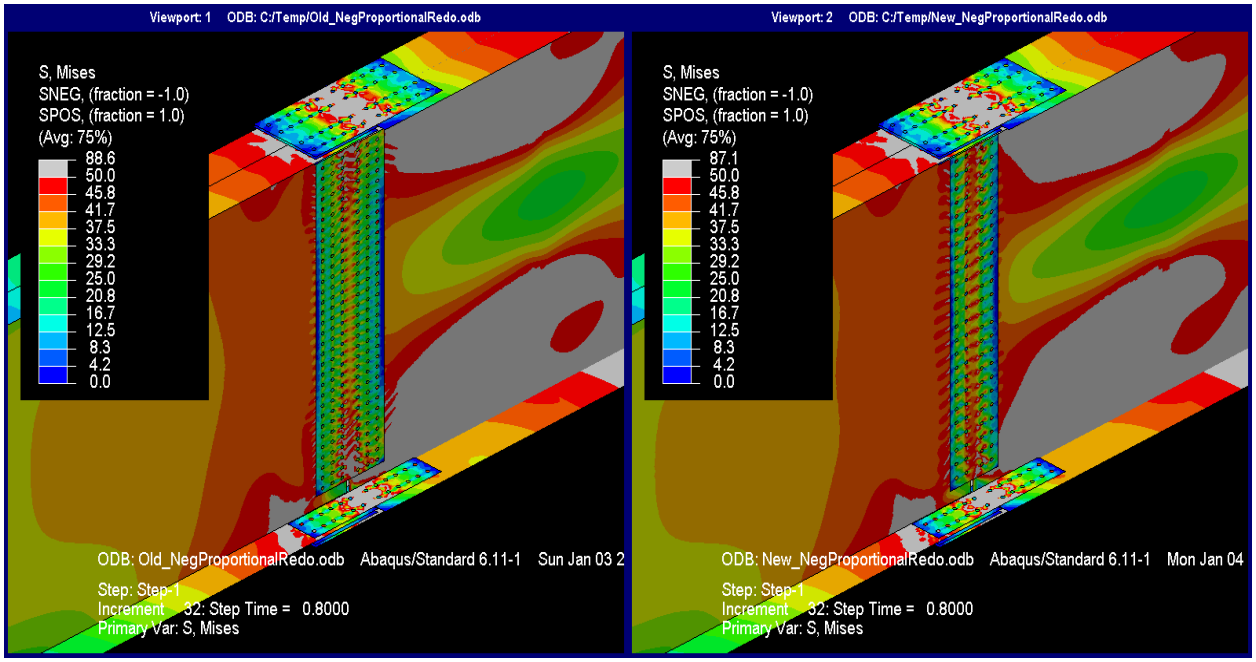

Source: FHWA

Figure 97. Illustration. Mises stresses at step 32.

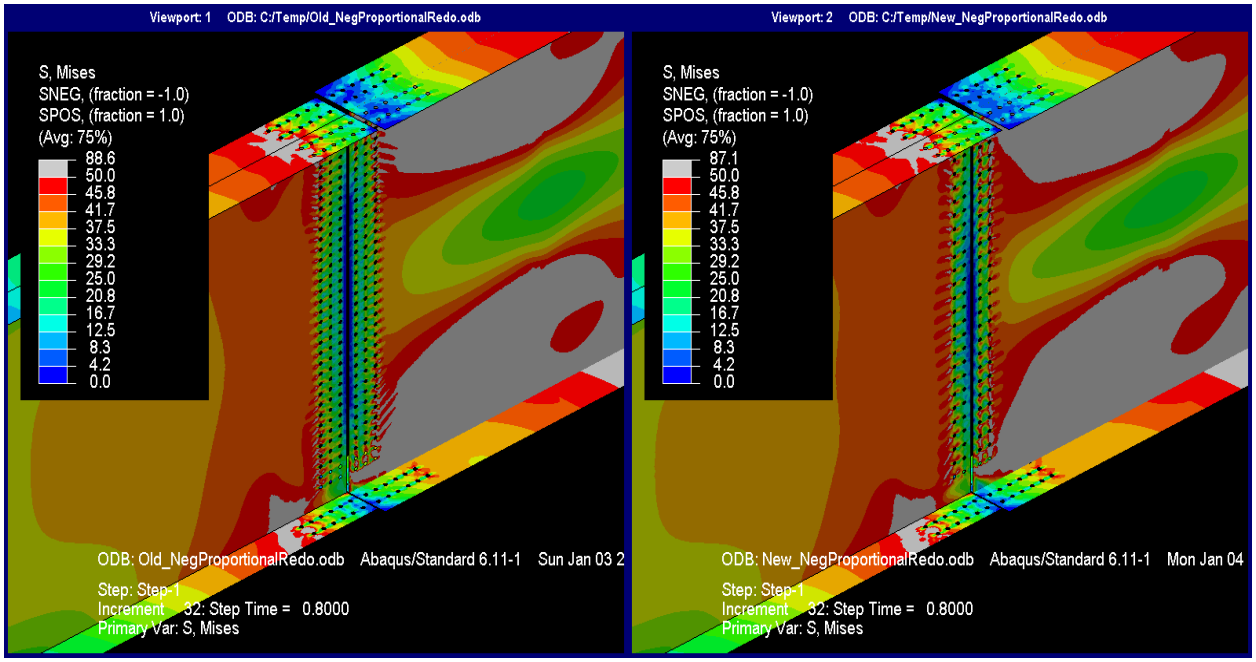

Source: FHWA

Figure 98. Illustration. Mises stresses at step 32 (splice plates not shown for clarity).

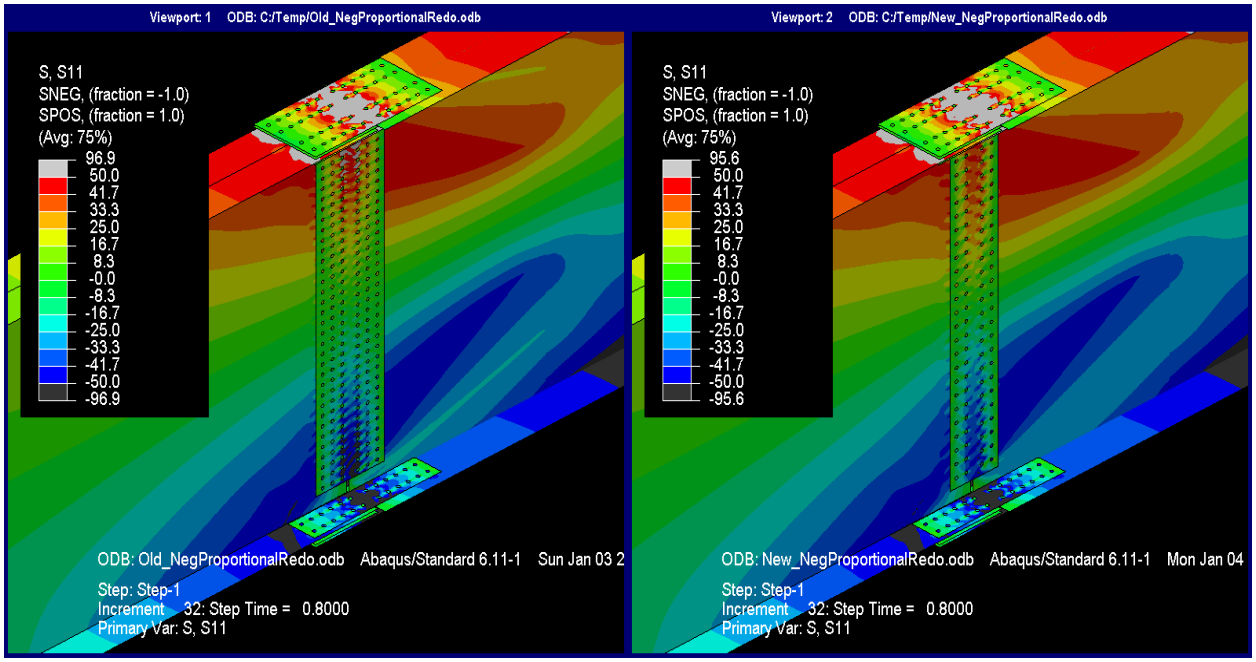

Source: FHWA

Figure 99. Illustration. Longitudinal stresses at step 32.

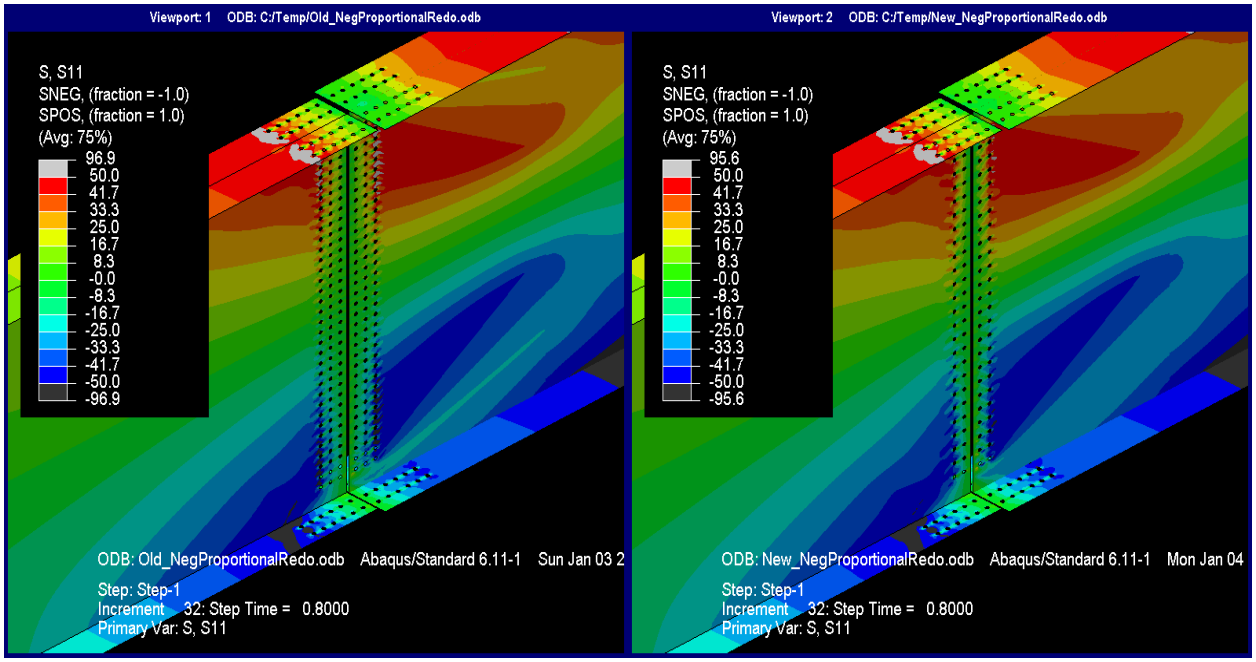

Source: FHWA

Figure 100. Illustration. Longitudinal stresses at step 32 (splice plates not shown for clarity).

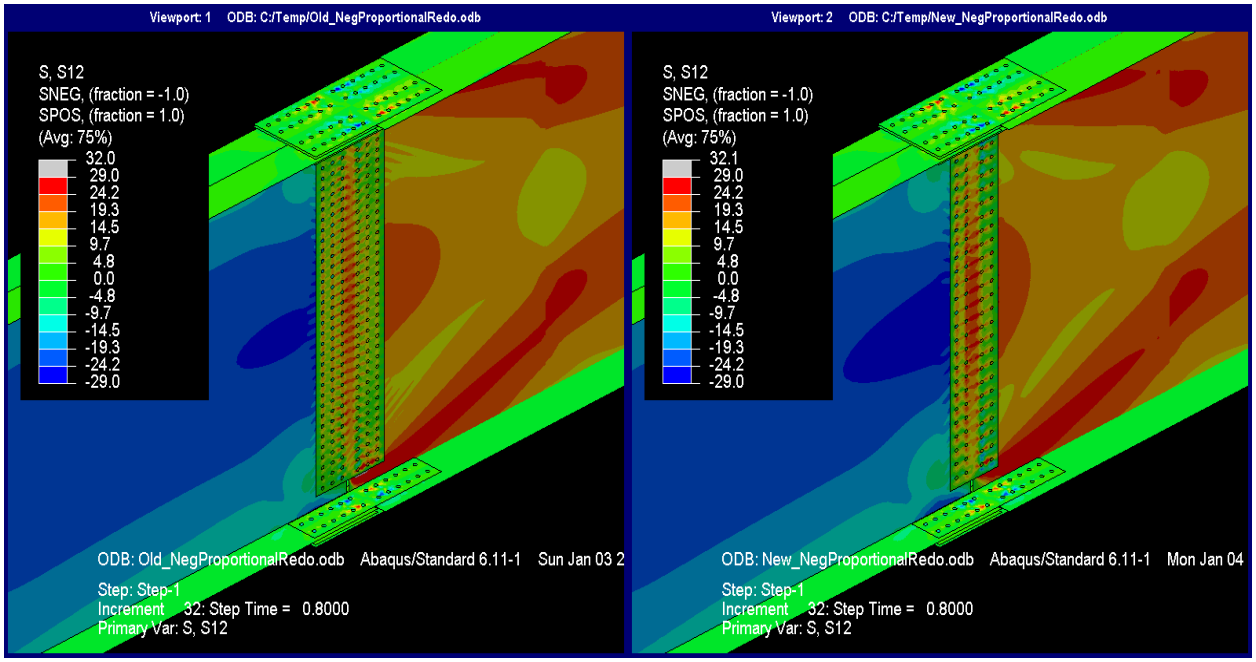

Source: FHWA

Figure 101. Illustration. Shear stresses at step 32.

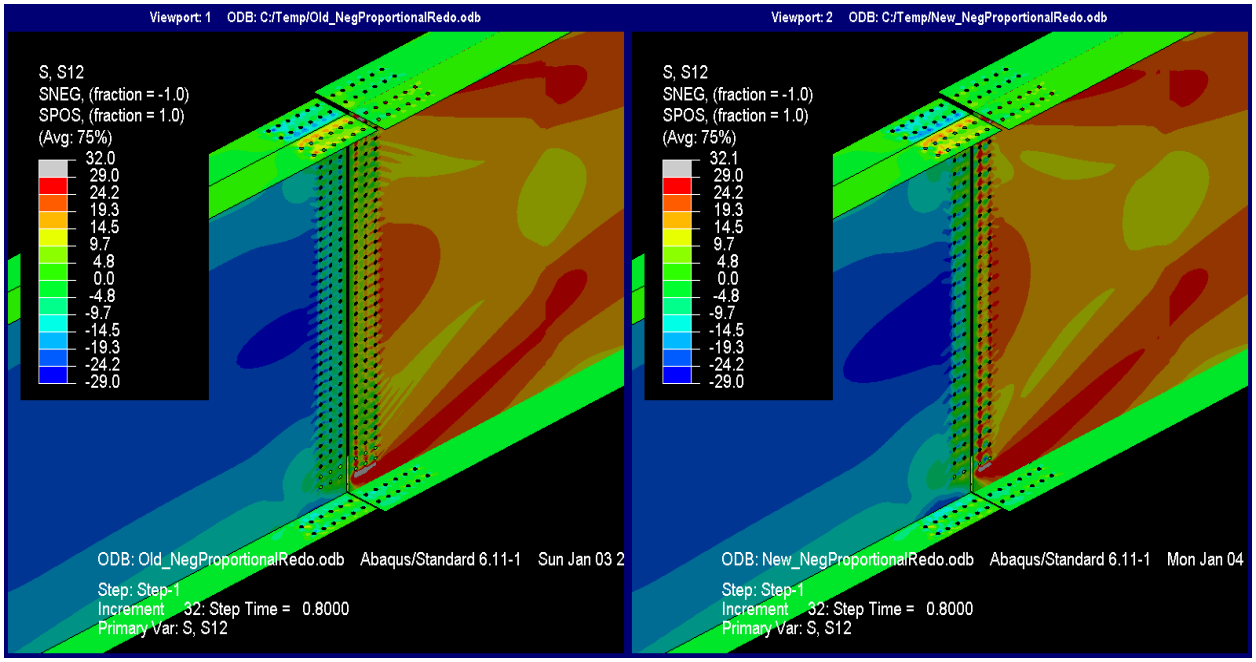

Source: FHWA

Figure 102. Illustration. Shear stresses at step 32 (splice plates not shown for clarity).

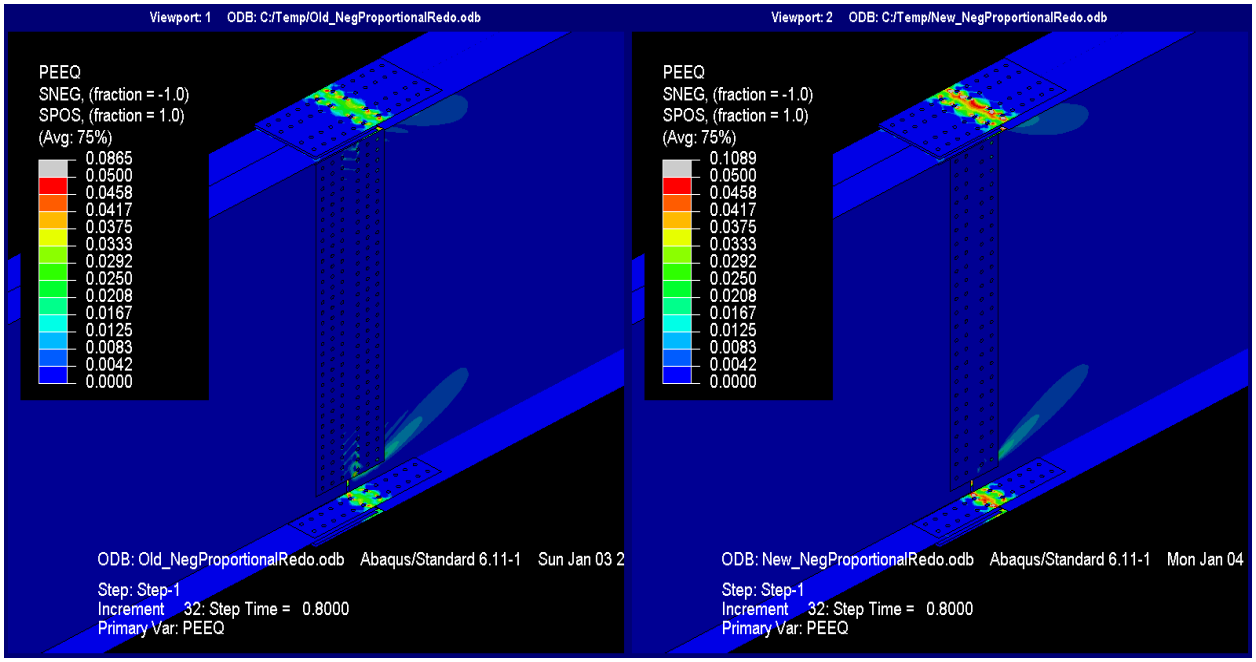

Source: FHWA

Figure 103. Illustration. PEEQ at step 32.

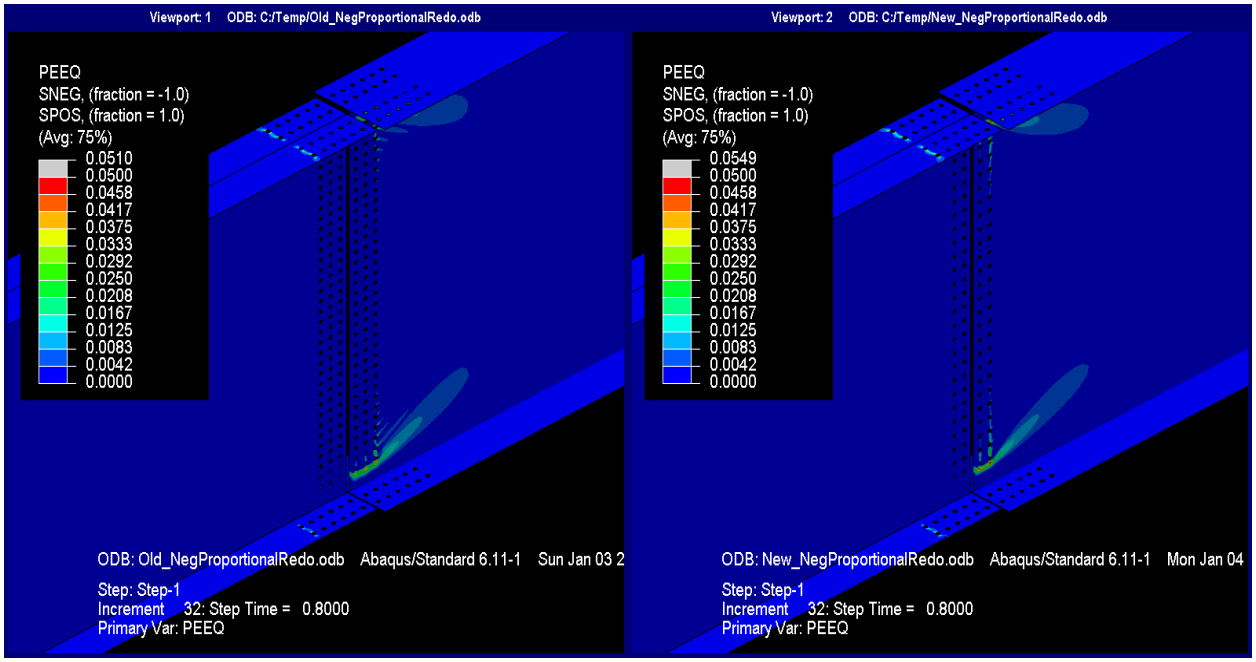

Source: FHWA

Figure 104. Illustration. PEEQ at step 32 (splice plates not shown for clarity).

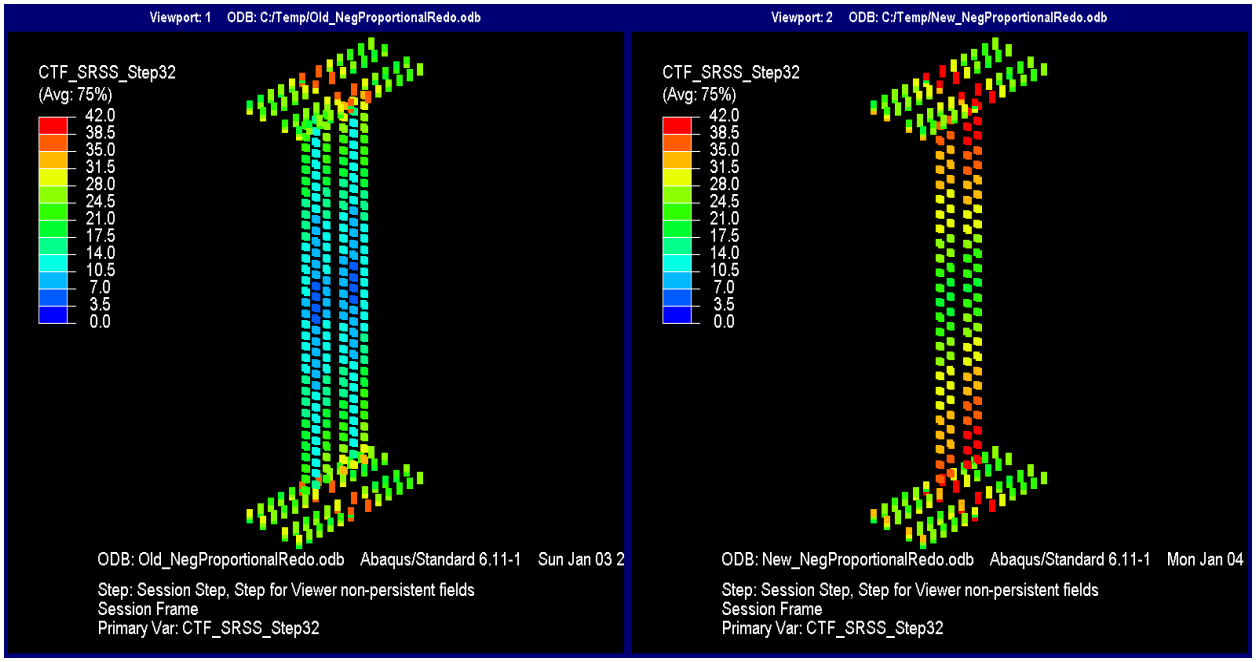

Source: FHWA

Figure 105. Illustration. Resultant forces on bolt shear planes at step 32.

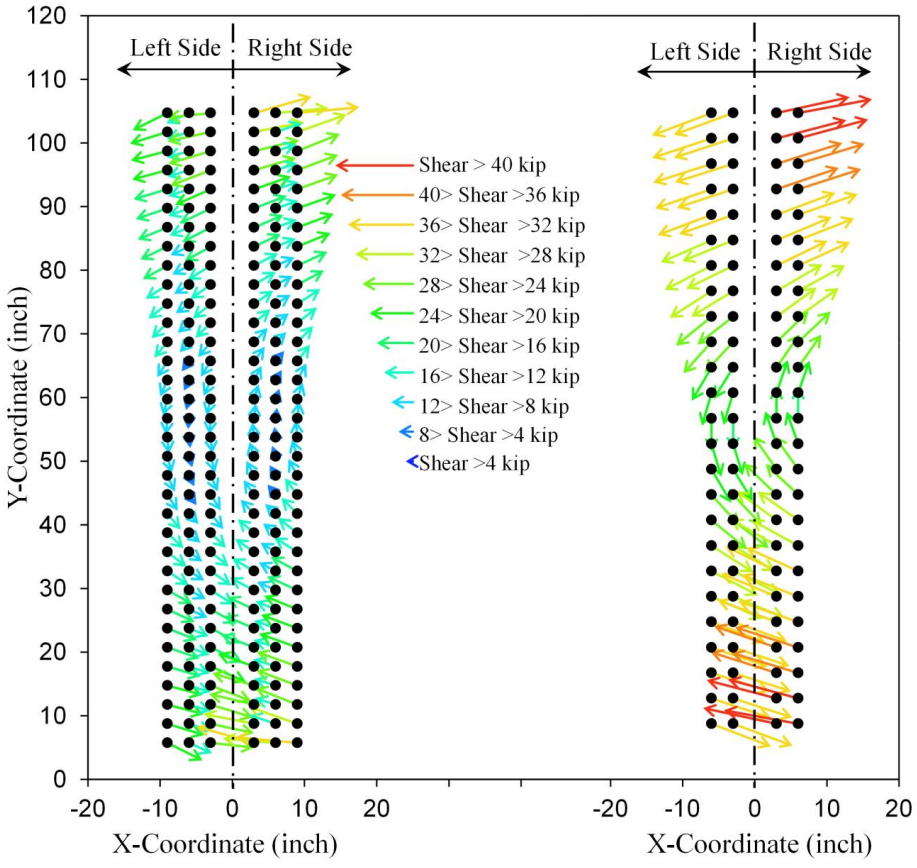

Source: FHWA

Figure 106. Graph. Web splice bolt shear vectors at step 32.

CONCLUSIONS

The following conclusions were reached from the results of the finite element analysis of an outlier connection on a girder with a 109-inch-deep web as well as based on the results of this study that compared and contrasted the current and new splice design methods:

- Both design methods are relatively insensitive to girder shear. That is, the models based on the current and new design methods generated similar results under shear-dominated loading. The only obvious difference was that the demand on the web bolts increased somewhat in the splice designed using the new method because fewer web bolts were required when using the new method.

- The larger web splices that were required to use the current design method were stiffer and attracted more moment into the web than the connection designed using the new method.

- The demand on the flange splices designed using the new method was slightly larger than the demand on the flange splices designed using the current method.

- The bolt force vector plots for the connection designed with each method demonstrated that the web contributed to moment transfer. Specifically, in the two combined loading scenarios investigated, the bolt vectors tended to show overall rotation around the girder neutral axis (proportional positive moment with shear) or girder centroid (proportional negative moment and shear), with a linear increase in force magnitude moving from the rotation center toward the flanges.

- The strength of the splice connection designed by either method provided a connection that exceeded the design force in the analysis and provided comparable connection stiffness. The web-splice connection designed using the new method for the 109-inch-deep girder was able to safely develop the factored shear resistance in combination with any flexural moment introduced into the splice. This was in light of the design method considering all bolts equally loaded by the vector component of shear and horizontal force despite the bolt force vectors showing linear variation from the rotation center out to the flanges.

ACKNOWLEDGEMENTS

The AASHTO SCOBS T-14 Committee formed the ad hoc task group to address the broad topic of simplifying the articles related to bolted field splice design in the *AASHTO LRFD Bridge Design Specifications*, and the author is grateful for the ability to participate in the process.[2] Thanks must also be given to Christopher Garrell of the National Steel Bridge Alliance (NSBA) for conducting all the LRFD Simon runs of various bridge configurations and Dr. Francesco Russo of Michael Baker International for conducting splice designs using NSBA splice. The helpful comments and guidance provided by Edward Wasserman of Modjeski and Masters, Inc., and Hormoz Seradj of the Oregon Department of Transportation in the development of the design method are also gratefully acknowledged. Lastly, the helpful advice of Dr. Karl Frank of Hirschfeld Industries and Michael Grubb of M.A. Grubb & Associates, LLC, on the conduct and analysis of the results from the finite element analyses is also gratefully acknowledged.

REFERENCES

1. Ibrahim, F.S. (1995). *Development of Design Procedures for Steel Girder Bolted Splices*, Ph.D. Dissertation, University of Texas at Austin, Austin, TX.

2. AASHTO. (2015). *AASHTO LRFD Bridge Design Specifications*, 7th Edition with 2015 Interims, American Association of State Highway and Transportation Officials, Washington, DC.

3. Research Council of Structural Connections. (2014). *Specification for Structural Joints Using High-Strength Bolts*, Research Council on Structural Connections, Chicago, IL.

4. AASHTO. (2017). *AASHTO LRFD Bridge Design Specifications*, 8th Edition, American Association of State Highway and Transportation Officials, Washington, DC.

5. ASTM A709/A709M. (2015). "Standard Specification for Structural Steel for Bridges," *Book of Standards Volume 01.04*, ASTM International, West Conshohocken, PA.

6. ASTM F3125/F3125M. (2015). "Standard Specification for High Strength Structural Bolts, Steel and Alloy Steel, Heat Treated, 120 ksi (830 MPa) and 150 ksi (1040 MPa) Minimum Tensile Strength, Inch and Metric Dimensions," *Book of Standards Volume 01.08*, ASTM International, West Conshohocken, PA.

7. Dassault Systèmes®. (2011). *Abaqus/CAE User's Manual Version 6.11-1*, Dassault Systèmes Simulia Corp, Providence, RI.

8. Moore, A.M., Rassati, G.A., and Swanson, J.A. (2008). *Evaluation of the Current Resistance Factors for High-Strength Bolts*. Obtained from: http://www.boltcouncil.org/files/Current-Resistance-factor-report_final.pdf. Site last accessed March 20, 2017.

HRDI-40/11-17(WEB)E